

THESIS



LIBRARY
Michigan State
University

This is to certify that the

thesis entitled

Silica Coatings on Bismaleimide Substrates

presented by

Chinmoy Mukherjee

has been accepted towards fulfillment of the requirements for

Master's degree in Materials Science

Eldon D. Case

Major professor

Date 5-19-99

O-7639

MSU is an Affirmative Action/Equal Opportunity Institution

PLACE IN RETURN BOX to remove this checkout from your record.

TO AVOID FINES return on or before date due.

MAY BE RECALLED with earlier due date if requested.

| DATE DUE | DATE DUE | DATE DUE |
|----------|----------|----------|
| | | |
| | | |
| | | |
| | | |
| | | |

1/98 c/CIRC/DateDue.p65-p.14

SILICA COATINGS ON BISMALEIMIDE SUBSTRATES

By

Chinmoy Mukherjee

A THESIS

Submitted to Michigan State University
In partial fulfillment of the requirements for the degree of

MASTER OF SCIENCE

Department of Materials Science and Mechanics

1999

ABSTRACT

SILICA COATINGS ON BISMALEIMIDE SUBSTRATES

By

Chinmoy Mukherjee

Neat (unreinforced) BMI specimens were coated with a thin, protective layer of a dense silicate ceramic material. Vickers indentation testing on the coated and uncoated BMI specimens was carried out to get an idea of point contact damage to a first approximation. Amount of silica coating spalled off from an indentation was measured as a function of indentation load and for different curing temperatures. Spalling for BMI specimens having coatings cured at 175° C for one hour (0.5% to 5%) was considerably less compared to spalling for BMI specimens (15% to 25%) with coatings cured at 150° C for 20 minutes. Crack spacings were characterized at constant loads for unabraded and abraded coatings, and their distribution studied. Mean crack spacings were independent of the indentation load for BMI specimens with coatings cured at 150° C for twenty minutes. However for BMI specimens with coatings cured at 175° C for one hour, the mean crack spacing increased 47% over a load range of 2.94 N to 196 N. The mean crack spacing normalized with respect to half the total crack dimension when plotted against indentation load is consistent with the power law relationship, μ a = φ P^E.

In addition, the silica coating slowed the uptake of water during water-immersion testing 1.7 times. An expression for the mass change as a function of time due to the diffusion of water into the BMI specimens was developed in Section 3.6.

ACKNOWLEDGEMENTS

I would like to thank my advisor Dr. Eldon D. Case, whose performance as an advisor was exemplary. His guidance and motivation enabled to bring out the best in me. I would like to thank my family for their support and encouragement. Also I would like to thank Ann Xiang (MS Candidate, MSM department, MSU) for her help in Visual Basic programming. This work was funded by the Research Excellence Fund of the State of Michigan, administered through the Composite Materials and Structures Center.

TABLE OF CONTENTS

| | | | | Page |
|-----|---------|-----------------|---|------|
| Lis | st of 7 | Γ a bles | | viii |
| Lis | st of l | Figures | | х |
| 1. | INT | RODU | UCTION | 1 |
| | 1.1 | Polyn | ner-ceramic combinations | 1 |
| | 1.2 | Bisma | aleimide chemistry | 2 |
| | 1.3 | Silica | coatings on BMI | 3 |
| 2. | EXI | PERMI | ENTAL PROCEDURE | 5 |
| | 2.1 | Mater | rials used | 5 |
| | 2.2 | Speci | men preparation | 6 |
| | 2.3 | Chara | acterization of coated BMI | 7 |
| | | 2.3.1 | Vickers indentation technique | 8 |
| | | 2.3.2 | Rockwell indentation technique | 8 |
| | | 2.3.3 | Measurement of silica film island gaps and crack lengths on silica coated BMI specimens | 9 |
| | | 2.3.4 | Measuring percentage of coating spalled off from an indentation | 9 |
| | 2.4 | Scanr | ning electron microscopy | 10 |
| | 2.5 | Coati | ng thickness measurements using ESEM | 10 |
| | 2.6 | Inter | crack spacing measurements | 11 |
| | 2.7 | Abrac | ling silica coated BMI specimens | 12 |
| | 2.8 | Mass | change upon immersion in water | 13 |

| 3. | RES | ULTS | AND DISCUSSION | 14 | |
|----|------|--------|---|-----|--|
| | 3.1 | Uncur | ed BMI and coating quality | 14 | |
| | 3.2 | Coatin | ng thickness effects | 14 | |
| | 3.3 | Vicke | ers indentation damage | 18 | |
| | | 3.3.1 | Comparison of the semi-macro indentor with the micro indentor | 18 | |
| | | 3.3.2 | Study of Vickers indentation damage | 20 | |
| | | 3.3.3 | Spalling area fraction as a function of curing conditions | 32 | |
| | | 3.3.4 | Indentation dimension analysis as a function of load for Vickers indents | 33 | |
| | | 3.3.5 | Vickers indent dimension as a function of loading rate and load time | 37 | |
| | 3.4 | Rocky | well indentation damage | 41 | |
| | 3.5 | ESEM | 1 observations and statistical analysis of crack pattern | 46 | |
| | | 3.5.1 | Mean crack spacing as a function of indentation load | 46 | |
| | | 3.5.2 | Comparison of scatter in spacings of abraded coatings versus unabraded coatings at constant loads | 74 | |
| | | 3.5.3 | Scatter increase with distance from the center of the indent | 78 | |
| | | 3.5.4 | Order statistics study to determine distribution of crack spacings | 84 | |
| | 3.6 | Mass | change measurements | 106 | |
| 4. | CON | CLUS | IONS | 113 | |
| 5 | मा म | TIRES | TUDIES | 117 | |

APPENDICES

| Appendix A. Curing and coating conditions for specimens used to measure coating thicknesses (Section 3.2). | 121 |
|--|-----|
| Appendix B. Curing and coating conditions for specimens used in mass absorption experiments, along with dimensions and time of water immersion (Section 3.6). | 122 |
| Appendix C. Curing and coating conditions for specimens used in scatter spacing measurements, along with R-square values for order statistic plots for different loads (Section 3.5). | 123 |
| Appendix D. Curing and coating conditions for specimens used to make Vickers Indentations and study effect of not precuring specimens (Section 3.3.42 and Section 3.3.4). | 125 |
| Appendix E. Curing and coating conditions for specimens used to study Hertzian indents (Section 3.4). | 126 |
| Appendix F. Curing conditions and dimensions for uncoated specimens used in varying load time and loading rate Vickers indentations (Section 3.3.5). | 127 |
| Appendix G. Curing and coating conditions for specimens used to calculate fractional spalled of area from indentations (Section 3.3.3). | 128 |
| Appendix H. Visual basic macro program to calculate the lowest P value corresponding to point ϕ , in a set of crack spacings for any given indentation load (Section 3.5.3). | 129 |
| Appendix I. Raw crack spacings data for 2.94 N and 4.9 N indentation loads for BMI specimen with unabraded silica coating cured at 150°C for 20 minutes (Figures 20 and 21) and 175°C for one hour (Figures 28 and 29). | 131 |
| Appendix J. Raw crack spacings data for 9.8 N and 49 N indentation loads for BMI specimen with unabraded silica coating cured at 150°C for 20 minutes (SUA1, Figures22 and 23) and 175°C for one hour (CR1, Figures 30 and 31) and, BMI with abraded coating cured at 150°C for 20 minutes. | 132 |
| Appendix K. Raw crack spacings data for 98 N and 196N indentation loads for BMI specimen with unabraded silica coating cured at 150°C for 20 minutes (SUA1, Figures 24 and 25) and 175°C for one hour (CR1, Figures 32 and 33). | 134 |

Appendix L. Indent dimension raw data, which was included in Figures 5a and 5b. Averages of indent dimensions (6 to 10 indents) were taken, when plotting indentation dimension versus indentation load.

137

LIST OF TABLES

| | Page |
|--|------|
| Table 1. The average of 6 total crack dimension values 2D, for indentations at 3 different loads in the semi-macro indentor (Specimen B, Appendix D) and the micro indentor (Specimen B1, Appendix D). | 19 |
| Table 2. The crack dimension measurement of a 9.8 N indent made by the semi macro indentor on specimen B1 (Appendix D), measured by the optical read out in the semi macro indentor and the micro indentor. | 19 |
| Table 3. Average Total indent dimension (2a) raw data as a function of indentation loads for figures 5a and 5b. | 24 |
| Table 4. Average of mean crack spacings for six indentations at each indentation load for the specimens listed in Appendix C. | 48 |
| Table 5. The pre-exponent φ and exponent ϵ obtained from least squares fitting of of figure 19 using equation 5. | 52 |
| Table 6. Mean crack spacing data for various indentation loads for BMI specimens with unabraded coatings cured at 150°C at 20 minutes and cured at 175°C at 60 minutes. | 54 |
| Table 7. MSF♠ values (equation 4) for BMI with unabraded and abraded coatings cured at 150°C for 20 minutes and BMI with unabraded coatings cured at 175°C for 20 minutes. | 57 |
| Table 8. Number of concentric cracks/unit length as a function of indentation load for BMI with unabraded and abraded silica coatings, cured at 150°C for 20 minutes and for unabraded silica coatings cured at 175°C for 1 hour. | 58 |
| Table 9. The standard deviations from mean crack spacings for BMI specimens with unabraded and abraded coatings cured at 150°C for twenty minutesand BMI specimens with unabraded coatings cured at 175°C for one hour. | 77 |
| Table 10. The distance of point, ϕ , from the center of the indent, along with the η values (equation 9), for various indentation loads. | 81 |
| Table 11. Coefficients α and β obtained from the least-squares fit of equation 17b to the M_N versus $t^{1/2}$ data. | 111 |

| Table A. Curing and coating conditions for specimens used to measure coating thicknesses (Section 3.2). | 121 |
|--|------------|
| Table B. Curing and coating conditions for specimens used in mass absorption experiments, along with dimensions and time of water immersion (Section 3.6). | 122 |
| Table C1. Curing and coating conditions for specimens used in scatter spacing measurements, along with mean spacing values at different loads (Section 3.5). | 123 |
| Table C2. R-square values for order statistics plots for indentations made on specimens listed in table C1. | 124 |
| Table D. Curing and coating conditions for specimens used to make Vickers Indentations and study effect of not precuring specimens (Section 3.3.42 and Section 3.3.4). | 125 |
| Table E. Curing and coating conditions for specimens used to study Hertzian indents (Section 3.4). | 126 |
| Table F. Curing conditions and dimensions for uncoated specimens used in varying load time and loading rate Vickers indentations (Section 3.3.5). | 127 |
| Table G. Curing and coating conditions for specimens used to calculate fractional spalled of area from indentations (Section 3.3.3). | 128 |
| Table I. Raw crack spacings data for 2.94 N and 4.9 N indentation loads for BMI specimen with unabraded silica coating cured at 150°C for 20 minutes (Figures 20 and 21) and 175°C for one hour (Figures 28 and 29). | 131 |
| Table J. Raw crack spacings data for 9.8 N and 49 N indentation loads for BMI specimen with unabraded silica coating cured at 150°C for 20 minutes (SUA1, Figures 22 and 23) and 175°C for one hour (CR1, Figures 30 and 31) and, BMI with abraded coating cured at 150°C for 20 minutes. | 132 |
| Table K. Raw crack spacings data for 98 N and 196N indentation loads for BMI specimen with unabraded silica coating cured at 150°C for 20 minutes (SUA1, Figures 24 and 25) and 175°C for one hour (CR1, Figures 32 and 33). | |
| Table L. Indent dimension raw data, which was included in Figures 5a and 5b. Averages of indent dimensions (6 to 10 indents) were taken, when plotting indentation dimension versus indentation load. | 134 137 |

LIST OF FIGURES

| | Page |
|---|-------|
| Figure 1. The thickness of silica coating on BMI substrates as a function of the spinning speed. The BMI (BMPM:DABPA=1:1.13 and BMPM:DABPA = 1:1, Appendix A) substrates were first precured at 200°C for 1 hour, then the coated specimens were cured at 150°C for 20 minutes. | 16 |
| Figure 2. Micrograph of ≈ 2.5 micron thick silica coating on BMI showing separated islands of the coating. The specimen, with substrate stoichiometry BMPM:DABPA=1:1 (Appendix A), was pre cured at 200° C for 1 hour, coated at 500 rpm for 20 seconds and then cured at 150° C for 20 minutes. | 17 |
| Figure 3(a). Schematic of delaminated silica coating on BMI substrate and Figure 3(b). Schematic of a spalled region of the silica coating on a BMI substrate. | 22 |
| Figure 4. Schematic of Vickers indent impressions on (a) an uncoated BMI specimen and (b) a coated BMI specimen. | 23 |
| Figure 5 (a). Logarithmic plot for indentation dimension versus indentation load for uncoated and coated BMI specimens of different chemistries (BMPM:DABPA = 1:1, 1:0.82, 1:1.13, Appendix D) and Figure 5 (b). Logarithmic plot for indentation dimension versus indentation load for uncoated and coated BMI specimens of the same stoichiometry (BMPM:DABPA = 1:1, Appendix D). | 25-26 |
| Figure 6. Micrograph of a Vickers indent made at a load of 49 N on an uncoated BMI specimen (BMPM: DABPA = 1:1, Specimen CR1, Appendix G). The BMI was precured at 200°C for 1 hour and again cured at 150°C for 20 minutes. | 27 |
| Figure 7. Micrograph of 9.8 N Vickers indent made on coated BMI specimen where the coating thickness was ≈ 0.15 microns. The specimens were precured at 200° C for 1 hour, coated at 3500 rpm for 20 seconds a) cured at 150° C for 20 minutes (Specimen CR1, Appendix G) and, b) cured at 175° C for one hour (Specimen CR3, Appendix G). | 28 |
| Figure 8. For the same indented specimen as shown in Figure 7a, a higher magnification view of the array of concentric cracks that comprise the indentation crack field. The center of the indent impression and a spalled region of the coating are shown. | 29 |

| Figure 9. Fraction of silica film spalled off from an indentation as a function of indentation load, for BMI with unabraded silica coatings cured | |
|--|----|
| at O - 150° C for 20 minutes, and Δ - 175° C for 1 hour. | 30 |
| Figure 10. Micrograph showing a coating delamination and crack associated with a pair of closely spaced 49 N Vickers indentations on a coated BMI specimen (BMPM:DABPA = 1:1, Specimen K2, Appendix D) This is the only example of a coating delamination that was observed in this study. | 35 |
| Figure 11. Micrograph showing a pair of closely spaced 9.8 N Vickers indentations on a coated BMI specimen (BMPM:DABPA = 1:1, Specimen CR2, Appendix G). | 36 |
| Figure 12. Indentation dimension plotted as a function of indentation load time at a loading rate of 50 microns/second, at loads of 4.9 N and 49 N for uncoated BMI specimens of three different chemistries (L1, L2 and L3, Appendix F). | 39 |
| Figure 13. Indentation dimension plotted as a function of loading rate at a load time of 10 seconds at loads of 4.9 N and 49 N, for uncoated BMI specimens of three different chemistires (L1, L2 and L3, Appendix F). | 40 |
| Figure 14. Rockwell indentation on the HRF scale depicting concentric circular crack pattern on a silica coated BMI specimen (R1, Appendix E). | 42 |
| Figure 15. Micrograph depicting the transition region from complete Hertzian cracks to incomplete hertzian cracks, in the same indent as Figure 14. | 43 |
| Figure 16. Micrograph depicts the incomplete Hertzian cracks at a higher magnification for the same indent as Figure 14. | 44 |
| Figure 17. Micrograph depicting the radial cracks originating from the end of the region that included the incomplete Hertzian cracks on the same indent as Figure 14. | 45 |
| Figure 18. Mean crack spacing data plotted versus various indentation loads for BMI specimens with unabraded coatings cured at 150°C at 20 minutes and cured at 175°C at 60 minutes. | 55 |
| Figure 19. Logarithmic plot of mean crack spacing data versus various indentation loads for BMI specimens with unabraded coatings cured at 150°C at 20 minutes and cured at 175°C at 60 minutes | 56 |

| Figure 20. Crack spacing data d _{ij} , for a Vickers indent made at a load of 2.94 N, on specimen SUA1 (Appendix C), plotted against the radial | |
|---|----|
| position from the center of the indent. | 59 |
| Figure 21. Crack spacing data d_{ij} , for a Vickers indent made at a load of 4.9 N, on specimen SUA1 (Appendix C), plotted against the radial position from the center of the indent. | 60 |
| Figure 22. Crack spacing data d_{ij} , for a Vickers indent made at a load of 9.8 N, on specimen SUA1 (Appendix C), plotted against the radial position from the center of the indent. | 61 |
| Figure 23. Crack spacing data d_{ij} , for a Vickers indent made at a load of 49 N, on specimen SUA1 (Appendix C), plotted against the radial position from the center of the indent. | 62 |
| Figure 24. Crack spacing data d_{ij} , for a Vickers indent made at a load of 98 N, on specimen SUA4 (Appendix C), plotted against the radial position from the center of the indent. | 63 |
| Figure 25. Crack spacing data d _{ij} , for a Vickers indent made at a load of 196 N, on specimen SUA4 (Appendix C), plotted against the radial position from the center of the indent. | 64 |
| Figure 26. Crack spacing data d_{ij} , for a Vickers indent made at a load of 9.8 N, on specimen SA1 (Appendix C), plotted against the radial position from the center of the indent. | 65 |
| Figure 27. Crack spacing data d_{ij} , for a Vickers indent made at a load of 49 N, on specimen SA1 (Appendix C), plotted against the radial position from the indent. | 66 |
| Figure 28. Crack spacing data d _{ij} , for a Vickers indent made at a load of 2.94 N, on an silica coated BMI specimen cured at 175°C for one hour (CR 3, Appendix C), plotted against the radial position from the center of the indent. | 67 |
| Figure 29. Crack spacing data d _{ij} , for a Vickers indent made at a load of 4.9 N, on an silica coated BMI specimen cured at 175°C for one hour (CR3, Appendix C), plotted against the radial position from the center of the indent. | 68 |
| Figure 30. Crack spacing data d _{ij} , for a Vickers indent made at a load of 9.8 N, on an silica coated BMI specimen cured at 175°C for one hour (CR3, Appendix C), plotted against the radial position from the center of the indent. | 69 |

| Figure 31. Crack spacing data d _{ij} , for a Vickers indent made at a load of 49 N, on an silica coated BMI specimen cured at 175°C for one hour (CR3, Appendix C), plotted against the radial position from the center of the | |
|--|----|
| indent. | 70 |
| Figure 32 . Crack spacing data d _{ij} , for a Vickers indent made at a load of 98 N, on an silica coated BMI specimen cured at 175°C for one hour (CR3, Appendix C), plotted against the radial position from the center of the indent. | 71 |
| Figure 33. Crack spacing data d _{ij} , for a Vickers indent made at a load of 196 N, on an silica coated BMI specimen cured at 175°C for one hour (CR3, Appendix C), plotted against the radial position from the center of the indent. | 72 |
| Figure 34. Crack spacing data d _{ij} , for a Hertzian indent made on the HRF scale, on specimen SUA3 (Appendix C), plotted against the radial position from the center of the indent impression. | 73 |
| Figure 35. Point ϕ , normalized by radial crack field dimension "a" for coated BMI specimens (SUA1, SUA4, Appendix C), plotted as a function of indentation load. | 83 |
| Figure 36. Schematic depicting uniform distribution of residuals. | 86 |
| Figure 37. For the distance between the i th and j th crack, d _{ij} , ordered residual spacings versus expected value of order statistics for a 2.94 N indent on an silica coated BMI specimen (SUA4, Appendix C) with an unabraded coating. | 87 |
| Figure 38. For the distance between the i th and j th crack, d _{ij} , ordered residual spacings versus expected value of order statistics for a 49 N indent on an silica coated BMI specimen (SUA4, Appendix C) with an unabraded coating. | 88 |
| Figure 39. For the distance between the i th and j th crack, d _{ij} , ordered residual crack spacings versus expected value of order statistics for a 9.8 N indent on an silica coated BMI specimen (SUA1, Appendix C) with an unabraded coating. | 89 |
| Figure 40. For the distance between the i th and j th crack, d _{ij} , ordered residual spacings versus expected value of order statistics for a 49 N indent on an silica coated BMI specimen (SUA1, Appendix C), with an unabraded coating. | 90 |

| residual crack spacings versus expected value of order statistics for a 98 N indent on an silica coated BMI specimen (SUA4, Appendix C), with an unabraded coating. | 91 |
|---|----|
| Figure 42. For the distance between the i th and j th crack, d _{ij} , ordered residual crack spacings versus expected value of order statistics for a 196 N indent on an silica coated BMI specimen (SUA4, Appendix C), with an unabraded coating. | 92 |
| Figure 43. For the distance between the i th and j th crack, d _{ij} , ordered residual spacings versus expected value of order statistics for a 9.8 N indent on a coated BMI specimen (SA1, Appendix C) with an abraded silica film. | 93 |
| Figure 44. For the distance between the i th and j th crack, d _{ij} , ordered residual spacings versus expected value of ordered statistics for a 49 N indent on a coated BMI specimen (SA1, Appendix C) with an abraded silica film. | 94 |
| Figure 45. For the distance between the i ^{ih} and j th crack, d _{ij} , ordered residual spacings versus expected value of ordered statistics for a 2.94 N indent on a coated BMI specimen cured at 175°C for one hour (CR3, Appendix H) with an abraded silica film. | 95 |
| Figure 46. For the distance between the i ^{ih} and j th crack, d _{ij} , ordered residual spacings versus expected value of ordered statistics for a 9.8 N indent on a coated BMI specimen cured at 175°C for one hour (CR3, Appendix C) with an abraded silica film. | 96 |
| Figure 47. For the distance between the i th and j th crack, d _{ij} , ordered residual spacings versus expected value of ordered statistics for a 9.8 N indent on a coated BMI specimen cured at 175°C for one hour (CR3, Appendix G) with an abraded silica film. | 97 |
| Figure 48. For the distance between the i ^{ih} and j th crack, d _{ij} , ordered residual spacings versus expected value of ordered statistics for a 49 N indent on a coated BMI specimen cured at 175°C for one hour (CR3, Appendix C) with an abraded silica film. | 98 |
| Figure 49. For the distance between the i ^{ih} and j th crack, d _{ij} , ordered residual spacings versus expected value of ordered statistics for a 98 N indent on a coated BMI specimen cured at 175°C for one hour (CR3, Appendix C) with an abraded silica film. | 99 |
| | |

| Figure 50. For the distance between the i ^{ih} and j th crack, d _{ij} , ordered residual spacings versus expected value of ordered statistics for a 196 N indent on a coated BMI specimen cured at 175°C for one hour (CR3, Appendix C) with an abraded silica film. | 100 |
|---|-----|
| Figure 51. For the distance between the i th and j th crack, d _{ij} , ordered residual spacings versus expected value of order statistics for a Rockwell indent on a coated BMI specimen (SUA3, Appendix C), with an unabraded silica film. | 101 |
| Figure 52. For the distance between the i^{ih} and j^{th} crack, d_{ij} , from the center of the indent until the point ϕ , ordered residual spacings versus expected value of order statistics for a 49 N Vickers indent on a coated BMI specimen (SUA1, Appendix C), with an unabraded silica film. | 102 |
| Figure 53. For the distance between the i th and j th crack, d _{ij} , from the point φ to the end of the indent, ordered residual spacings versus expected value of order statistics for a 49 N Vickers indent on a coated BMI specimen (SUA1, Appendix C), with an unabraded silica film. | 103 |
| Figure 54. For the distance between the i th and j th crack, d _{ij} , from the center of the indent until the point φ, ordered residual spacings versus expected value of order statistics for a 196 N Vickers indent on a coated BMI specimen (SUA4, Appendix C), with an unabraded silica film. | 104 |
| Figure 55. For the distance between the i th and j th crack, d _{ij} , from the point φ to the end of the indent, ordered residual spacings versus expected value of order statistics for a 196 N Vickers indent on a coated BMI specimen (SUA4, Appendix C), with an unabraded silica film. | 105 |
| Figure 56. Schematic of the diffusion of water into the BMI during water immersion testing. | 107 |
| Figure 57. Normalized mass change, M_N , versus $t^{1/2}$ for BMI specimens with (a) all 6 sides coated and (b) uncoated BMI specimens (BMPM:DABPA = 1:0.82). The solid curves represent a least -squares fit of the data to equation (17b). | 112 |

1.0 INTRODUCTION

1.1 Polymer ceramic combinations

This thesis deals with applying continuous ceramic coatings to polymeric materials. Although continuous ceramic coatings on polymeric materials are relatively novel, additions of ceramics to bulk polymeric materials are common, especially for ceramic fiber reinforcement of polymers such as in fiberglass. In addition, for biomedical use, several weight percent barium sulfate (BaSO₄) dispersed in PMMA bone cement (a fixative for medical implants composed mainly of a monomeric methyl methacrylate and particulate PMMA) makes the bone cement radiopaque and hence renders the bone cement "readable" on medical x-rays [1]. Powdered silica, calcium carbonate, and clay are often used as inexpensive extenders for polymers [2]. Mica platelets can increase the impact strength and the flexural modulus, improve resistance to chemical attack, and decrease moisture up-take for thermoplastics [3]. However, each of these applications feature ceramics in particulate, fiber, or platelet form being added to the bulk of a polymer material, rather than producing a ceramic coating on the surface of the polymer.

Duchatelhard et al. applied thin alumina films to PMMA using RF magnetron sputtering [4,5]. Alumina coatings improve the wetability of PMMA, which is advantageous in dental applications, where saliva wetability of materials is quite important [6]. This thesis however focuses on a technique for depositing and characterizing a thin, adherent coating on the surface of bismaleimide (BMI), which is a polymeric material that is of considerable interest for aerospace applications due to its (i) ease of processing and (ii) excellent high temperature properties. Prior to crosslinking,

BMI is a viscous liquid, enabling BMI to be processed with methods similar to those used to process epoxy resin. Upon curing, the glass transition temperature of BMI is about 300°C, which can be considered for aerospace applications.

However, as is the case for many polymeric systems, the physical and mechanical properties of BMI are affected by organic solvents and moisture [15]. In addition, BMI-carbon composites are susceptible to galvanic corrosion when in contact with metallic surfaces. Thus, although BMI has the advantages of processing ease and good thermal properties, BMI's performance could be substantially improved by decreasing its susceptibility to solvent attack, ingress of water, and (in the case of BMI-carbon components) galvanic corrosion. A thin continuous surface coating might be able to seal out moisture and solvents, and if the layer were electrically insulating, it could reduce galvanic corrosion. To be effective such a coating would need to adhere well to the BMI surface.

1.2 Bismaleimide Chemistry

The cure reaction characteristics and kinetics in the liquid and glassy-state of BMPM-DABPA BMI composite matrices have been studied by Fourier transform infrared spectroscopy (FTIR), differential scanning calonmetry (DSC) and gel permeation chromatography (GPC) [7, 8, 9, 11, 12]. In the 100-200°C range the BMPM BMI reacts with the DABPA to form an "ene" adduct. The "ene" adduct is pentafunctional as a result of (i) three carbon-carbon double bonds, capable of chain extension and crosslinking, and (ii) two hydroxyl groups capable of etherification by hydroxyl dehydration.

BMI is a crosslinked polymer glass and as such its mechanical properties depend on the detailed topography of the crosslinked network [13]. For example, depending on the crosslinked conditions, the elastic modulus of BMI varies from 3.55 GPa to 4.12 GPa [15] and the room temperature density changes from 1.2375 g/cm³ to 1.2473 g/cm³ [16].

The relative rates in the liquid-state and the principal cure reactions involving the five reactive "ene" group species have been fully characterized in the 200°-350°C temperature range [12]. Morgan et. al [7] have used the infrared bands at 3473 cm⁻¹ and 1179 cm⁻¹ to monitor the disappearance of hydroxyl groups and appearance of the ether groups respectively for the etherification reaction by hydroxyl dehydration. Recent work [14] has identified infrared bands associated with the cure reactions of the allyl (A) at 915 cm⁻¹ and 995 cm⁻¹, propenyl (B) at 931 cm⁻¹ and 975 cm⁻¹ and maleimide (C) at 690, 713, 827 and 1639 cm⁻¹ double bonds respectively.

1.3 Silica coatings on BMI

This thesis investigates fabricating continuous silica coatings on unreinforced BMI substrates. Spin rates and curing conditions are adjusted to obtain uniform, apparently uncracked silica coatings on BMI substrates. Coating thicknesses are measured for varying spin rates. Vickers indentations were made on uncoated and silica coated BMI substrates and their indentation pattern evaluated. Spalling area fractions on Vickers indentation and uniformity of silica coatings for the silica coated BMI substrate was studied as a function of indentation load for varying curing temperatures.

Crack spacings in silica coated BMI substrates were evaluated at constant indentation loads for BMI with unabraded and abraded (Section 2.7 and Section 3.5.2) silica coatings cured at 150°C, and for BMI with unabraded silica coatings cured at 150°C and 175°C. Scatter in crack spacings was evaluated as a function of the radial position from the indent at at a constant indentation load (Section 3.5.3). Mean crack spacings were plotted as a function of indentation loads for the curing temperatures of 150°C and 175°C (Section 3.5.1). Distribution of crack spacings was studied by doing an order statistic study (Section 3.5.4). Water uptake at room temperature was compared for uncoated and silica coated BMI (Section 3.6).

2. EXPERIMENTAL PROCEDURE

2.1 Materials Used.

The Bismaleimide (BMI) resin system (MatrimidTM 5292, Ciba-Geigy [14]), used was a two component system based on 4,4'-bismaleimidodiphenylmethane (BMPM) and 0,0'-diallyl bisphenol alcohol (DABPA). The amber, viscous DABPA liquid monomer was poured into a magnetic stir-activated beaker and heated on a hot plate at 130°C, then yellow BMPA crystalline powder was added slowly and mixed until a homogeneous solution was achieved. This prepolymer mixture was degassed in a vacuum oven set at a temperature of 130°C for 20 minutes. This mixture was then poured into a preheated (90°C) mold and cured in a nitrogen atmosphere oven for 1 hour at 177°C followed by additional 1 hour curing at 200°C. During processing, the stoichiometric ratio of BMPA:DABPA was varied such that the BMI specimens included in this study had BMPM: DABPA ratios of 1:0.82, 1:1 and 1:1.13. All BMI substrates included in this study were initially cured for 1 hour at 177°C followed by a cure for one hour at 200°C. Depending on the curing conditions, the elastic modulus of BMI varies from 3553 MPa to 4122 MPa [15], the room temperature density ranges from 1.2375 g/cm³ to 1.2473 g/cm³ [16], the activation energy for diffusion varies from about 21.8 kJmol⁻¹ to 33.5 kJmol⁻¹.

The silica coatings that were applied to the BMI were an organic-based liquid (Emulsitone company, New Jersey) that was spun-onto the BMI substrates. The liquid is converted to an amorphous silica film upon pyrolysis.

2.2 Specimen Preparation

Using a low speed diamond saw (IsometTM Buehler), the BMI substrate specimens were cut into 1 cm X 1 cm X 0.4 cm sections. Tap water was used as coolant instead of oil to prevent contamination of the BMI. After sectioning with the diamond saw, the specimens were ground using a 600-grit abrasive paper and then polished using $5 \mu m$, $0.3 \mu m$, and $0.05 \mu m$ alumina abrasive powders.

The polished BMI specimens were pre-cured (The specimens when received had already been cured at 177°C/1hour and then at 200°C/1hour) prior to coating in order to reduce shrinkage of the BMI during the subsequent coating procedure. The precuring was done in air for 60 minutes to 120 minutes in a resistively-heated oven (Stabil-Therm® Gravity oven, Model – B-2729-Q, Blue Signal) at temperatures ranging from 180°C to 265°C. A mercury thermometer, with a least count of 2°C was used to record temperature in the furnace.

The BMI specimen surfaces to be coated were cleaned first with deionized water, then with acetone and then blotted dry with a paper towel. Afterwards the silica coating was applied to the BMI surface.

The BMI specimens were adhered to the center of a petri-dish with an adhesive tape and placed on the high speed spinner which holds the petri-dish by vacuum assist. The spinner was turned on before applying the film and the spin rate and timer settings were adjusted to that needed in the experiment.

Five to six drops of the silica film solution was applied on the center of the BMI surface using a pasteur pipette. The specimens were then spun for 20 seconds on a substrate spinner at rates ranging from 500 to 4000 rpm to yield a range of coating

thicknesses. The specimens were then cured in air at 150° C \pm 2° C for 20 minutes in the resistively-heated oven.

Two coating protocols were used for coating the BMI: (1) only one specimen surface coated and (2) all six-specimen surfaces coated (for mass absorption experiments, Section 3.6). To coat all six sides, 5 sides of a precured BMI specimen were coated, leaving the bottom surface uncoated. The coated specimen was then cured in air at 150°C for 20 minutes, then the single uncoated specimen surface was coated with silica coating at 3000 rpm for 20 seconds. The entire specimen was cured using the same temperature and time used to cure the other five specimen surfaces.

Two coated BMI specimens SA1 and SA2 (Appendix C) were used in scatter spacing studies (Section 3.5.2). The curing and coating conditions are given in Appendix C. After curing the two BMI coated substrates, the specimens were polished on a polishing wheel at 175 rpm for 45 seconds to introduce defects larger than the pre-existing defects. Both specimens were cleaned using de-ionized (DI) water and blotted dry using Kleenex paper.

2.3 Characterization of coated BMI

In this study, we evaluate the BMI coatings using two types of tests: (1) Vickers and Hertzian indentation damage and (2) mass change upon water immersion. For the indentation tests we compared the single-side coated and uncoated specimens. For the water immersion tests, we compare uncoated specimens with specimens coated on all six surfaces.

2.3.1 Vickers Indentation technique

All indented BMI specimens were polished and precured prior to indentation. Two commercial hardness testers were used to generate Vickers indentation cracks in both uncoated and single-side coated specimens using a loading rate of 70 microns/second, a loading hold time of 10 seconds. The semi-macro indenter (Buehler, Lake Bluff, IL) had a load range of 2.94 N to 196N and the micro indenter (Model: M-400-G1, LECO Corporation) had a load range of 0.098 N to 9.8 N. The dimensions of the resulting crack damage were measured using a digital readout attachment to the Vickers indenters (both the indenters had a similar digital readout attachment), which could be read to ± 0.1 micron.

2.3.2 Rockwell Indentation Technique

Single-side coated BMI specimens were cleaned and dried prior to indentation. A standard Rockwell indenter (Wilson Mech. Instrument CO. INC., N.Y.) was used at a load of major load of 60 kg and 1.5875 X 10⁻³m steel ball indentor at a loading time of 10 seconds. This scale is the Rockwell-F scale. A minor load of about 10kg is first applied to set the penetrator in position on the specimen, and a reference position is established on the dial gauge. The dial is then set at zero before the major load (between 60kg and 150kg) is subsequently applied. This major load is the total load applied and the depth measurement (hardness calculated from depth) depends solely on the increase in depth due to the load increase from minor to major. The specimen was then removed and imaged using scanning electron microscopy.

2.3.3 Measurement of silica film island gaps and crack lengths on silica coated BMI specimens

BMI specimens with chemistries (BMPM:DABPA = 1:1, 1:0.82, 1:1.13) were coated at speeds varying from 500 to 4000 rpm. All of the above BMI specimens were observed under an optical microscope at 200 X prior to indentation. The optical lens used was the one attached to the semi-macro Vickers indentor. The specimens on which the silica film formed islands (Figure 2) were subjected to measurements on the optical microscope. The gaps between islands of silica film were measured were made using the digital readout, which was attached to the lens. Two cursors are placed at the two points between which you want the measurements taken and the reading is observed from the digital readout. For each specimen 10 readings were taken and the average calculated. For the specimens on which film was absent but some surface cracks were present, the crack lengths and the distances between the parallel cracks were measured with the optical microscope. Results were calculated from average of five readings.

2.3.4 Measuring percentage of coating spalled off from an indentation

Three BMI specimens with coating thickness of approximately 0.15 microns, were indented at loads ranging from 2.94 N to 196 N and imaged using scanning electron microscopy. Micrographs were taken at magnifications ranging from 300 X to 720 X. The fractional spalled area was calculated using an image analysis software NIH image FAT 5.0. The fractional spallation area, f_S , was calculated from f_S = spalled area/total indented area. Grid point method was used to verify the results from the image analysis software, and agreed to within \pm 2%. For the grid point method the fractional spalled

area f_S = number of grid points intersecting the spalled area/total number of grid points intersecting the diamond-shaped crack zone.

2.4 Scanning electron microscopy

Scanning electron microscopy was used in imaging coated and uncoated BMI specimens. Two different scanning electron microscopes were used. One was an SEM (JEOL, LaB₆) and the other was an environmental scanning electron microscope (ESEM, Philips-Electroscan 2020 environmental scanning electron microscope, equipped with a LaB₆ filament).

Surfaces to be imaged of all indented specimens used for SEM studies was gold coated using an Emscope Sputter coater at a current of 20 mA, vacuum of 0.08-0.12 Torr and coating time of 90 to 120 seconds. Specimen sides were made conductive by applying carbon paint.

Specimens imaged using ESEM, did not have to be gold coated nor painted using carbon paint, as the ESEM allows imaging of non conductive specimens.

2.5 Coating Thickness Measurements Using ESEM

The environmental scanning electron microscope was used to estimate the thickness of the silica coating on the BMI. BMI specimens of chemistries (BMPM:DABPA = 1:1 and 1:1.13 and 1:0.82, Appendix A) precured at 200°C for 1 hour were coated at spinning speeds varying from 500 rpm to 4000 rpm with the silica coating and then cured in air at 150°C for 20 minutes. The coated specimens were sectioned,

using a low speed diamond saw, so that the thickness values could be measured near the center of the specimen.

Coated BMI specimens were then placed in the ESEM at tilt angles varying from 7^0 to 12^0 and at an accelerating voltage of 20 kV in order to facilitate the coating thickness measurements. The true coating thickness h is given by $h = h_W/\cos\theta$ where h_W is the measured coating thickness and θ the tilt angle in the ESEM.

Since the ESEM allows observation of nonconductive specimens without an electrically-conductive coating, no conductive coating was applied to the surfaces of either the silica coated or the uncoated BMI specimens. The lack of a conductive coating is an advantage in this study, as such a coating could obscure details of cracks and other surface features on the BMI specimens.

2.6 Inter-crack spacing measurements

For this set of experiments only coated BMI and abraded coated BMI specimens were considered. Six of the BMI specimens were precured at 200°C for 1 hour, then coated with silica film at 4000 rpm for 20 seconds and finally cured at 150°C for 20 minutes, but one of the specimens were cured at 175°C for 60 minutes. For the BMI with abraded coatings the specimen surface after coating was polished using 0.03 µm alumina polishing powder solution on a wheel for 45 seconds to abrade the surface. In all 7 BMI specimens of chemistries (BMPM:DABPA = 1:1, Appendix C) were used. Two types of indents considered:

- a) Vickers Indent at indentation loads ranging from 2.94 N to 196 N
- b) Rockwell-F scale Indent at 588 N indentation load

The specimens were imaged using scanning electron microscopy at magnifications of 3000X to 3500X, and an accelerating voltage of 20 kV. The BMI specimen was held to the specimen holder by an adhesive tape. For the Vickers Indent, images were taken along a radial crack till the end of the crack zone.

The crack spacing were individually measured from the micrographs by using a ruler with a least count of 1 mm. If the crack spacing measured from the ruler was d mm, then the true length of the spacing was given by

$$D_0 = (d/M) X 1000 \text{ microns}$$

where.

M = magnification

The crack spacings were plotted as a function of radial spacing using MS Excel software.

Similarly, the crack spacings were calculated along one of the radii for the Rockwell indent and plotted as a function of radial position. The Rockwell indent spacings also were imaged at magnifications of 3000X to 3500X using scanning electron microscopy.

2.7 Abrading silica coated BMI specimens

Silica coated BMI specimens after curing were abraded on a polishing cloth using a 0.03 micron alumina polishing solution for 30 to 45 seconds. The polishing wheel was spun at 175 rpm. The specimen was held by hand without any other mechanical pressure.

2.8 Mass change upon immersion in water

The coated (all six sides) and uncoated BMI were weighed using an electronic balance (Denver Instrument Company, M-Series Analytical balance, Model M-220D), to an accuracy of ±0.0001g. The coated and uncoated BMI were placed in two separate beakers containing room temperature deionized water. The ratio of the volume of water/specimen surface area ranged from 50 cm to 60 cm for each of the water immersion trials. After two hours the uncoated and coated BMI were removed from the deionized water. The specimen was dried using tissue paper and exposing it to air for 3 to 4 minutes. The masses of the uncoated and coated BMI were measured. The uncoated and coated BMI specimens were returned to their respective deionized water containers. The mass measurement procedure was repeated every two hours up to 10 hours after the initial immersion in the deionized water.

3. RESULTS AND DISCUSSION

3.1 Uncured BMI and coating quality

Four BMI specimens (Appendix D) that were not precured prior to coating showed sets of nearly parallel cracks which were about 70 to 140 microns apart that were distributed uniformly over the 1 cm X 1 cm specimen faces. The cracks were about 3 to 5 mm long, with side-branching cracks that extended about 1 to 3mm from the main cracks. On average there were about 1 or 2 branching cracks that originated from one of the set of parallel cracks. The specimens were observed in an optical microscope attached to the Semi-Macro Indentor at 200X. All measurements were made using the digital readout attached to the Semi-Macro Indentor, as discussed in Section 2.3.3.

3.2 Coating thickness effects

Spin rates between 500 rpm and 4000 rpm produced (after curing) coating thicknesses from 2.5 microns to 0.15 microns (Figure 1). Coating thickness were measured as a function of spin rates for silica coated BMI specimens of varying stoichiometry. Thirty specimens were used, six each of T1, T2 and T3 types of specimens (BMPM:DABPA = 1:1.13, Appendix A), six of T4 specimens (BMPM:DABPA = 1:1, Apendix A) and six of T7 (BMPM:DABPA = 1:0.82, Appendix A).

The coated surfaces were observed as a function of the spinning speed. For this six each of T5 (BMPM:DABPA = 1:1.13, Appendix A), T6 (BMPM:DABPA = 1:1, Appendix A), and T8 types of specimens were used (BMPM:DABPA = 1:0.82, Appendix A), none of which had to be sectioned, as they were not used for thickness

measurements. For coating thickness in the thickness range between 1.66 (1000 rpm) to 2.5 microns (500 rpm), the coating was discontinuous, as determined both by unaided eye observations and a 200X optical microscope connected to the Semi-Macro indentor. For coatings spun at 500 rpm and 1000 rpm, islands of silica coating (Figure 2) were observed. For the 500 rpm specimens the distance between the silica islands was on average about 12 microns, and for 1000 rpm specimen the distance between the islands was about 6.3 microns. The measurements were made using the digital readout connected to the semi-macro indentor as described in Section 2.3.3.

Coatings spun at 1500 rpm (coating thickness \approx 0.6 microns) had parallel cracks with spacings of about 100 to 150 microns with lengths ranging from 3 to 4 mm, with occasional side branching cracks that ranged in length from about 1mm to 2.5mm. Coatings with thicknesses less than about 0.3 microns (corresponding to spin rates of 2000 rpm and greater) were not cracked and no gaps were apparent in either the optical microscope or the ESEM for the 0.8 cm \times 1 cm (T5, Appendix A) and 1 cm \times 1 cm (T6 and T7) specimen surfaces.

Coatings with thicknesses less than about 0.3 microns (2000 rpm and above) were not cracked and no gaps were apparent in either the optical microscope or the ESEM for the 0.8 cm X 1 cm (T5, Appendix A) and 1 cm × 1 cm (T6 and T7) specimen surfaces.

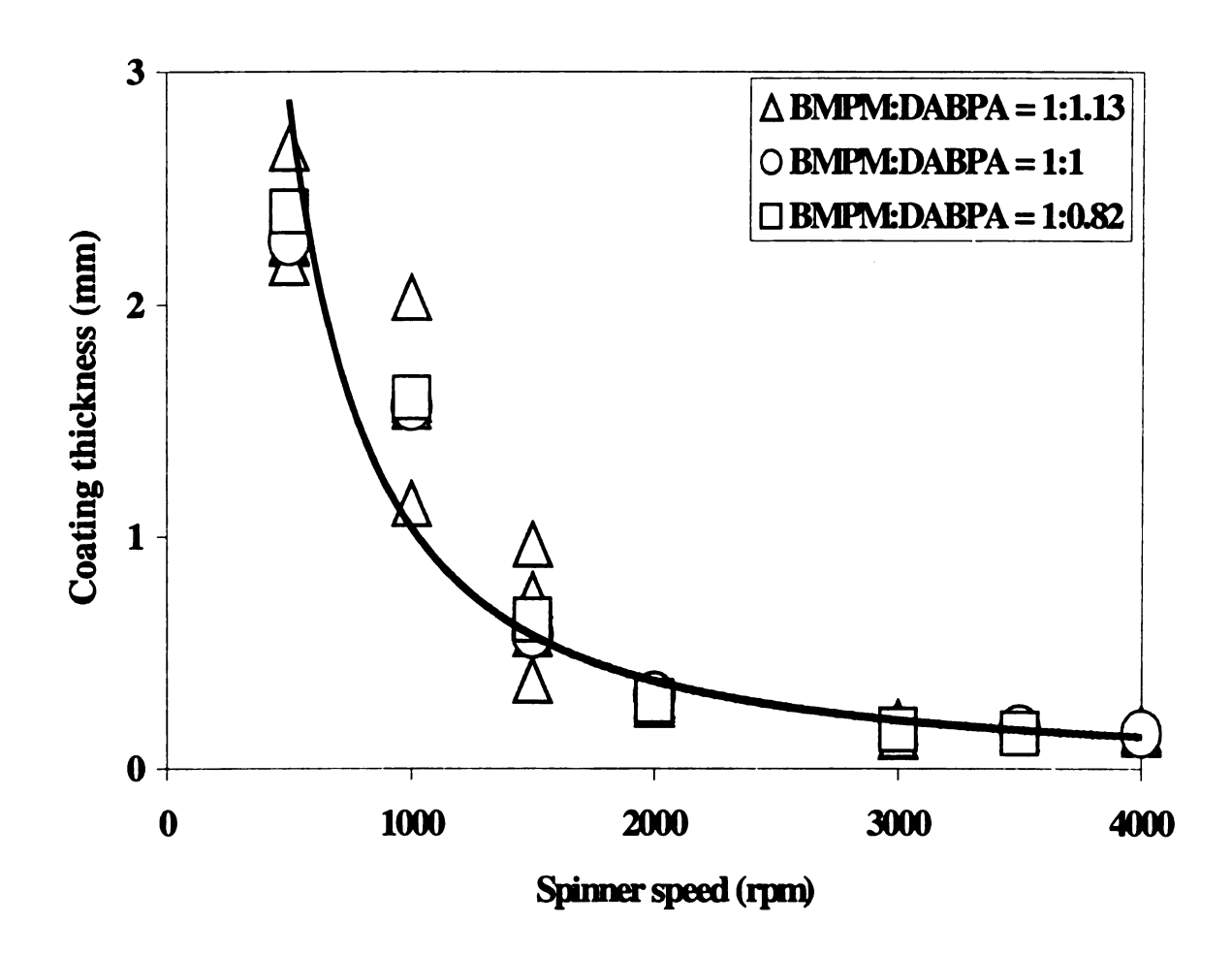


Figure 1. The thickness of silica coating on BMI substrates as a function of the spinning speed. The BMI (BMPM:DABPA=1:1.13 and BMPM:DABPA = 1:1, Appendix A) substrates were first precured at 200°C for 1 hour, then the coated specimens were cured at 150°C for 20 minutes.

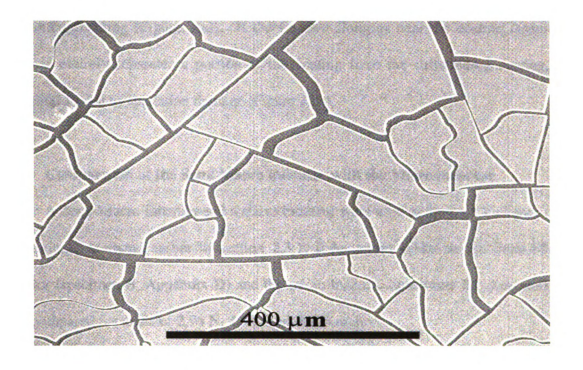


Figure 2. Micrograph of ≈ 2.5 micron thick silica coating on BMI showing separated islands of the coating. The specimen, with substrate stoichiometry BMPM:DABPA=1:1 (Appendix A), was pre cured at 200° C for 1 hour, coated at 500 rpm for 20 seconds and then cured at 150° C for 20 minutes.

3.3 Vickers Indentation damage

This thesis shall discuss the coating damage in terms of cracks, delaminations, and spalls. We shall use the term delamination to denote a fracture along or near the coating/specimen interface for which part of the coating remains attached to the surrounding coating (Figure 3(a)). If the fracture along or near the coating /specimen interface entirely separates a portion of the coating from the surrounding coating, we shall refer to that as spallation damage (Figure 3(b)).

3.3.1 Comparision of the Semi Macro indentor with the Micro indentor

A Semi-Macro Indentor and a micro indentor were used to produce Vickers indentations, as stated earlier in section 2.3.1. Indentations taken on the Semi-Macro indentor (specimen B, Appendix D) and the micro indentor (specimen B1, Appendix D) were compared for loads of 2.94 N, 4.9 N and 9.8 N each.

Six readings were taken at each load, on each of the indentors and averages compared. Also, an indent made at 9.8 N on specimen B1 on the semi-macro indentor was measured using the digital readout on the semi-macro as well as the micro indentor.

The indentations made on the semi-macro and micro indentors are very much comparable at the same loads (Tables 1 and 2) with regards to nature of the indent impressions and their dimensions. Thus, we use both the indentors at various loads to extend the range of loads at which we make indentations.

Table 1. The average of 6 total crack dimension values 2a, for indentations at 3 different loads in the semi-macro indentor (Specimen B, Appendix D) and the micro indentor (Specimen B1, Appendix D).

| Specimen | Indentor | *2a _{coat} (µm) / P (N) | | | | |
|-----------------|------------|----------------------------------|--------------|-------------|--|--|
| B (Appendix 4) | Semi-Macro | 122.3 / 2.94 | 167.7 / 4.9 | 239.5 / 9.8 | | |
| B1 (Appendix 4) | Micro | 124.27 / 2.94 | 165.17 / 4.9 | 236.7 / 9.8 | | |

^{*} Each 2a_{coat} reading is an average of 6 readings.

Table 2. The crack dimension measurement of a 9.8 N indent made by the semi macro indentor on specimen B1 (Appendix D), measured by the optical read out in the semi macro indentor and the micro indentor.

| Optical read-out | Load (N) | Indentor used | 2a _{coat} (μm) |
|------------------|----------|---------------|-------------------------|
| used | | | |
| Semi-macro | 9.8 N | Semi-macro | 237.1 |
| Micro | 9.8 N | Semi-macro | 237.3 |

3.3.2 Study of Vickers Indentation Damage

The indentation behavior of brittle films on brittle substrates, has been considered in number of studies [18, 19, 20]. However, we will consider the point contact damage by doing Vickers indentation on a brittle (silica) film on a compliant (polymer – BMI) substrate. Vickers indentation damage to a first approximation compares well with damage caused during handling and fabricating components [21].

For the silica-coated BMI specimens, the adhesion of the silica coatings to the BMI is surprisingly strong. Both uncoated and silica-coated BMI specimens were indented using a Vickers Semi-macroindentor at loads of 2.94 N to 196 N and a microindentor at loads of 0.098 N to 9.8N (Figures 4 (a), 4 (b), 5 (a) and 5 (b)). The uncoated specimens showed a square-pyramidal indent impression. The total crack dimension, 2a_{uncoat} (Note: For coated BMI we call the total crack dimension 2a_{coab} and for the uncoated BMI the total crack dimension is called 2a_{uncoat}, Figures 5 (a), 5 (b) and 6), for the uncoated BMI varied from about 530 microns at 2.94 N to about 1040 microns at 196 N. The absence of radial cracks in the uncoated BMI, is interesting as polymers tend to have low fracture toughness values K_{ic} (K_{ic} - fracture toughness in plain strain, [22]). This absence of radial cracks can be attributed to the low hardness value, H (H = P/2a²), where P is Vickers indentation load and, "a" is half the total crack dimension for a Vickers indentation), and high critical load, Pc (the critical load required to initiate a crack) to initiate cracks. P_c is proportional to $(K_{ic})^4/(H)^3$ { $P_c = \lambda_0 (K_{ic})^4/(H)^3$ }[23, 24, 25], where λ_0 is a geometric constant, which is about 1.6×10^4 for a Vickers indentation [25]. From the above relationship, $P_c = \lambda_0 (K_{ic})^4/(H)^3$ [25], we estimate the critical Vickers indentation load required to propagate radial cracks in BMI to be 322 N to 840 N

(assuming K_{ic} (BMI) = 1 MPa m^{1/2}, Hardness (BMI) = 317.48 ± 50.03 from Section 3.3.4). Since the P_c for BMI (322 N to 840 N), was higher than the maximum indentation load (196 N), which could be obtained using the Semi-macro Vickers indentor, it is consistent with the fact that we did not obtain any radial cracks.

For the silica-coated specimens, Vickers indentation produced cracks in the silica coating in a pattern of concentric diamond-shaped cracks, centered on the indent impression (Figures 4(b), 7 (a), 7 (b) and 8). The outer edge of the array of diamond shaped cracks corresponded very well with the indent impression for the uncoated BMI specimens. Cracks towards the outer region tend to bow outward slightly, than compared to the cracks towards the center of the indent impression (Figures 7 (a) and 7 (b)). The total crack dimension 2a_{uncoat} for the uncoated specimen and the outer edge of the "crack zone", 2a_{coat}, for the coated material agree to within about two-percent in all cases. Also the crack zone dimension 2a agrees very closely even for specimens coated at different spinning speeds and different chemistries (BMPM:DABPA = 1:1, 1:0.82 and 1:1.13, Figures 5 (a) and 5 (b)). Twelve specimens (Appendix D) were used in this study. Of the twelve specimens four were uncoated specimens and eight were coated. All crack field measurements were made using the digital readout attached to the semi-macro indentor. For each load, the crack-region measurements 2a, was an average of readings from 6 to 10 indentations. The 2a, for each indentation was an average of the two diagonals of the Vickers indentation (Figures 4(a) and 4(b)). A total of 514 Vickers indentations were made in this study.

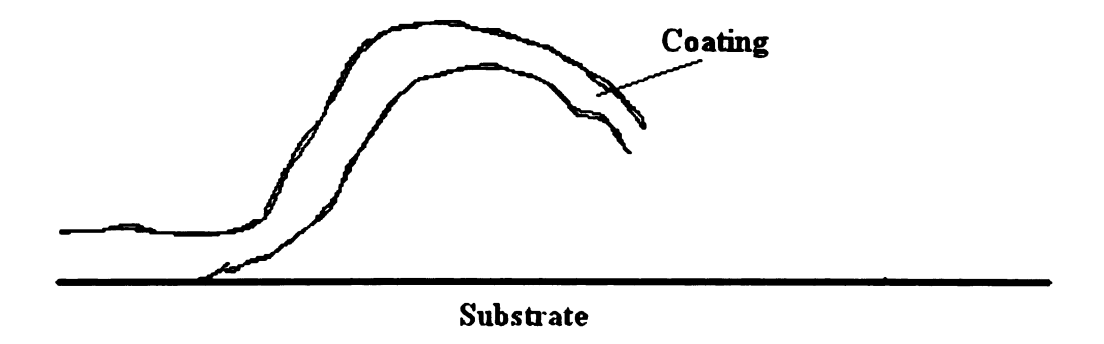


Figure 3 (a). Schematic of delaminated silica coating on BMI substrate

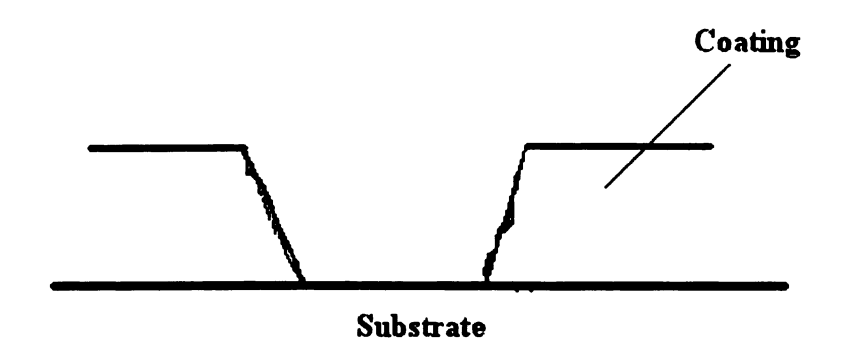


Figure 3 (b). Schematic of a spalled region of the silica coating on a BMI substrate

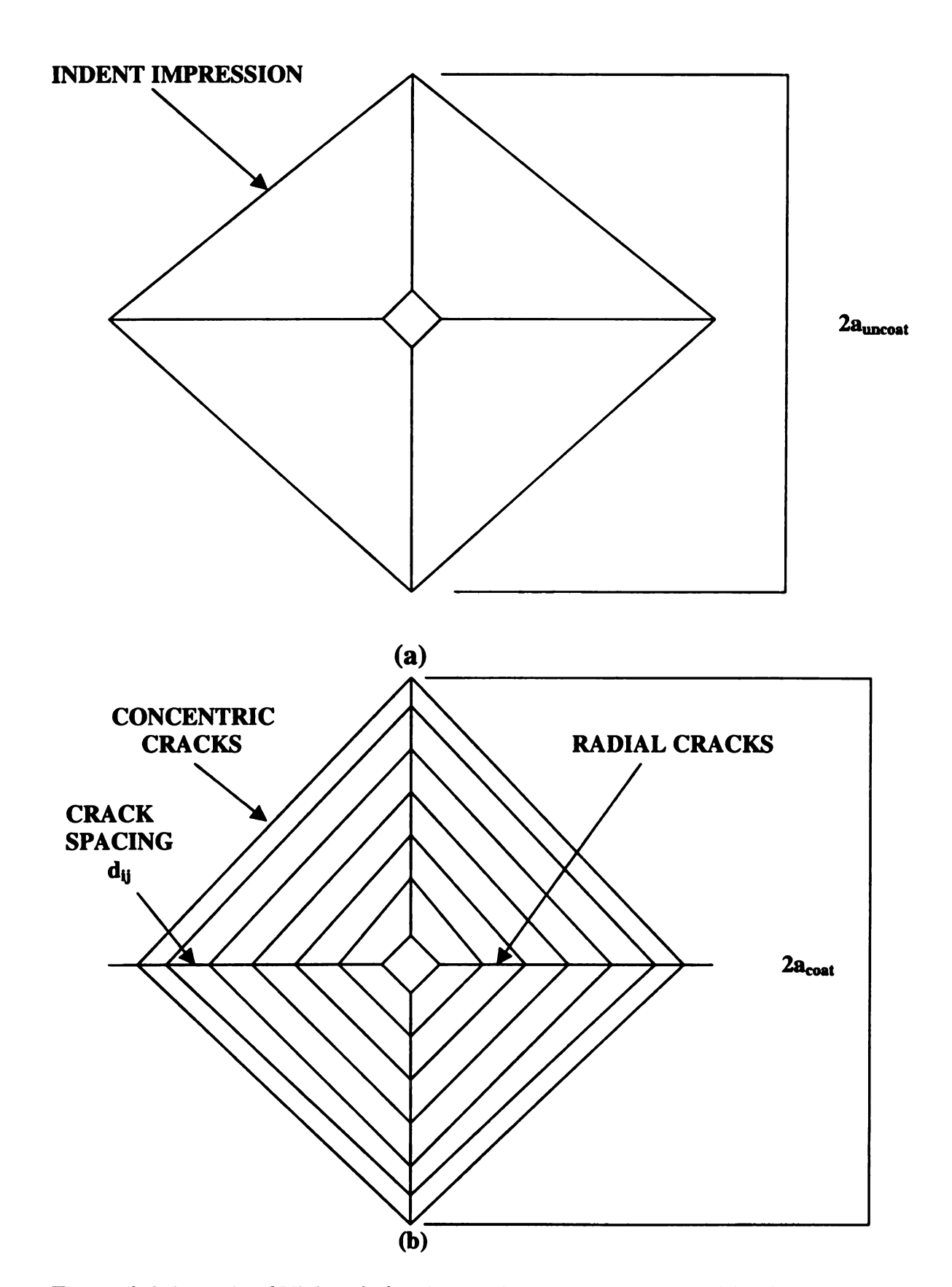


Figure 4. Schematic of Vickers indent impressions on (a) an uncoated BMI specimen and (b) a coated BMI specimen.

Table 3. Average Indentation dimension for specimens A, B, C, D, E, A1, B1, C1, F1, F2, G1, and G2 (Appendix D) raw data for figures 5a and 5b

| (2a ₁) | B (2a ₂) | $C(2a_2)$ | D (2a ₁) | \mathbf{E} (2a ₂) | A1 (2a ₁) | B1 (2a ₂) | $C1 (2a_2)$ | Load (N) A (2a ₁) B (2a ₂) C (2a ₂) D (2a ₁) E (2a ₂) A1 (2a ₁) B1 (2a ₂) C1 (2a ₂) F1 (2a ₁) F2 (2a ₂) G1 | F2 (2a ₂) | | G2 |
|--------------------|----------------------|-----------|----------------------|---------------------------------|-----------------------|-----------------------|-------------|--|-----------------------|------------|-----------|
| - | | | | | | | | | | $(2r_2)^*$ | $(2r_2)!$ |
| | | | | | 20.1 | 20.3 | 1.61 | 1 | | | |
| | | | | | 30.1 | 32.9 | 28.7 | 7 | | | |
| | | | | | 47.7 | 48.8 | 47.2 | 2 | | | |
| | | | | | 71.2 | 70.5 | 8.69 | 8 | | | |
| | | | | | 102.9 | 99.1 | 104 | 4 | | | |
| 134.5 | 122.3 | 132.5 | 123.9 | 132 | 129.1 | 124.3 | 125.5 | 5 130.8 | 120.4 | | |
| 176 | 167.7 | 167.9 | 165.5 | 167.2 | 175.1 | 165.2 | 162.3 | 3 171.6 | 164.6 | | |
| 237.6 | 239.5 | 231.1 | 232.2 | 234.1 | 236.4 | 236.7 | 228.5 | 5 234.9 | 224.8 | | |
| 524.4 | 526.9 | 517.8 | 511.6 | 516.3 | | | | 521.2 | 514.3 | | |
| 745.3 | 749.7 | 744.3 | 721.1 | 728.6 | | | | 725.2 | 725.8 | | |
| 1031.9 | 1043.4 | 1042.3 | 1036.8 | 1042.1 | | | | | | | |
| | | | | | | | | | | 1339.1 | 1312.8 |

All 2a readings are in microns.

2r, is in microns and is diameter of total Rockwell indent, excluding the transition region with incomplete Hertzian cracks

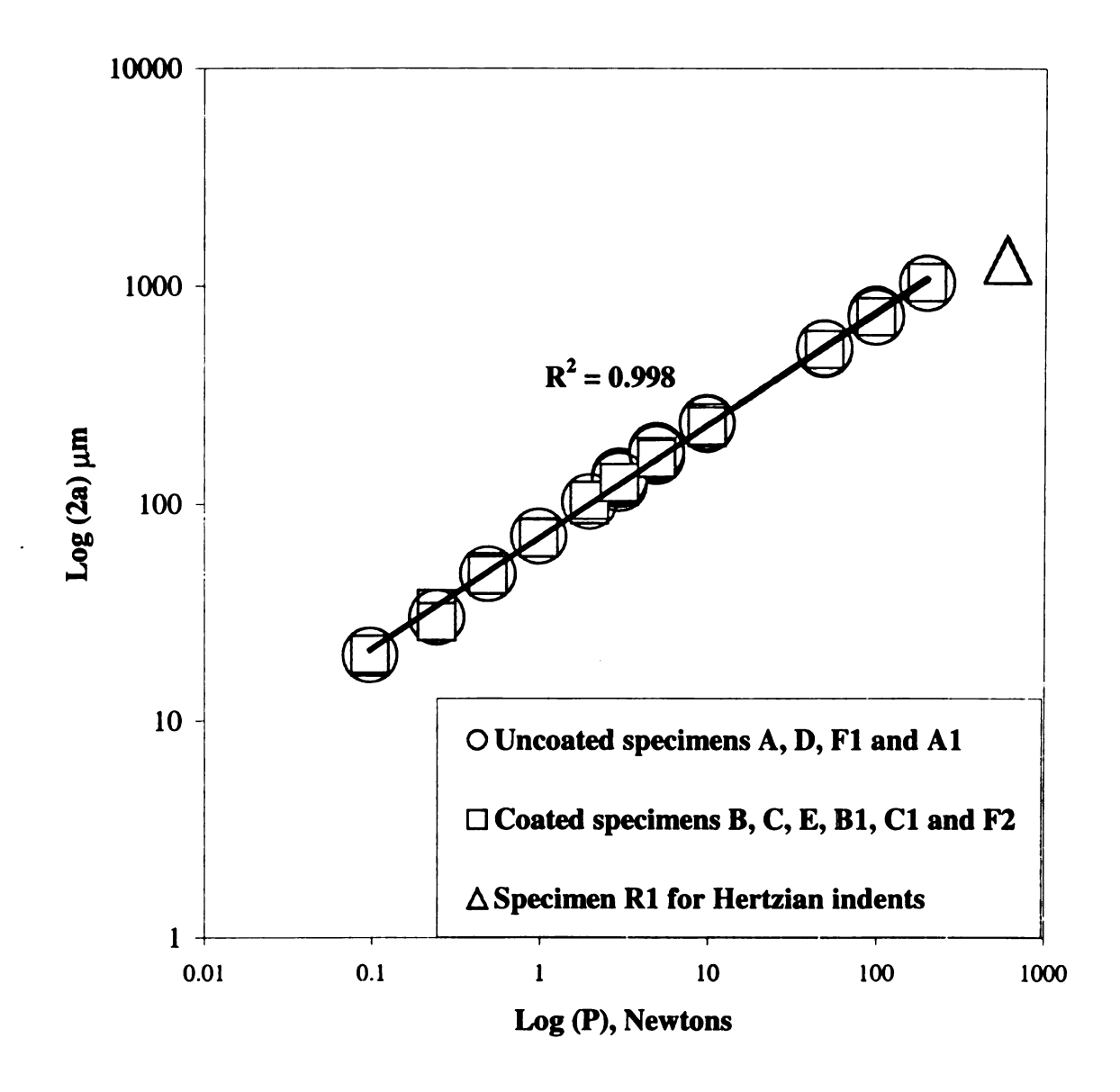


Figure 5a. Logarithmic plot for indentation dimension 2a versus indentation load for uncoated and coated BMI specimens of different chemistries (BMPM:DABPA = 1:1, 1:0.82 and 1:1.13, Appendix D).

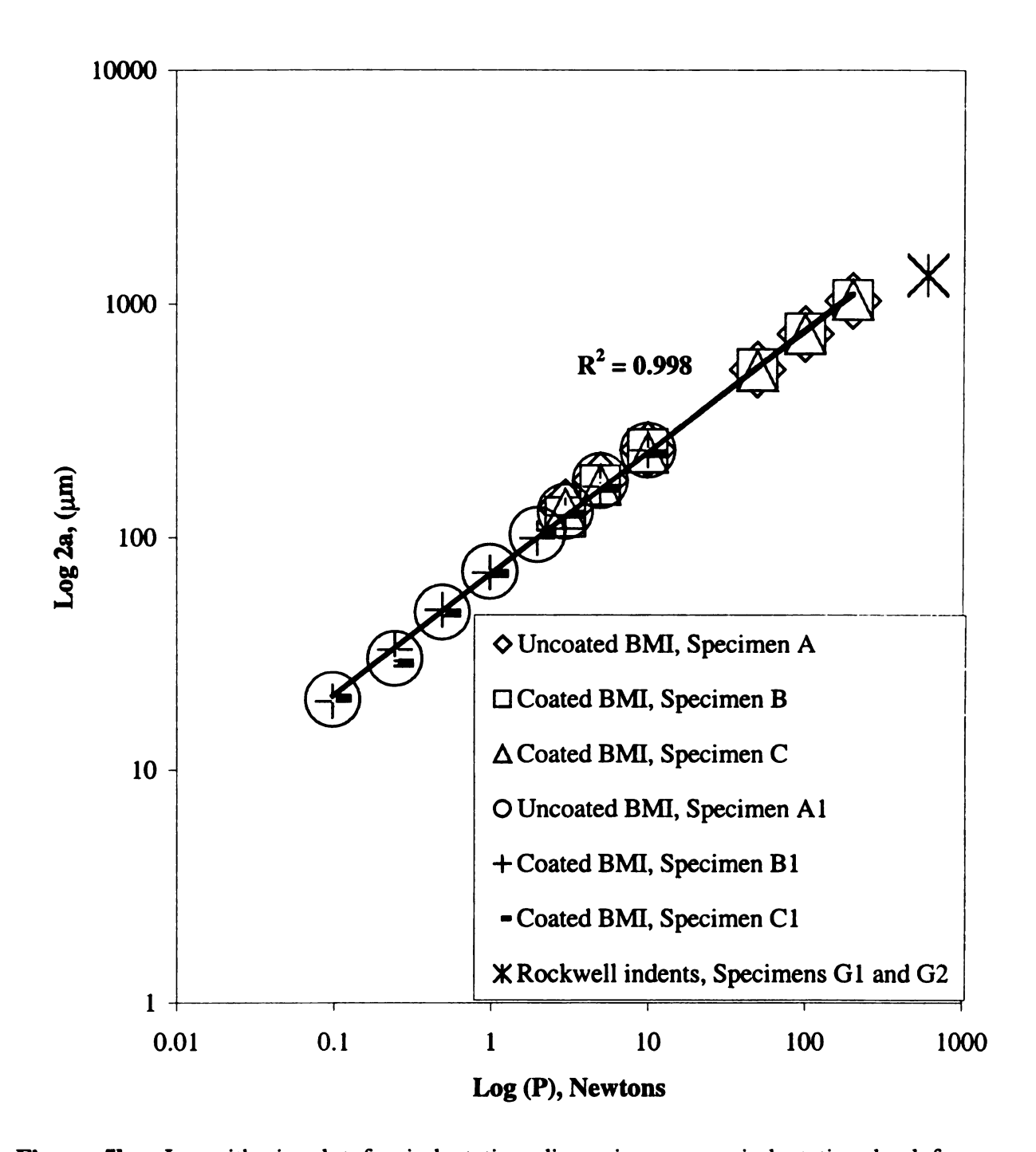


Figure 5b. Logarithmic plot for indentation dimension versus indentation load for coated and uncoated BMI specimens of the same stoichiomery (BMPM:DABPA = 1:1, Appendix D).

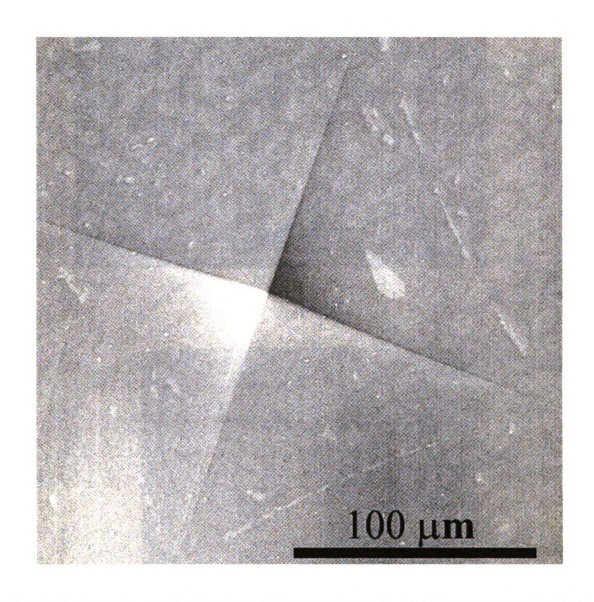
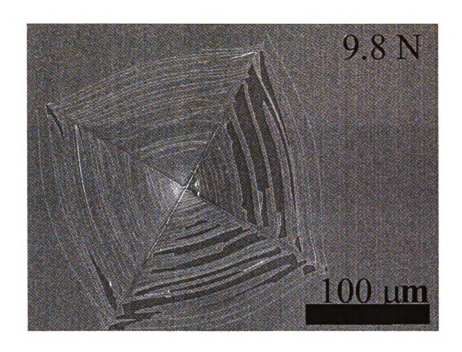


Figure 6. Micrograph of a Vickers indent made at a load of 49 N on an uncoated BMI specimen (BMPM: DABPA = 1:1, Specimen CR1, Appendix G). The BMI was precured at 200° C for 1 hour and again cured at 150° C for 20 minutes.



100 µm

(a)

Figure 7. Micrograph of 9.8 N Vickers indent made on coated BMI specimen where the coating thickness was = 0.15 microns. The specimens were precured at 200° C for 1 hour, coated at 3500 rpm for 20 seconds a) cured at 150° C for 20 minutes (Specimen CR1, Appendix G) and, b) cured at 175° C for one hour (Specimen CR3, Appendix G).

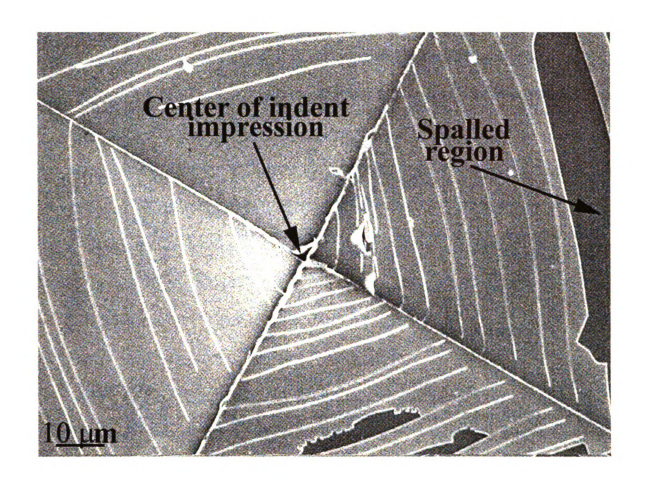


Figure 8. For the same indented specimen as shown in Figure 7a, a higher magnification view of the array of concentric cracks that comprise the indentation crack field. The center of the indent impression and a spalled region of the coating are shown.

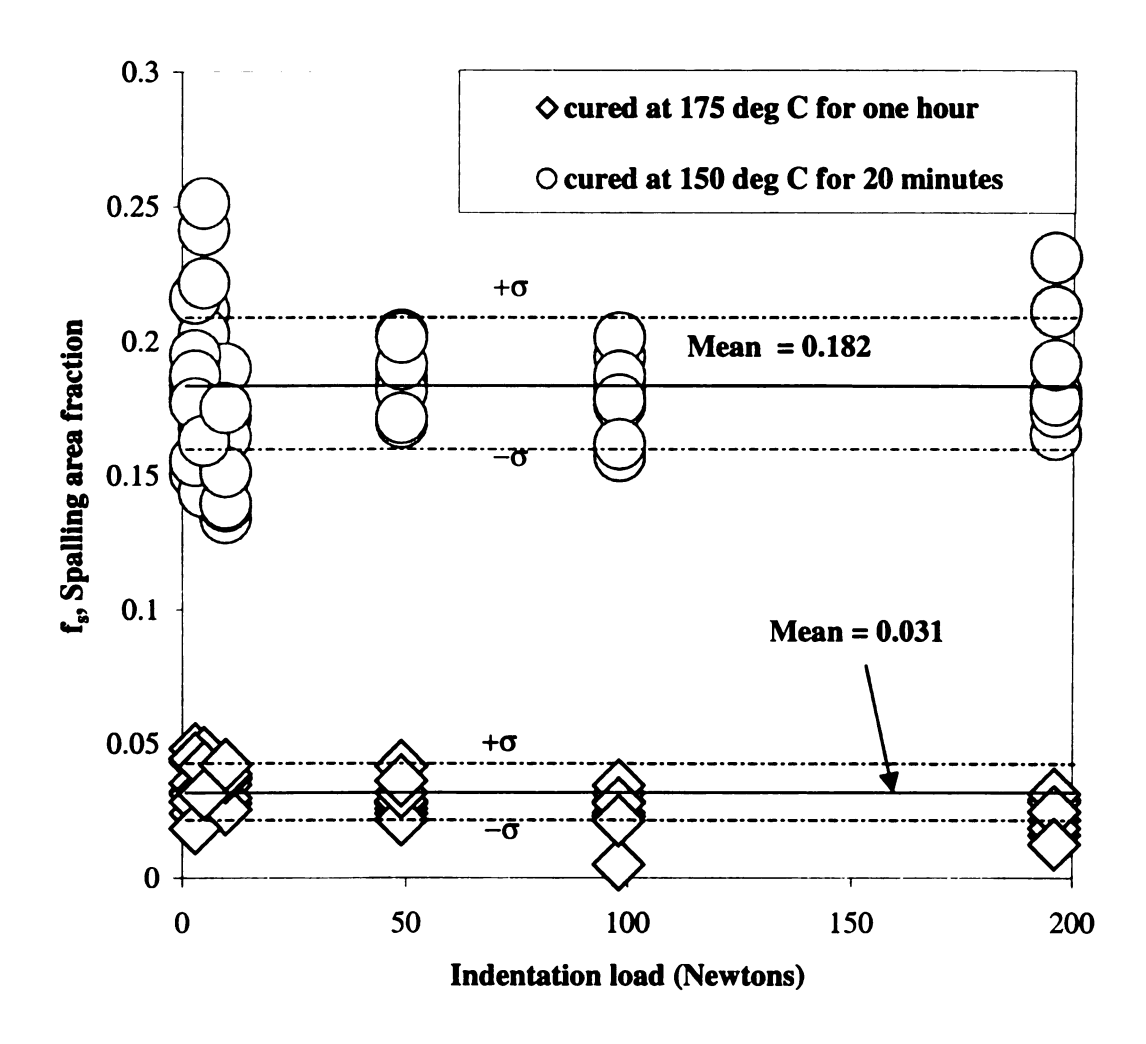


Figure 9. Fraction of silica film spalled off from an indentation as a function of indentation load, for BMI with unabraded silica coatings cured at O - 150° C for 20 minutes, and Δ - 175° C for 1 hour.

Vickers indentation damage of the coated BMI specimens yielded evidence of coating delamination (Figure 10) only in one case. For specimen K1, (Appendix D) two Vickers indentations at loads of 49 N were made so that the center of each indent was 480 microns apart. Some more close sets of indentations were carried out to check for other occurrences of delaminations.

Six additional pairs of closely spaced indentations at 49 N were made on specimens K1 and K2 (Appendix D). In addition to the above pairs of indents, two sets of four closely spaced indents were made at 49 N on specimen K2 (Appendix D), so that the center of the indents were about 400 to 460 microns from each other. In one case two closely spaced indents were made at, 98 N on specimen K2, so that the center of indents were 700 microns apart. In two cases a pair of indents of loads of 9.8 N were made so that the center of indents were 180 microns apart (specimen CR2, Appendix G).

None of the closely spaced indentations, other than the one shown in Figure 10, produced a delamination that could be observed by either optical microscopy or by ESEM observations (Figure 11). However, spallation of the coatings was observed over a small fraction of the indentation-damaged coatings (Figures 3(b), 7 (a), 7 (b) and 8).

The lack of coating delaminations in all but one case, suggests that the delamination produced in that one case (Figure 10), may be due to an interfacial coating defect, near the indentation site. We can also say the film delamination on indentation is not a trend. This observation, is in agreement with the work done by Li et al [26], who observed coating cracking on indenting 0.1 micron thick DLC coatings on a polycarbonate substrate using a diamond like three sided Berkovich indentor. The substrate/coating system that was indented by Li et al [26], was comparable in Young's modulus values for

both the substrate and coating and coating thickness values. Young's moduli of polycarbonate and DLC are 3.3 GPa and 130 GPa respectively [26], as compared to the Young's moduli of BMI and fused silica, which are 3.6 GPa – 4.1 Gpa [15] and 72 Gpa [27] respectively. The silica coating indented by us was 0.15 to 0.3 microns thick compared to the 0.1 micron thick DLC coating indented by Li et al [26]. However indentation loads used in this study ranged from 0.098 to 196 N, compared to the 0.7 N load used by Li et al [26]

3.3.3 Spalling area fraction as a function of curing conditions

Three coated BMI specimens were cured at varying conditions as listed in Appendix G. To quantify the extent of coating spallation as a function of indentation load, the three BMI specimens with coating thicknesses of approximately 0.15 microns, were indented at loads ranging from 2.94 N to 196 N and imaged using scanning electron microscopy. Micrographs were taken at magnifications ranging from 300 X to 720 X. The fractional spalled area were calculated as described in Section 2.3.4

Fractional spalled area, $f_{S,}$, was calculated for nine indents at each load (Figure 9), for the BMI cured at different conditions. For the indents on the BMI cured at 150° C for 20 minutes, $f_{S,}$ varied from 0.14 to 0.25 (Figure 7 (a)). However the indents for the BMI specimen cured at 175° C for one hour had a much reduced $f_{S,}$ ranging from 0.02 to 0.05 (Figure 7 (b)). The indents for the coated BMI cured at 200° C for one hour and 250° C for one hour also had $f_{S,}$ in the range 0.02 to 0.04 However these specimens had a network of cracks.

Thus at curing conditions of 175° C for one hour, the adhesion of the silica coating to the BMI is very good and might be of further interest in fabrication of the film on a larger scale, due to the narrow temperature window which controls the adhesion. The cracking of silica film at the higher curing temperatures ($\geq 200^{\circ}$ C) might have been due to relief of thermal stresses, but should be further investigated.

3.3.4 Indent dimension analysis as a function of load for Vickers indents.

As determined by least-squares fitting, the load, P, versus indentation damage dimension (Figures 5a and 5b) was consistent with the relationship

$$P = 2Ba^{n}$$
 (1)

where the parameter "a" measures the dimension of: (i) half the indent dimension for the uncoated BMI specimens (Figure 4a) or (ii) the crack damage field of concentric diamond-shaped cracks for the silica-coated BMI specimens (Figure 4b). The B value from least squares fitting was 317.48 ± 50.03 MPa, and exponent n was 1.933 MPa ± 0.05 . The form of equation 1 is consistent with the functional form of load-crack length relationships found in the literature for brittle materials [21], i.e.

$$P = 2Ha^2 (2)$$

Thus B corresponds to the hardness values H, which can be approximated to be same for both the coated and uncoated specimens, as the "2a" values for uncoated and coated BMI agreed to within $\pm 2\%$ of each other for the various indentation loads. Thus we can say the Hardness value, is hardness of the BMI substrate itself. This confirms with the fact that the thin silica coatings (0.15 microns to 0.3 microns), did not affect the value of H, measured from Vickers indentations, in the indentation load we considered.

The hardness value obtained from Vickers indentations, are consistent with hardness values in literature for other rigid polymers like epoxy resin, acrylic resin, and a series of aromatic polyesters, ranging from 200 MPa to 400 Mpa [23, 28, 29, 30]. Also the H/E values, where the elastic modulus, E, ranges from 3.6 GPa to 4.1 GPa for BMI is approximately 0.07 and are consistent with H/E ratios found in literature PMMA [28]. The constant slope of the log (2a) versus log (P) plot (Figures 5 (a) and 5 (b)), implies that hardness of BMI is independent of the indentation load. This is consistent with data from the literature for other rigid polymers, where the hardness of PMMA, high density polyethylene, an epoxy resin and an acrylic resin is load independent at higher Vickers indentation loads [23, 31, 32].

To understand the array of diamond-shaped cracks, one can think of an analogy to loading a membrane with a circular punch. Such loading will result in a conical depression of circular cross section. For the BMI, which has a relatively low elastic modulus, the subsidence of the surface local to the indentor (for the case of a Vickers indentation crack) may roughly correspond to a cone of pyramidal cross section. Thus the regions of the coating that are significantly deflected undergo cracking.

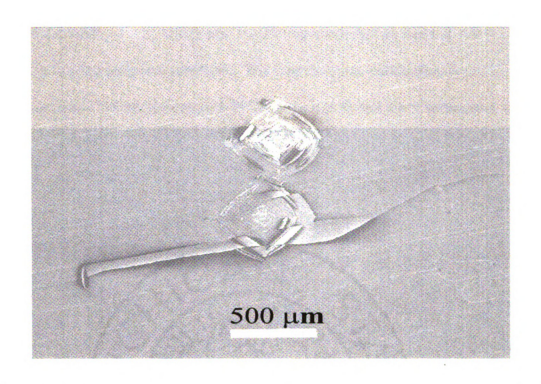


Figure 10. Micrograph showing a coating delamination and crack associated with a pair of closely spaced 49 N Vickers indentations on a coated BMI specimen (BMPM:DABPA = 1:1, Specimen K2, Appendix D) This is the only example of a coating delamination that was observed in this study.

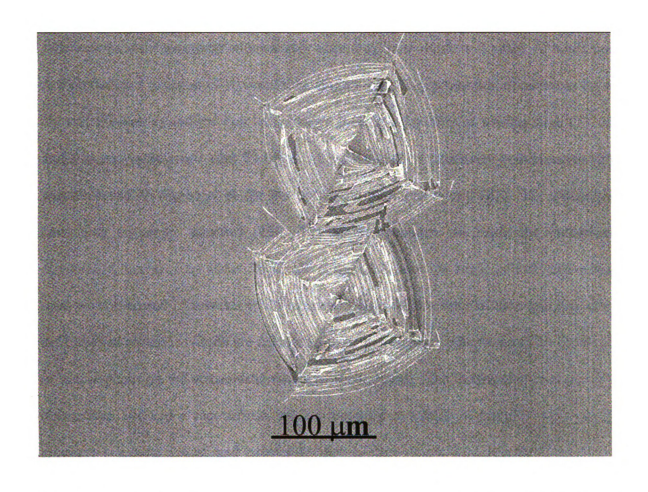


Figure 11. Micrograph showing a pair of closely spaced 9.8 N Vickers indentations on a coated BMI specimen (BMPM:DABPA = 1:1, Specimen CR2, Appendix G).

3.3.5 Vickers Indentation dimension as a function of loading rate and load time

Three uncoated BMI specimens (Appendix F) of different stoichiometries (BMPM:DABPA = 1:1, 1:0.82 and 1:1.13) were indented at loads of 4.9 N and 49 N at varying loading rates and load times. The load time was varied from 5 to 35 seconds at a loading rate of 50 microns/second for both the 4.9 N and 49 N indentation loads. The indentations were measured immediately after they were made and again 72 hours later and plotted as a function of the load time (Figure 12). The indentation dimensions for all the stoichiometries and the two loads varied little as a function of loading time [23, 32] and also recovered much after 72 hours. A similar lack of sensitivity to indentation time was observed by Paglia et al for the polymeric materials epoxy (KIT 36) and acrylic (moulding transoptic powder) [23]. For the indentations we made the indentation dimensions increased by about 3% to 5% (Figure 12) over the range of indentation load time we considered (5 seconds to 35 seconds). Thus BMI's viscoelasticy will not affect the hardness readings, which are calculated from the Vickers indent dimension 2a, which in turn depends on the viscoelastic nature of the material. The indentations measured 72 hours later, showed a recovery in crack dimension of 0.01% to 0.05%. Thus elastic recovery is almost absent, and indentation dimension changes very little as a function of elapsed time since indentation.

The three BMI specimens used for the varying load times experiment were also used to study the dependence of indentation dimension on loading rates at loads of 4.9 N and 49 N at a load time of 10 seconds. The indent dimensions 2a varied 0.5 % to 1% on varying loading rates from 40 microns/second to 200 microns/second (Figure 13).

Thus varying load rates and indentation load times would have given us, very similar hardness values. Also indentations measured after a certain time would give us similar hardness values.

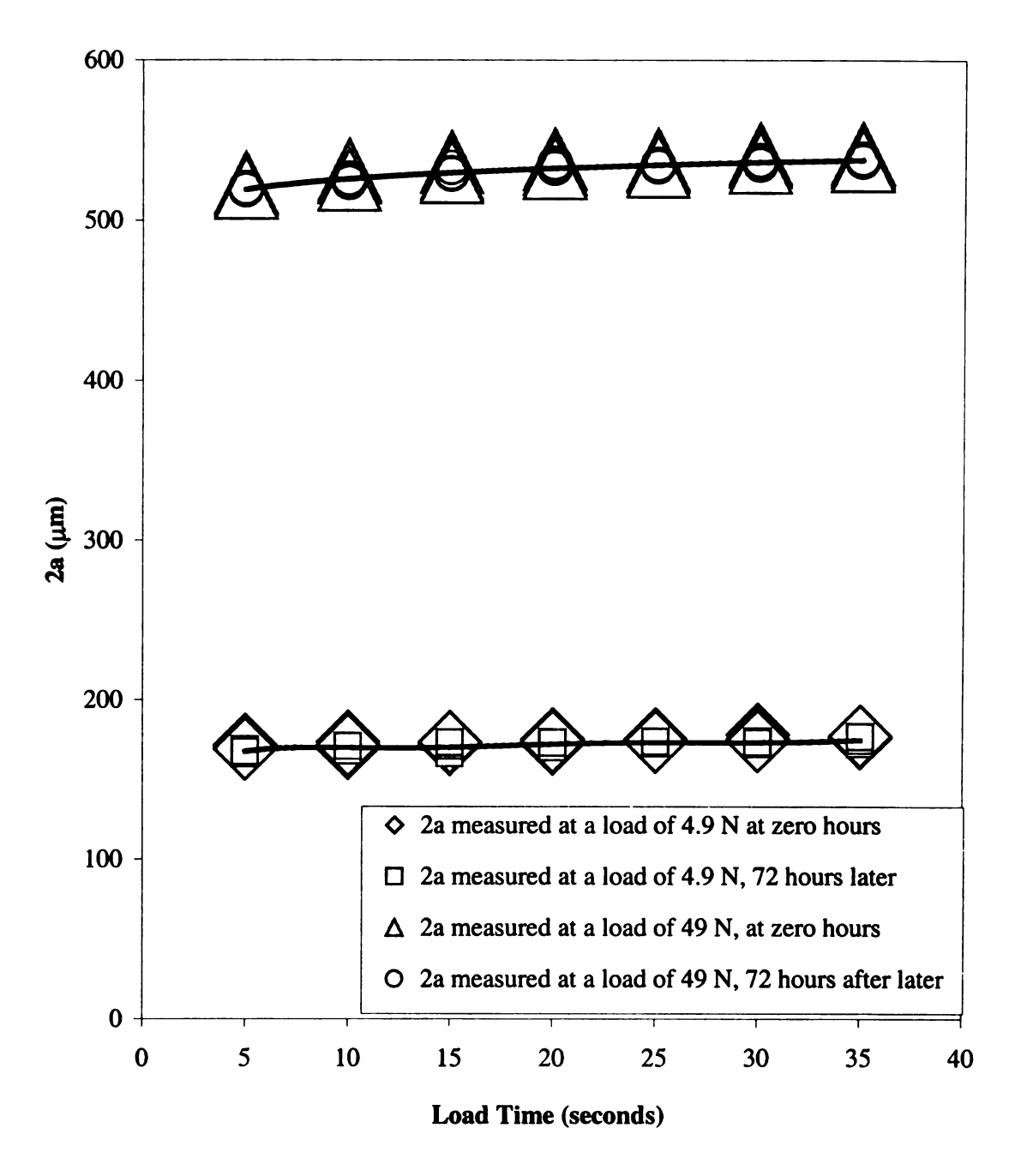


Figure 12. Indentation dimension plotted as a function of indentation load time at a loading rate of 50 microns/second, at loads of 4.9 N and 49 N for uncoated BMI specimens of three different chemistries (L1, L2 and L3, Appendix F).

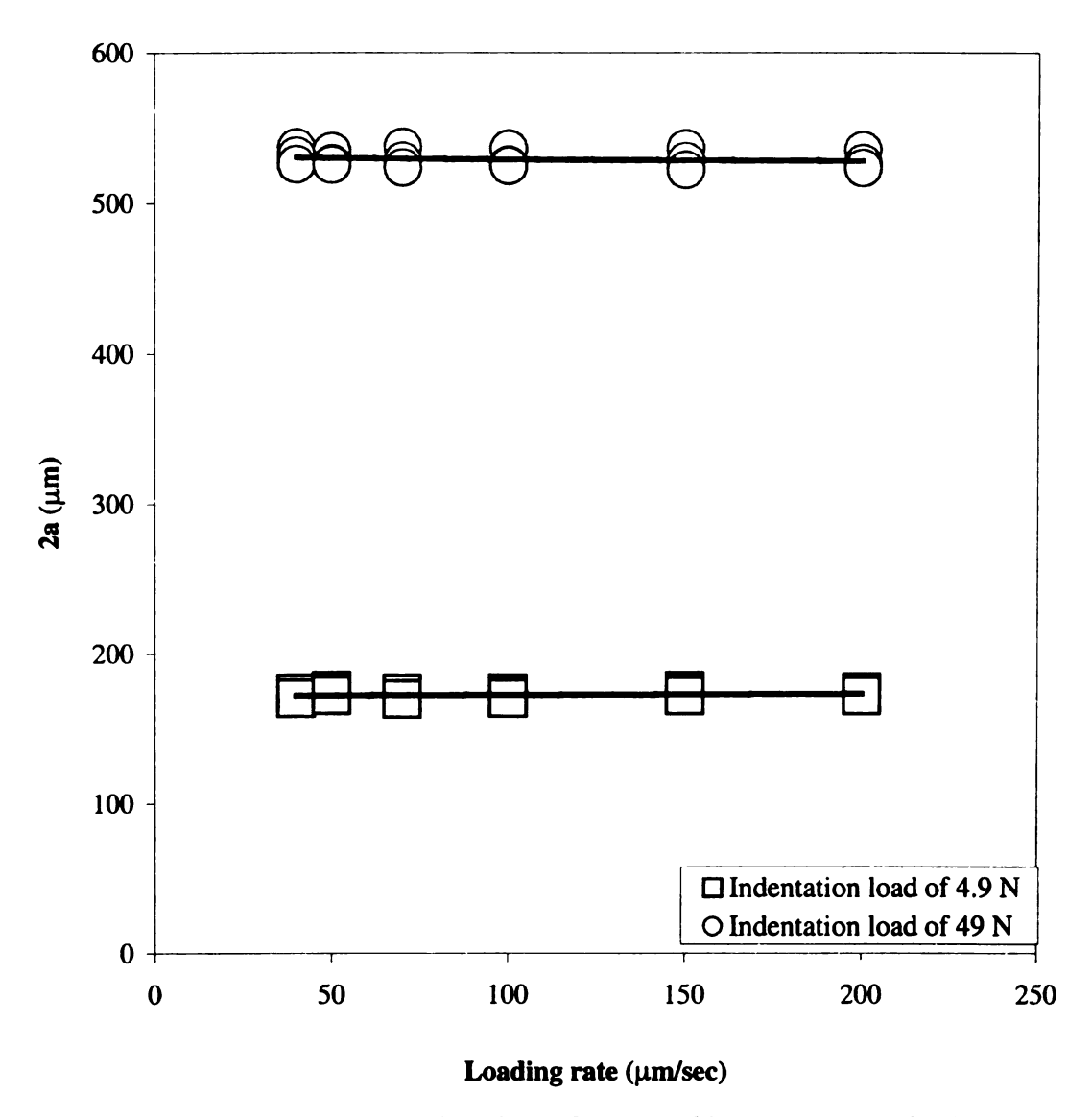


Figure 13. Indentation dimension plotted as a function of loading rate at a load time of 10 seconds at loads of 4.9 N and 49 N, for uncoated BMI specimens of three different chemistires (L1, L2 and L3, Appendix F).

3.4 Rockwell Indentation damage

Two coated BMI specimens (Appendix E) were indented using the Rockwell Hardness Tester, on the Rockwell-f Scale (Load 588 N). Rockwell indentation on the silica coated BMI produced cracks in the silica coating in a pattern of concentric circular shaped cracks (Figures 14 and 15), centered on the indent impression. Radial cracks originated from the edge of the indent (Figure 17) and were 450 to 850 microns long. There was a transition region between the edge of the indent and the beginning of the radial cracks (Figures 15 and 16) which comprised of incomplete Hertzian cracks. The transition region measured from 75 to 85 microns. For five Hertzian indents 0.06 to 0.08 of the total indent area was spalled off.

The fraction spalled off f_S was calculated using a grid point method. Eight micrographs were required to cover the Hertzian indent at a magnification of 600 X. Grids were drawn on the eight micrographs and the fractional spallation area, f_S , was calculated from f_S = number of grid points intersecting the spalled area/total number of grid points intersecting the circular crack zone. The diameter of the circular indent region was approximately 1340 microns (this measurement excludes the transition region and the outgoing radial cracks).

The total indentation dimension (1340 microns) for the hertzian indent when plotted on Figures 5 (a) and 5 (b), was 30% lesser than that the indentation dimension at 588 N from extrapolating the least squares fit for the Vickers indents data. From this we can conclude that the load dominates the indentation damage, with very little dependence on the shape and material of the diameter.

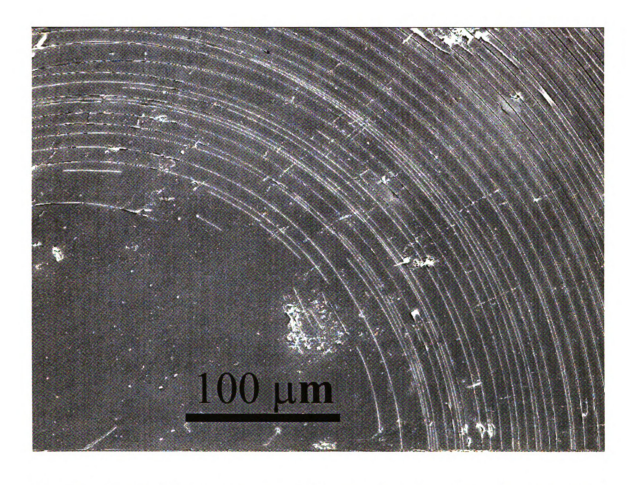


Figure 14. Rockwell indentation on the HRF scale depicting concentric circular crack pattern on a silica coated BMI specimen (R1, Appendix E).

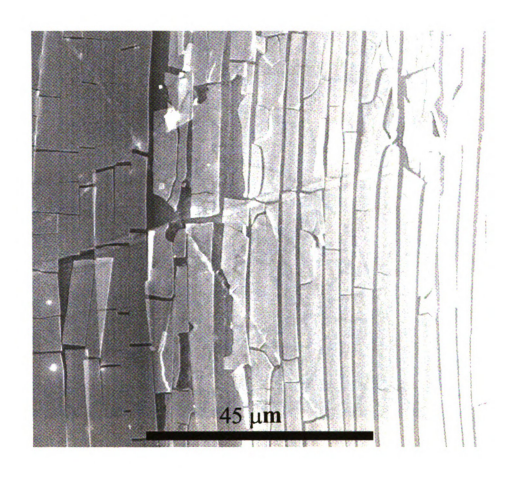


Figure 15. Micrograph depicting the transition region from complete Hertzian cracks to incomplete hertzian cracks, in the same indent as Figure 14.



Figure 16. Micrograph depicts the incomplete Hertzian cracks at a higher magnification for the same indent as Figure 14.



Figure 17. Micrograph depicting the radial cracks originating from the end of the region that included the incomplete Hertzian cracks on the same indent as Figure 14.

3.5 ESEM observations and statistical analysis of crack pattern

3.5.1 Mean crack spacing as a function of indentation load

Seven specimens (Appendix C) were indented at loads ranging from 2.94 N to 196 N, using the semi macro Vickers indentor. Hertzian indents were made using the Rockwell Hardness Tester on the F-scale. Crack spacings d_{ij} (distance along the radius between one crack and the adjacent crack, (Figure 4 (b)) were measured (Section 2.6). For each of the eighty-four Vickers indents (six at each indentation load) and for the six Rockwell indents made on the F-scale, crack spacing values were plotted as a function of the radial position from the center of the indent.

The mean crack spacings μ were calculated for each indent by using the following equation

$$\mu = \frac{\sum_{i=1, j=2}^{i=N-1, J=N} d_{ij}}{N}$$
(3)

where

N = the total number of cracks for an indent in between the center of the indent dimension and the end of the indent dimension.

The average of six mean crack spacing values, MS were calculated for each indentation load (Table 4).

The ratio of mean crack spacings at two different loads can be calculated by

$$MSF = \frac{MS_x}{MS_y} \tag{4}$$

Where

MSF = Ratio in average of six mean crack spacing values of indents made at load ofx Newtons to an average of six mean crack spacing values of indents made at a load of y Newtons.

 MS_x = Average of six mean crack spacing values for x Newton load indents on a coated BMI specimen

 MS_y = Average of six mean crack spacing values for y Newton load indents on a coated BMI specimen.

Table 4. Average of mean crack spacings for six indentations at each indentation load for the specimens listed in Appendix C.

| Specimen | MS _{2.94} | MS4.9 | MS _{9.8} | MS49 | MS98 | MS ₁₉₆ | MS _{Rock} |
|----------|--------------------|---------------|-------------------|---------------|---------------|-------------------|--------------------|
| | (μ m) | (μ m) | (μ m) | (μ m) | (μ m) | (μ m) | (μ m) |
| SUA1 | | 4.7 | 4.8 | 4.6 | 4.6 | | |
| SUA2 | | | 4.7 | 4.7 | | | 1 |
| SUA3 | | | | | | | 4.6 |
| SUA4 | 4.7 | | - | 5.0 | | 4.7 | |
| SA1 | | | 4.4 | 4.5 | | | |
| SA2 | | | 4.4 | 4.3 | | | |
| CR1 | 4.9 | 5.3 | 6.0 | 6.3 | 6.7 | 7.2 | |

For the specimens SUA1 and SUA2 with unabraded coatings cured at 150° C for 20 minutes (Appendix C) crack spacings were plotted as a function of the radial position from the center of the indent for Vickers indents made at loads of 2.94 N (Figure 20), 4.9 N (Figure 21), 9.8 N (Figure 22), 49 N (Figure 23), 98 N (Figure 24) and 196 N (Figure 25). Thirty-six such indents were made, six each for each of the six loads. The mean crack spacings, μ , for six indents at each of the loads were calculated and averages MS taken for the six readings (Table 4). The mean crack spacing varied from 4.3 microns to 5.0 microns for the BMI specimens with unabraded coatings (Tables 4 and 6, Figure 18) for the various indentation loads. The MSF values for the specimens with unabraded coatings ranged from 0.98 to 1.01 (Table 7).

Similarly for the BMI specimens SA1 and SA2 (Appendix C), with coatings cured at 150° C for 20 minutes and then abraded using the 0.03 μ m alumina polishing cloth (Section 2.7), six indentations each at 9.8 N and 49 N (Table 4) were made. The mean crack spacings were calculated for each of the indentations and the averages MS for the mean crack spacings calculated at each indentation load. The averages MS of the mean crack spacing μ for various indentation loads varied in between 4.3 microns and 4.7 microns (Table 4). The MSF value for the BMI specimen with abraded coatings was 0.97 (Table 7).

From the MSF values for both the abraded and unabraded coated BMI specimens $(MSF_{Minimum} = 0.97, MSF_{Maximum} = 1.01)$, we can say that, the average of mean crack spacings varied only by \pm 3% for the range of loads at which mean crack spacings were measured (2.94 N to 196 N, change in load factor of 66.67). Thus we can say that the mean crack spacing is a very weak function of indentation load.

To further investigate the nature of crack spacings, six Rockwell indents on specimen SUA3 (Appendix C, Table 4). Crack spacings were plotted as a function of the radial position from the center of the indent (Figure 34). The average MS_{Rock} of six mean crack spacing values for the Rockwell-f scale indent was 4.6 μ m (Table 4). The Rockwell indents were not performed on the same specimen as the Vickers was.

MSF values were calculated by comparing the average of the mean crack spacing for the Rockwell indent to the average of the mean crack spacings for various Vickers indentation loads varied from 0.98 to 1.01 (Table 7). Thus we can say that the average mean crack spacing values for the Vickers indents are within \pm 2% to the mean crack spacing values for the Rockwell-f scale indent. Thus even after increasing indentation loads by a factor of 200 (2.94 N to 588 N) the average of mean crack spacing values changed only by \pm 2%. Thus the mean crack spacing value is a very weak function of indentation load. Changing the indenter material (diamond to steel) and shape (diamond pyramid to spherical) varied average of the mean crack spacings by \pm 2%. This observation confirms with the fact that the mean crack spacing is a weak function of the indentor material and shape.

For the coated BMI with unabraded coatings cured at 175°C for one hour (CR1, Appendix C), the crack spacings, d_{ij}, were plotted as a function of radial position from the center of the indent for indentation loads of 2.94 N to 196 N (Figures 28, 29, 30, 31, 32 and 33). However for the coated BMI cured at 175°C for one hour the mean crack spacings showed a clear dependence on indentation load as compared to the BMI specimens with unabraded coatings cured at 150°C for twenty minutes. The average of

2.5

pl

the mean crack spacings increased with increase in indentation loads from 4.9 microns at 2.94 N, to 7.2 microns at 196 N (an increase of 47%, Table 6, Figure 18).

The mean crack spacings normalized by half the total indent dimension "a" plotted as a function of the indentation load for the BMI specimens with unabraded coatings cured at 150°C for twenty minutes and 175°C for one hour (Figure 19) using the log-log scale on least squares fitting gives R² values of 0.997 and 0.996 respectively. From this we can say that the mean crack spacings normalized by the half the total indent dimension "a", is consistent with the power law relationship

$$\mu / a = \varphi P^{\varepsilon} \tag{5}$$

where

 φ = pre-exponential factor

 $\varepsilon = exponent$

From the standard error of estimates of φ (0.006 and 0.005) for the two curing conditions $150^{\circ}\text{C}/20$ minutes and $175^{\circ}\text{C}/1$ hour listed in Table 5, we can say that the φ values can be considered similar, as the s.e.e. values (0.005 and 0.006) are greater than the difference in φ values for the two different curing conditions (0.1230-0.1224 = 0.0006 = s.e.e (φ)/10). Similarly for the two curing conditions $150^{\circ}\text{C}/20$ minutes and $175^{\circ}\text{C}/1$ hour, we can say that the ε values can be considered different, as the s.e.e. values (0.0253 and 0.023) are less than the difference in ε values for the two different curing conditions (-0.4153 + 0.4981 = 0.0828 = 4 × s.e.e. (ε)). Thus the ε values might be influenced by the two different curing temperatures but must be further explored.

Table 5. The pre-exponent φ and exponent ϵ obtained from least squares fitting of of

figure 19 using equation 5.

| Specimen curing conditions | φ ± s.e.e. * | ε ± s.e.e. ** |
|----------------------------|--------------------|----------------------|
| 150°C/20 minutes | 0.1224 ± 0.006 | -0.4981 ± 0.0253 |
| 175 ⁰ C/1 hour | 0.1230 ± 0.005 | -0.4153 ± 0.0230 |

*
$$\varphi$$
 (175/1) - φ (150/20) = 0.1230-0.1224 = 0.0006 < s.e.e. (φ)

**
$$\epsilon$$
 (175/1) – ϵ (150.20) = –0.4153 + 0.4981 = 0.0828 > s.e.e (ϵ)

The number of cracks/unit length were calculated (Table 8), and varied from $0.20~\mu m^{-1}$ to $0.22~\mu m^{-1}$ for the BMI with unabraded and abraded coatings cured at 150^{0} C for 20 minutes. However the number of cracks/unit length for the BMI with unabraded coatings cured at 175^{0} C for one hour decreased with increase in indentation load, from $0.21~\mu m^{-1}$ to $0.14~\mu m^{-1}$ (Table 8) as the indentation load went up from 2.94~N to 196~N respectively.

Table 6. Mean crack spacing data for various indentation loads for BMI specimens with unabraded coatings cured at 150°C at 20 minutes and cured at 175°C at 60 minutes.

| Indentation Load (N) | CR1, μ (μm) | SUA1, μ (μm) |
|----------------------|-------------|--------------|
| 2.94 | | 4.9 |
| 4.9 | 5.4 | 4.3 |
| 9.8 | 6.0 | 4.3 |
| 49 | 6.3 | 5 |
| 98 | 6.6 | 4.8 |
| 196 | 7.2 | 4.7 |
| 2.94 | 4.9 | 5 |
| 4.9 | 5.3 | 4.5 |
| 9.8 | 5.9 | 4.4 |
| 49 | 6.5 | 4.9 |
| 98 | 6.7 | 4.3 |
| 196 | 7.3 | 4.4 |
| 2.94 | 4.9 | 4.6 |
| 4.9 | 5.2 | 4.7 |
| 9.8 | 6.1 | 4.6 |
| 49 | 6.4 | 4.9 |
| 98 | 6.6 | 4.6 |
| 196 | 7.1 | 4.7 |
| 2.94 | 4.9 | 4.9 |
| 4.9 | 5.3 | 4.8 |
| 9.8 | 6.0 | 4.7 |
| 49 | 6.3 | 4.7 |
| 98 | 6.8 | 4.6 |
| 196 | 7.1 | 4.5 |
| 2.94 | 5.1 | 4.7 |
| 4.9 | 5.5 | 4.5 |
| 9.8 | 6.1 | 4.9 |
| 49 | 6.3 | 4.4 |
| 98 | 6.8 | 4.5 |
| 196 | 7.3 | 4.7 |
| 2.94 | 4.8 | 4.4 |
| 4.9 | 5.3 | 4.8 |
| 9.8 | 5.9 | 4.5 |
| 49 | 6.3 | 4.2 |
| 98 | 6.5 | 4.8 |
| 196 | 7.2 | 4.5 |

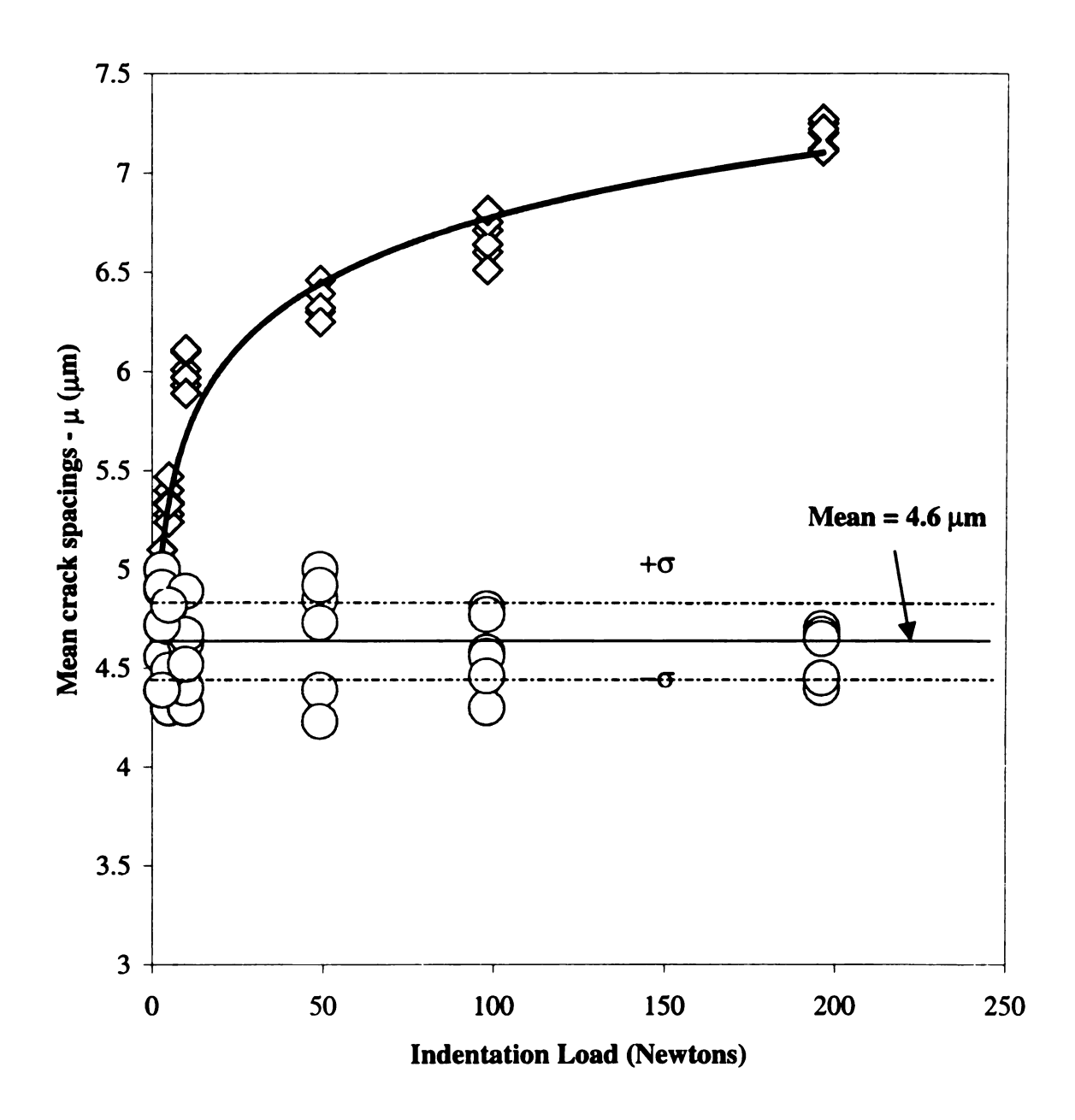


Fig 18. Mean crack spacing data plotted versus various indentation loads for BMI specimens with unabraded coatings cured at 150°C at 20 minutes and cured at 175°C at 60 minutes.

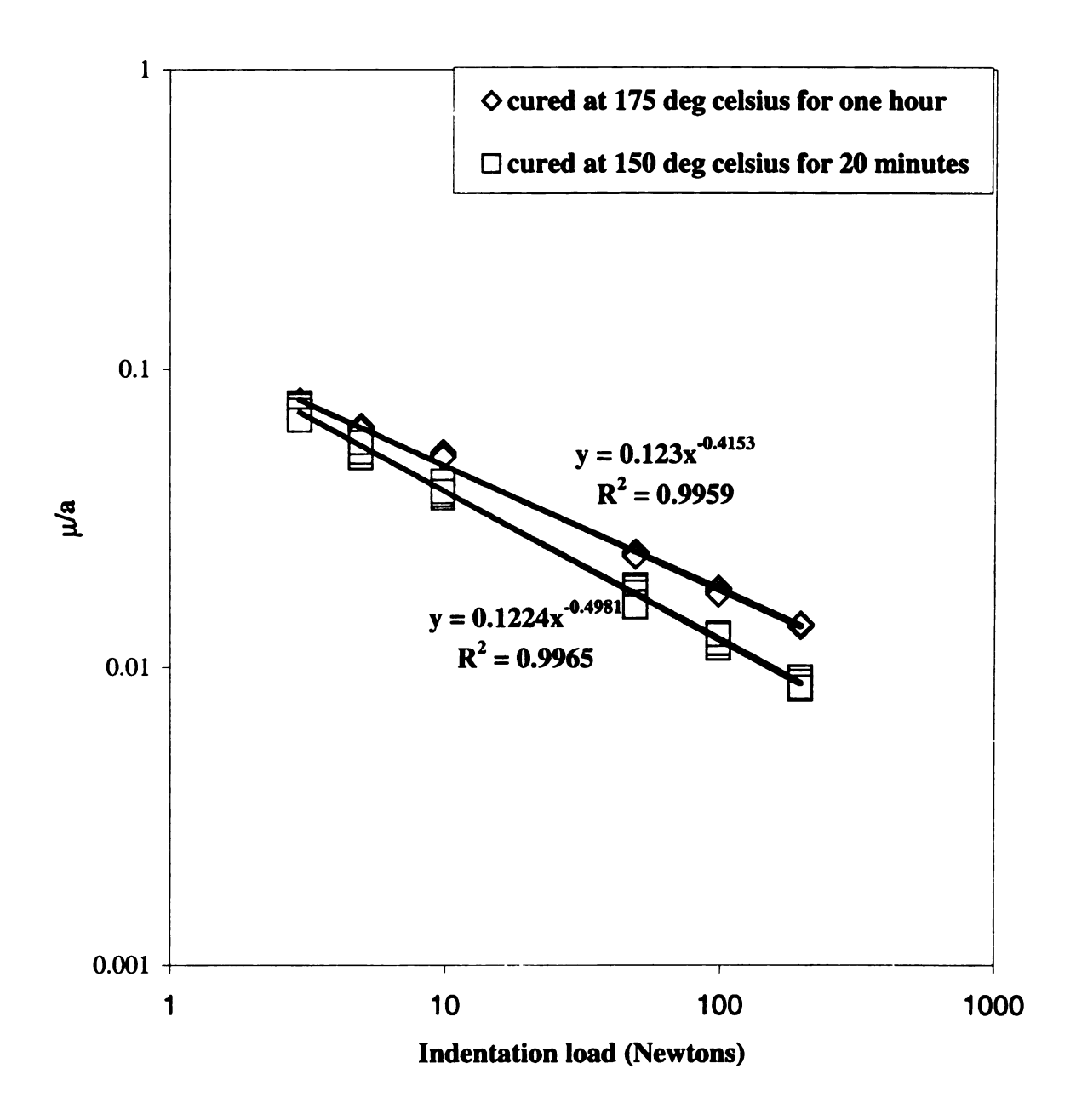


Figure 19. Logarithmic plot of mean crack spacing data versus various indentation loads for BMI specimens with unabraded coatings cured at 150°C at 20 minutes and cured at 175°C at 60 minutes.

Table 7. MSF♠ values (equation 4) for BMI with unabraded and abraded coatings cured at 150°C for 20 minutes and BMI with unabraded coatings cured at 175°C for 20 minutes.

| MSF 4 | SUA* | SA** | CR∀ |
|--------------------------|------|------|------|
| MSF _{4.9/2.94} | 0.98 | | 1.08 |
| MSF _{9.8/2.94} | 1.01 | | 1.22 |
| MSF 49/2.94 | 0.99 | | 1.29 |
| MSF _{98/2.94} | 0.98 | | 1.37 |
| MSF _{196/2.94} | 1.01 | | 1.47 |
| MSF _{49/9.8} | 0.98 | 0.97 | |
| MSF _{Rock/2.94} | 0.98 | | |
| MSF _{Rock/4.9} | 0.98 | | |
| MSF _{Rock/9.8} | 0.97 | | |
| MSF _{Rock/49} | 0.99 | | |
| MSF _{Rock/98} | 1.01 | | |
| MSF _{Rock/196} | 0.99 | | |

[♠] MS values used to calculate MSF are an average of 6 readings for each indentation load.

^{*} MSF values for BMI with unabraded silica coatings cured at 150°C for 20 minutes.

^{**} MSF values for BMI with abraded silica coatings cured at 150°C for 20 minutes. ∀MSF values for BMI with unabraded silica coatings cured at 175°C for one hour.

Table 8. Number of concentric cracks/unit length as a function of indentation load for BMI with unabraded and abraded silica coatings, cured at 150°C for 20 minutes and for unabraded silica coatings cured at 175°C for 1 hour.

| Indentation load | NSUA* | NSA** | NCR∀ |
|------------------|-----------------------------|--------------------|-----------------------------|
| (Newtons) | (μ m) ⁻¹ | (μm) ⁻¹ | (μ m) ⁻¹ |
| 2.94 | 0.21 | | 0.21 |
| 4.9 | 0.22 | | 0.19 |
| 9.8 | 0.22 | 0.22 | 0.17 |
| 49 | 0.21 | 0.22 | 0.16 |
| 98 | 0.22 | | 0.15 |
| 196 | 0.21 | | 0.14 |

^{*} Number of concentric cracks/unit length for BMI with unabraded silica coatings cured at 150°C for 20 minutes.

^{**} Number of concentric cracks/unit length for BMI with abraded silica coatings cured at at 150°C for 20 minutes.

[∀] Number of concentric cracks/unit length for BMI with unabraded silica coatings cured at 175°C for one hour.

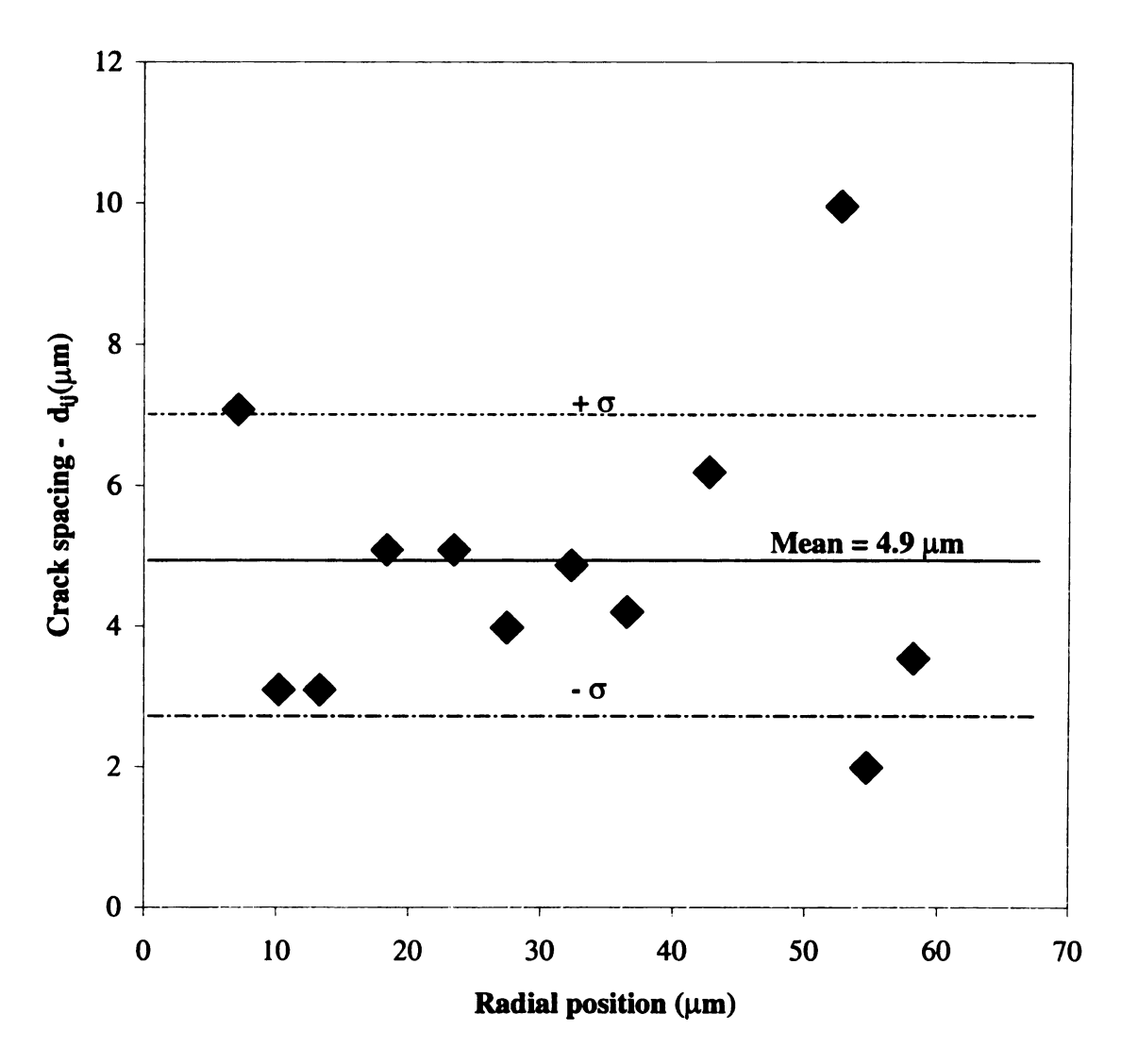


Figure 20. Crack spacing data d_{ij} , for a Vickers indent made at a load of 2.94 N, on specimen SUA1 (Appendix C), plotted against the radial position from the center of the indent.

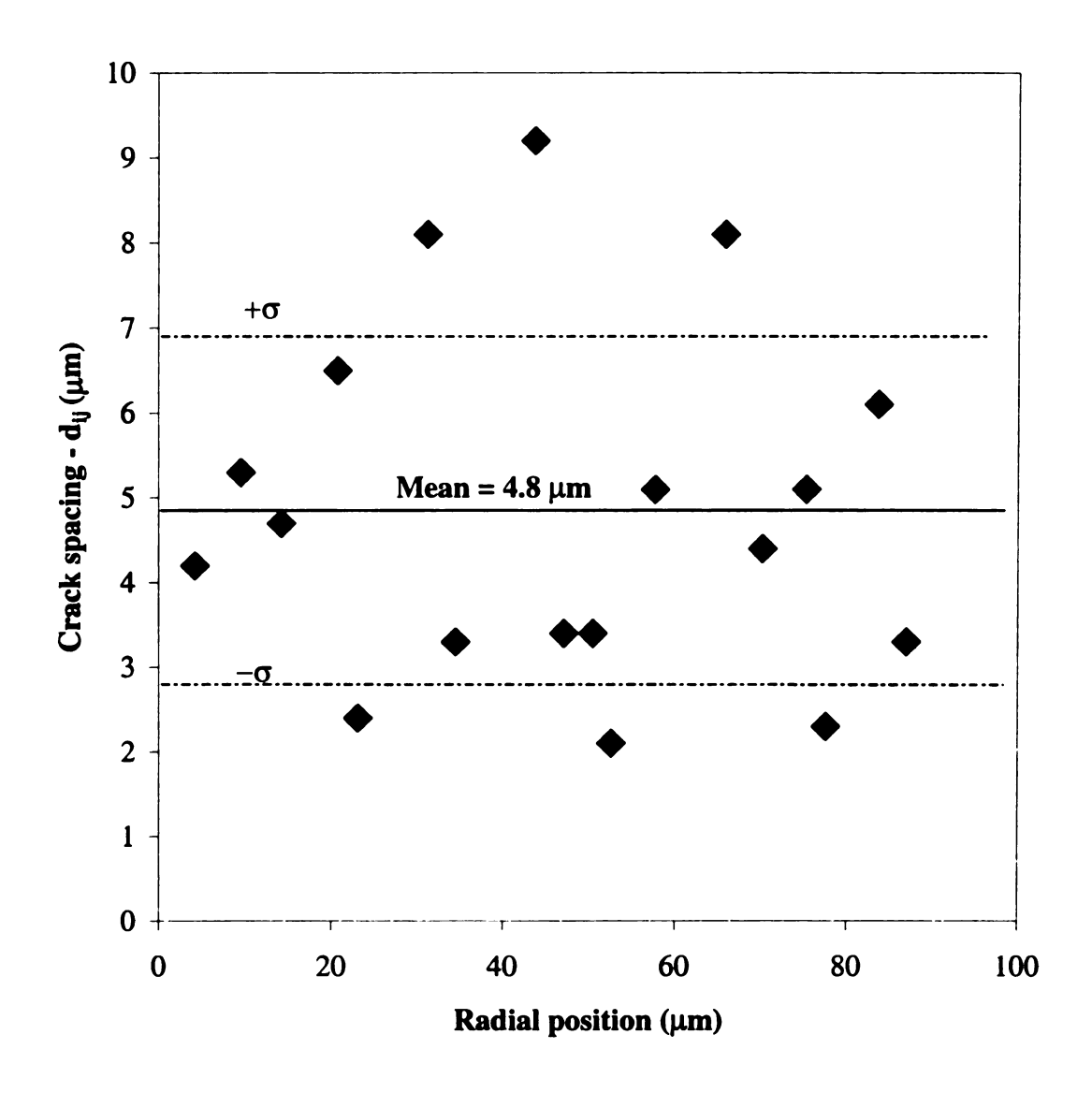


Figure 21. Crack spacing data d_{ij} , for a Vickers indent made at a load of 4.9 N, on specimen SUA1 (Appendix C), plotted against the radial position from the center of the indent.

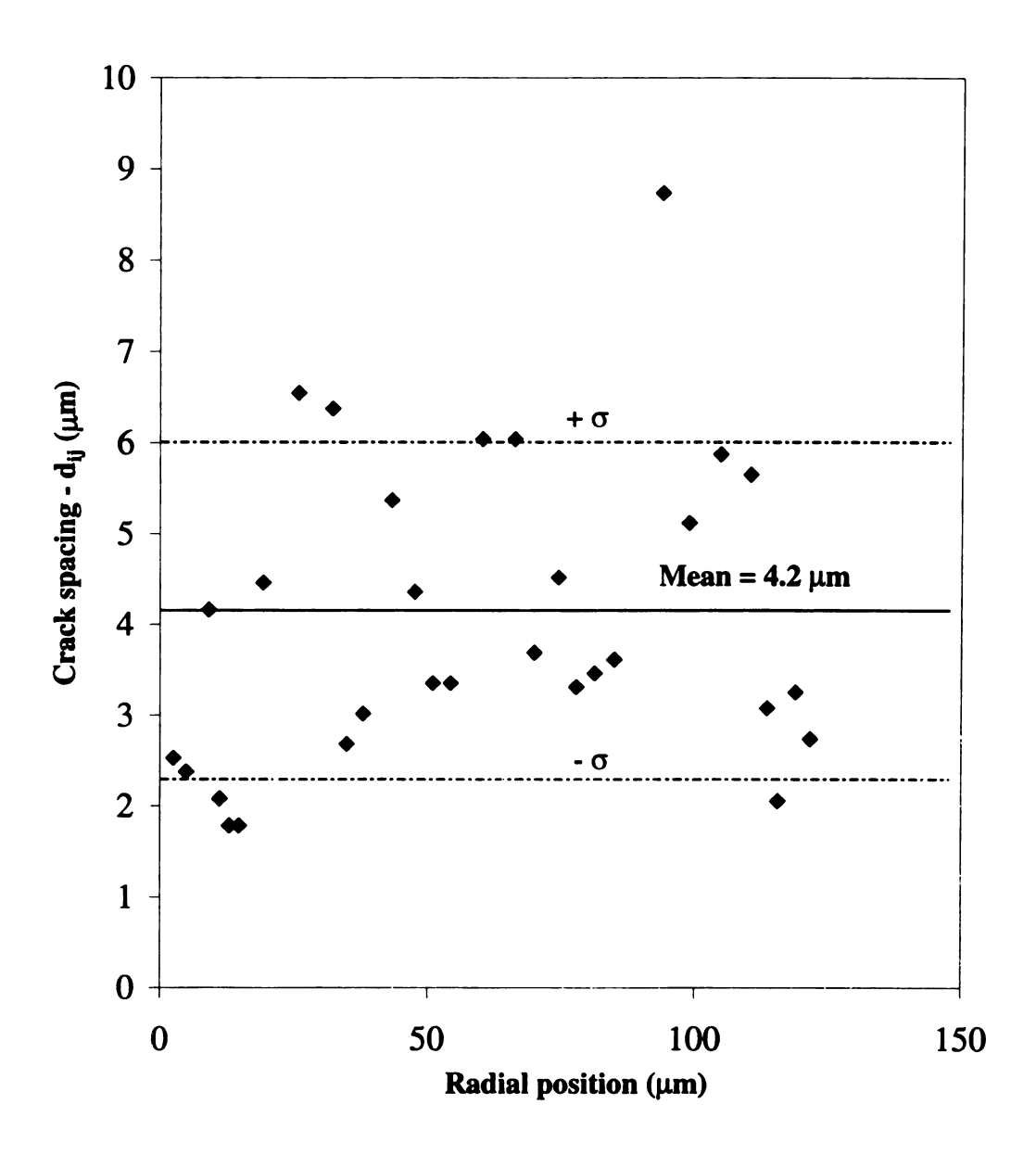


Figure 22. Crack spacing data d_{ij} , for a Vickers indent made at a load of 9.8 N, on specimen SUA1 (Appendix C), plotted against the radial position from the center of the indent.

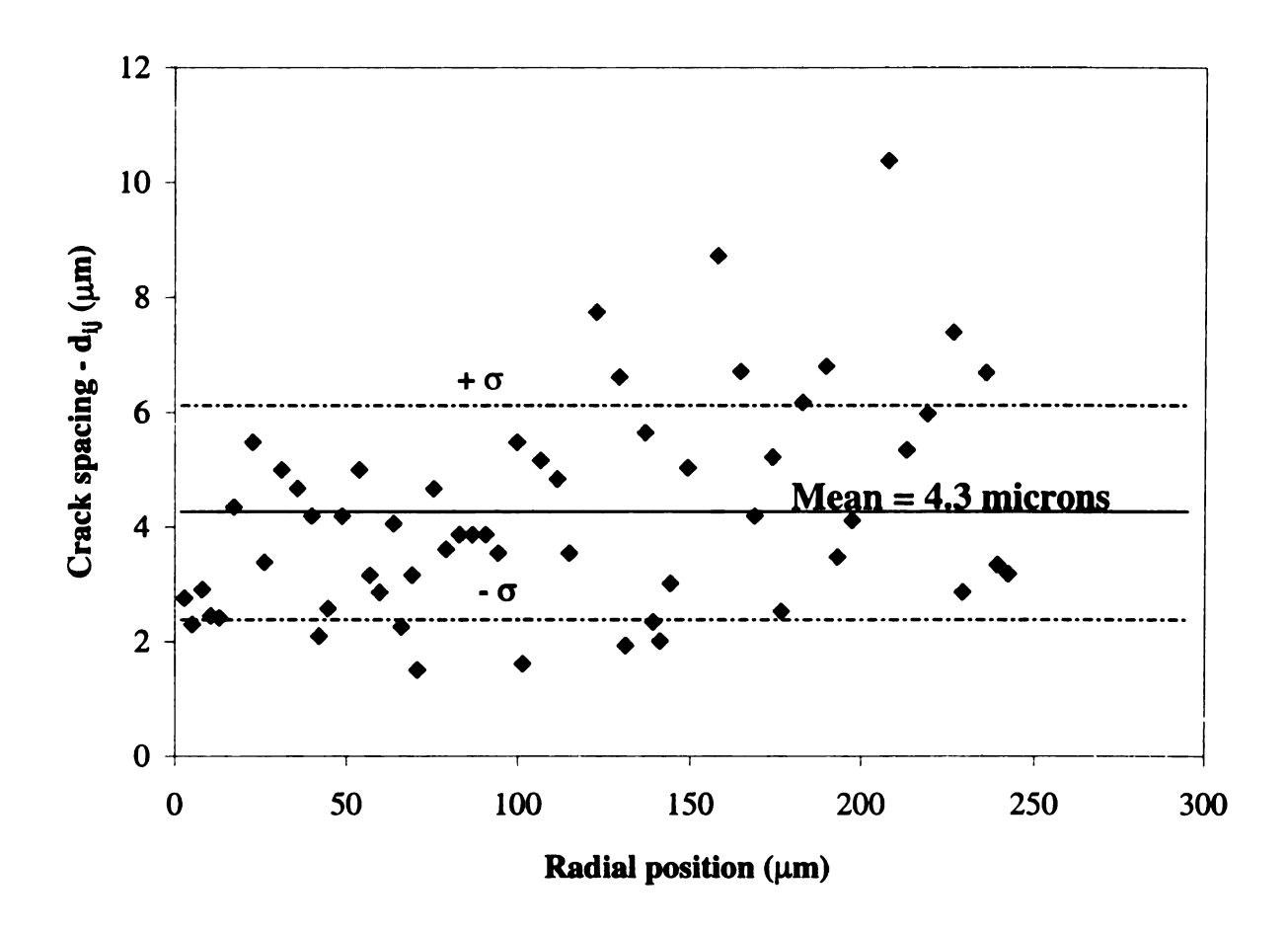


Figure 23. Crack spacing data d_{ij} , for a Vickers indent made at a load of 49 N, on specimen SUA1 (Appendix C), plotted against the radial position from the center of the indent.

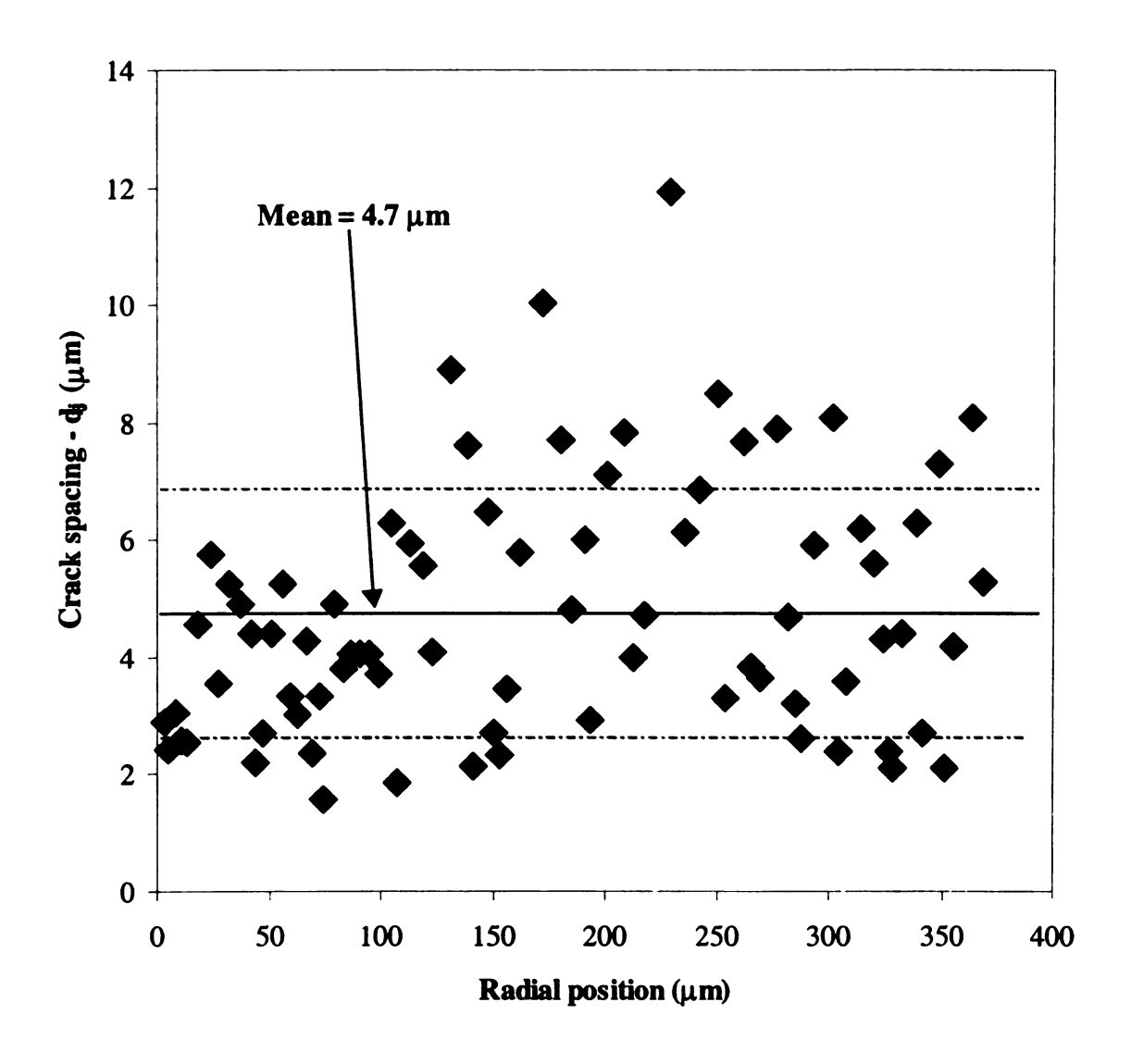


Figure 24. Crack spacing data d_{ij} , for a Vickers indent made at a load of 98 N, on specimen SUA4 (Appendix C), plotted against the radial position from the center of the indent.

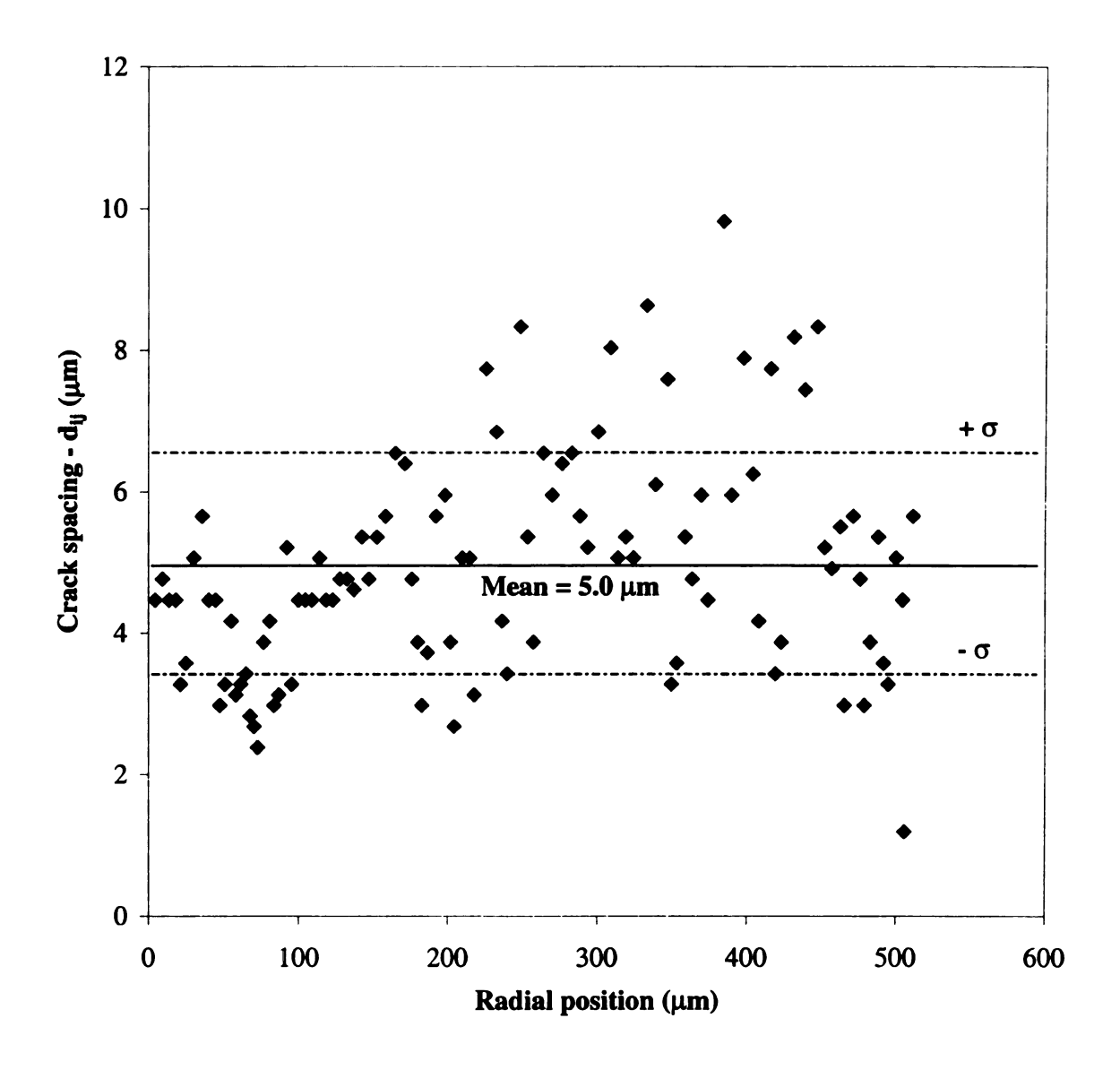


Figure 25. Crack spacing data d_{ij}, for a Vickers indent made at a load of 196 N, on specimen SUA4 (Appendix C), plotted against the radial position from the center of the indent.

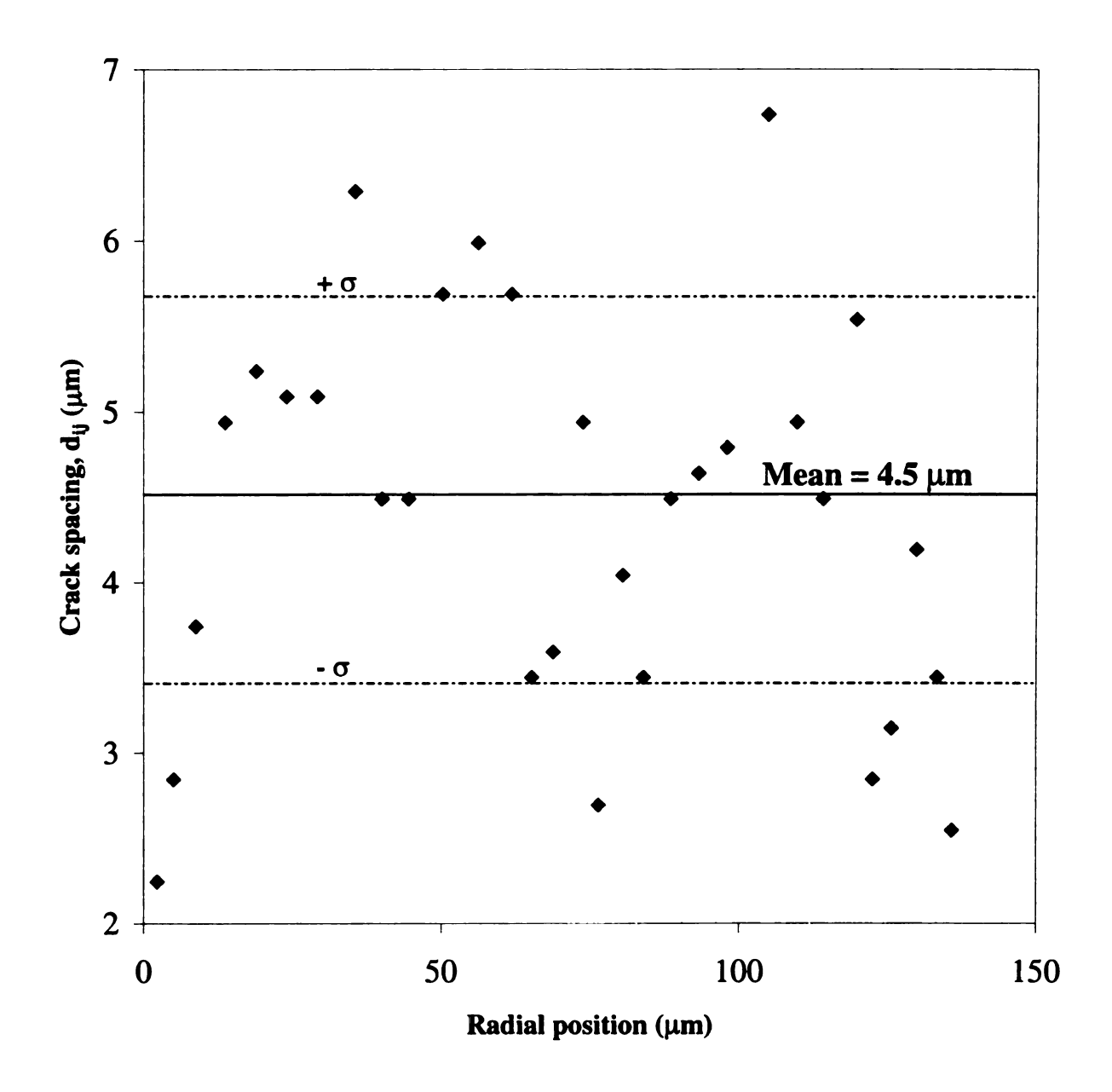


Figure 26. Crack spacing data d_{ij}, for a Vickers indent made at a load of 9.8 N, on specimen SA1 (Appendix C), plotted against the radial position from the center of the indent.

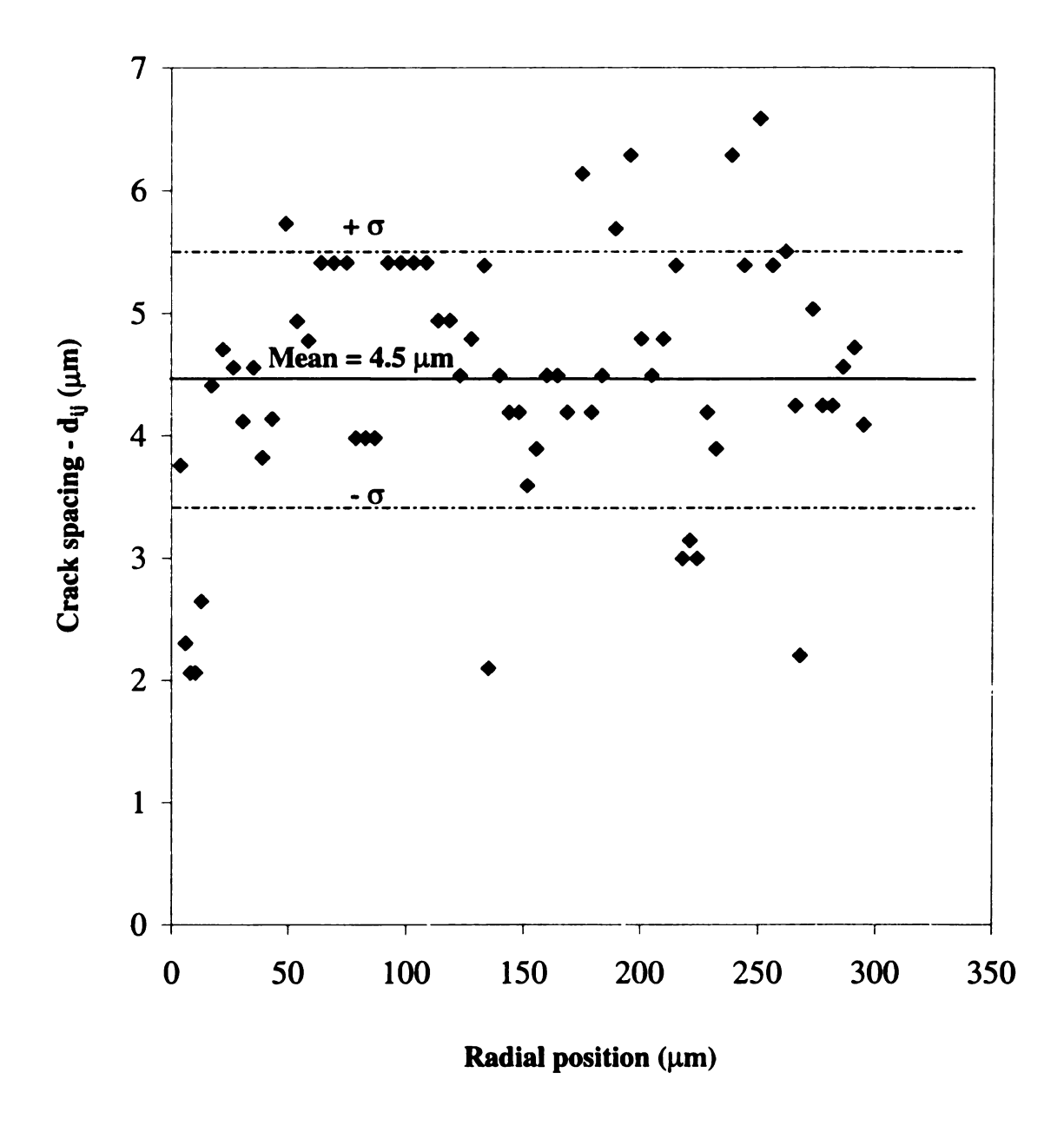


Figure 27. Crack spacing data d_{ij} , for a Vickers indent made at a load of 49 N, on specimen SA1 (Appendix C), plotted against the radial position from the indent.

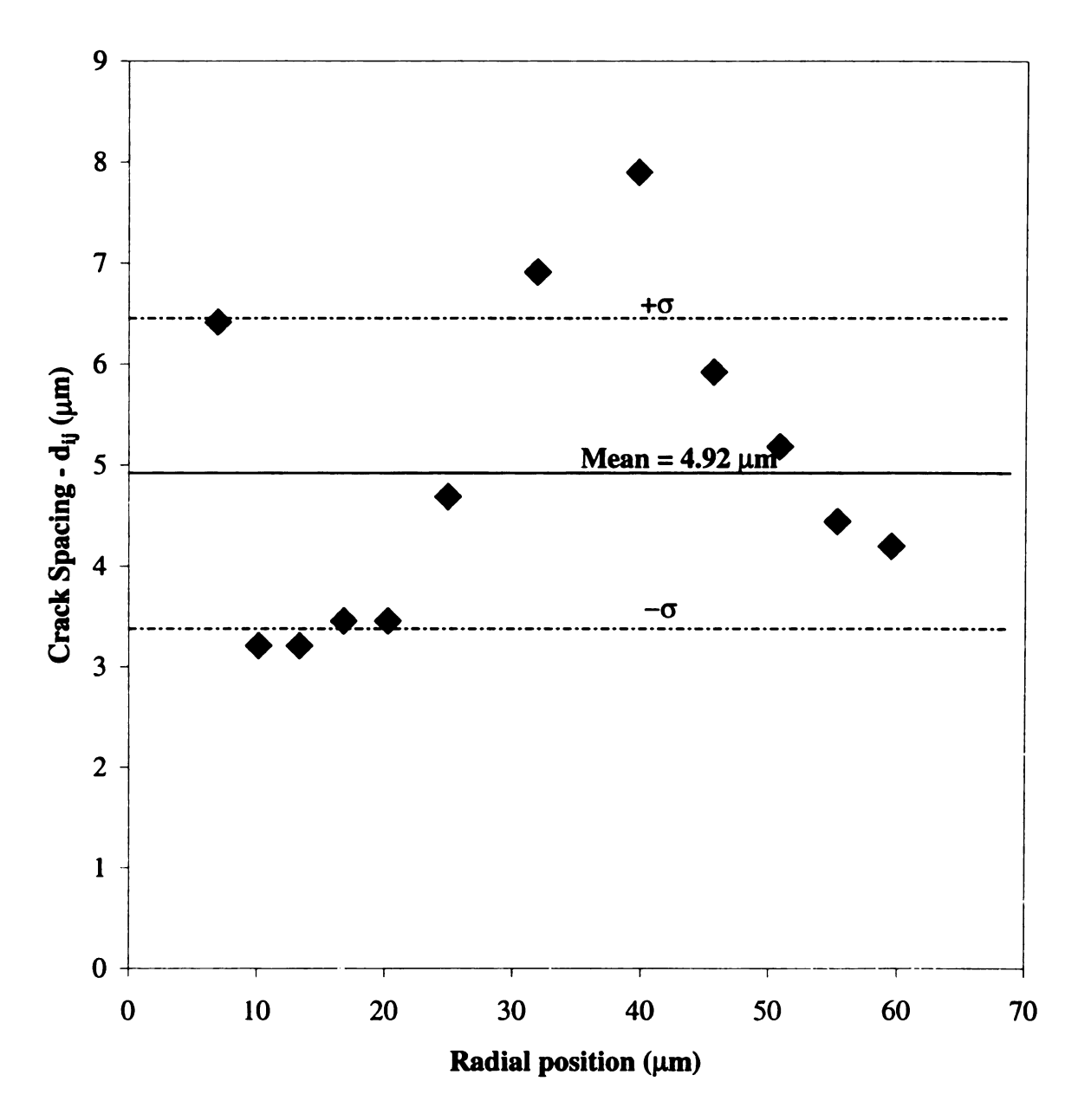


Figure 28. Crack spacing data d_{ij} , for a Vickers indent made at a load of 2.94 N, on an silica coated BMI specimen cured at 175° C for one hour (CR3, Appendix C), plotted against the radial position from the center of the indent.

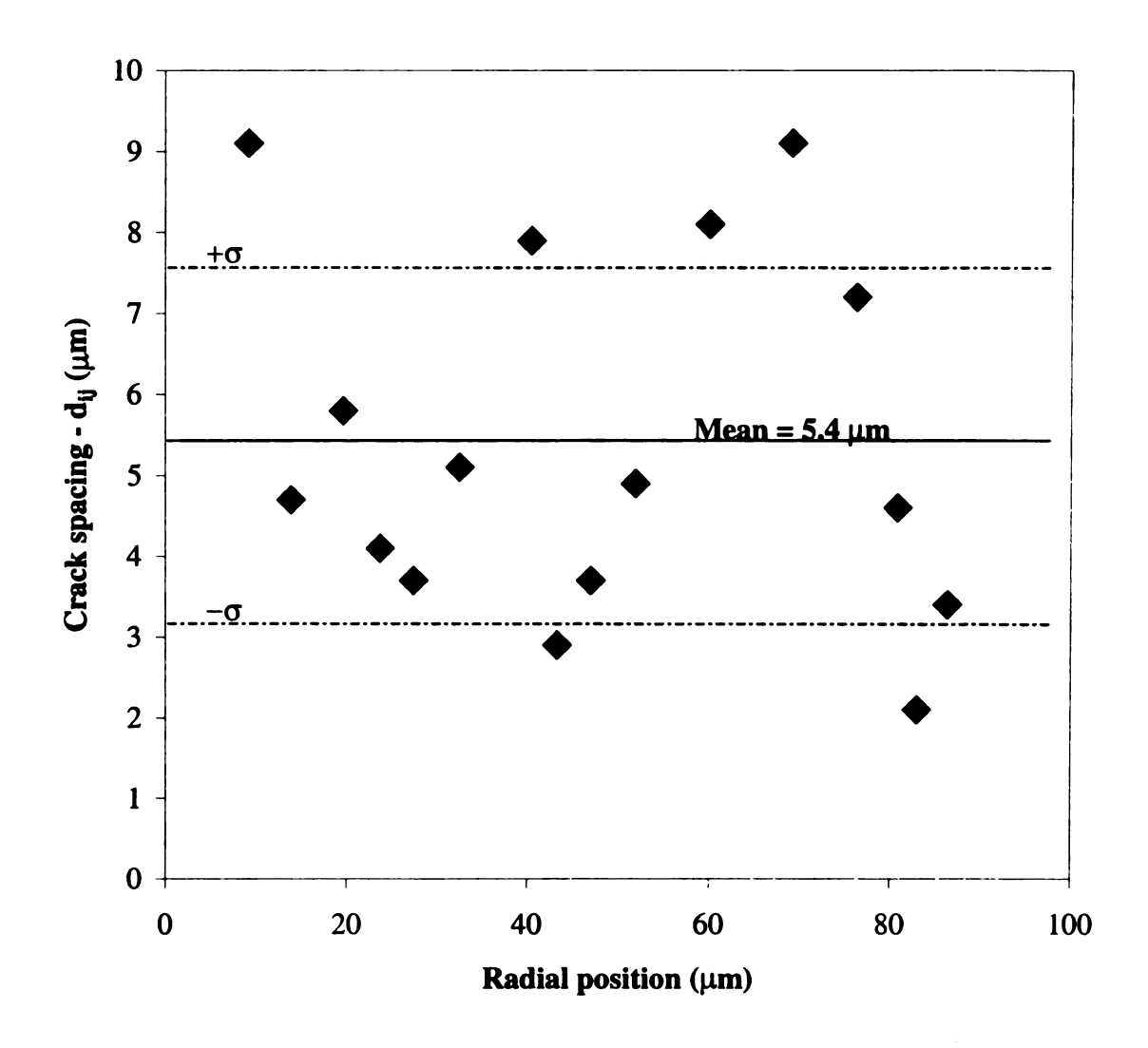


Figure 29. Crack spacing data d_{ij} , for a Vickers indent made at a load of 2.94 N, on an silica coated BMI specimen cured at 175^{0} C for one hour (CR3, Appendix C), plotted against the radial position from the center of the indent.

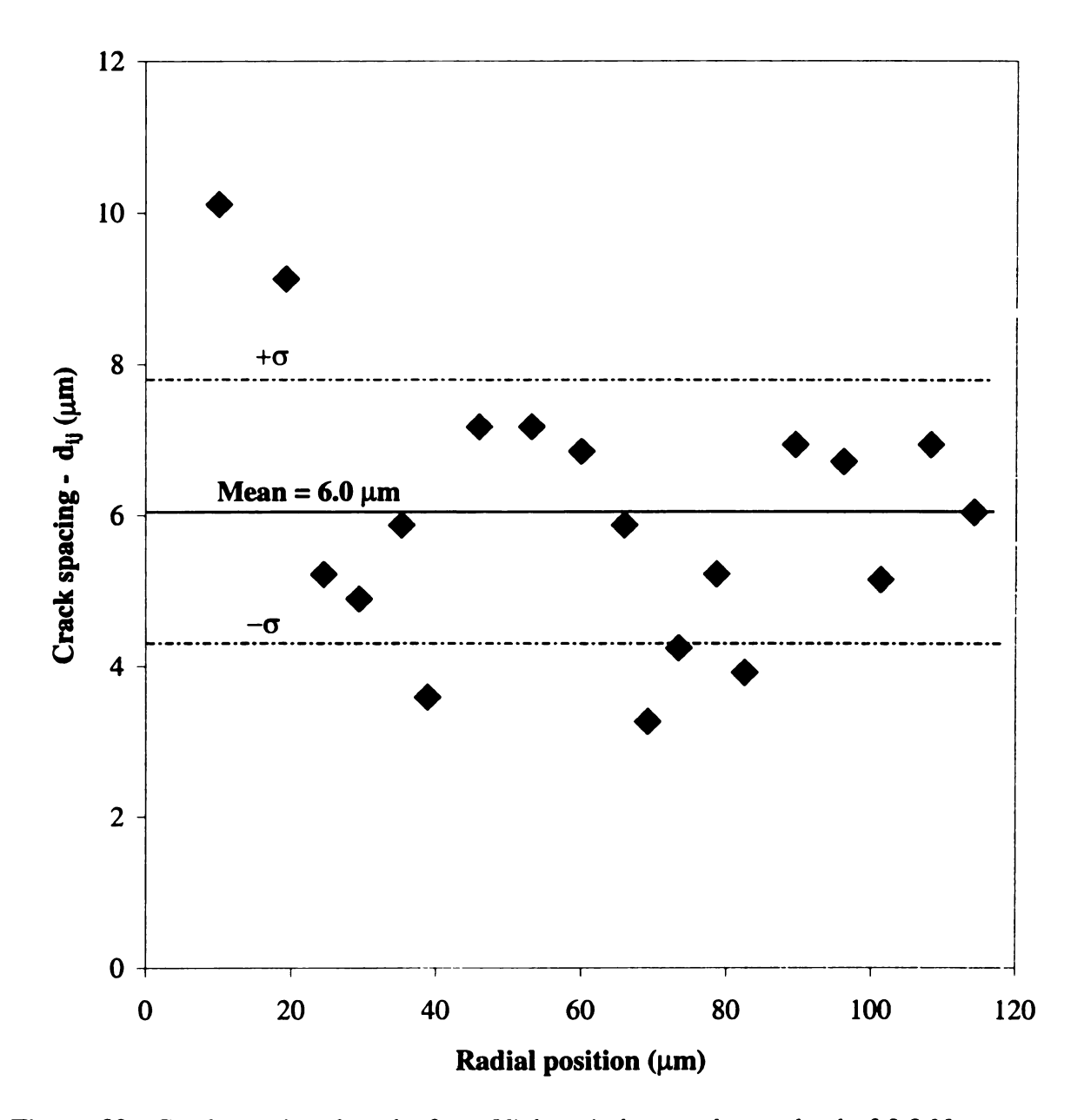


Figure 30. Crack spacing data d_{ij} , for a Vickers indent made at a load of 9.8 N, on an silica coated BMI specimen cured at 175° C for one hour (CR3, Appendix C), plotted against the radial position from the center of the indent.

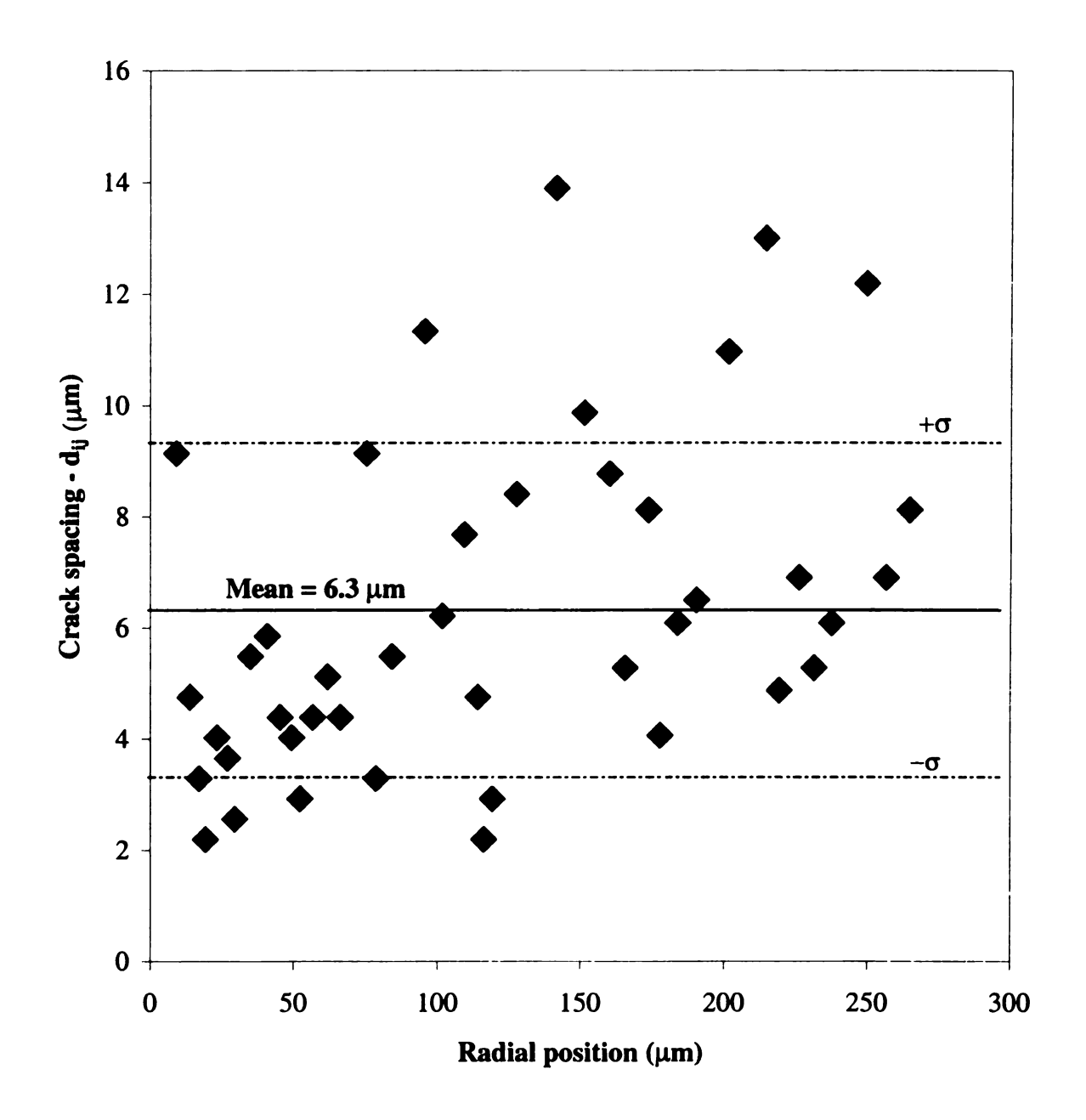


Figure 31. Crack spacing data d_{ij} , for a Vickers indent made at a load of 49 N, on an silica coated BMI specimen cured at 175° C for one hour (CR3, Appendix C), plotted against the radial position from the center of the indent.

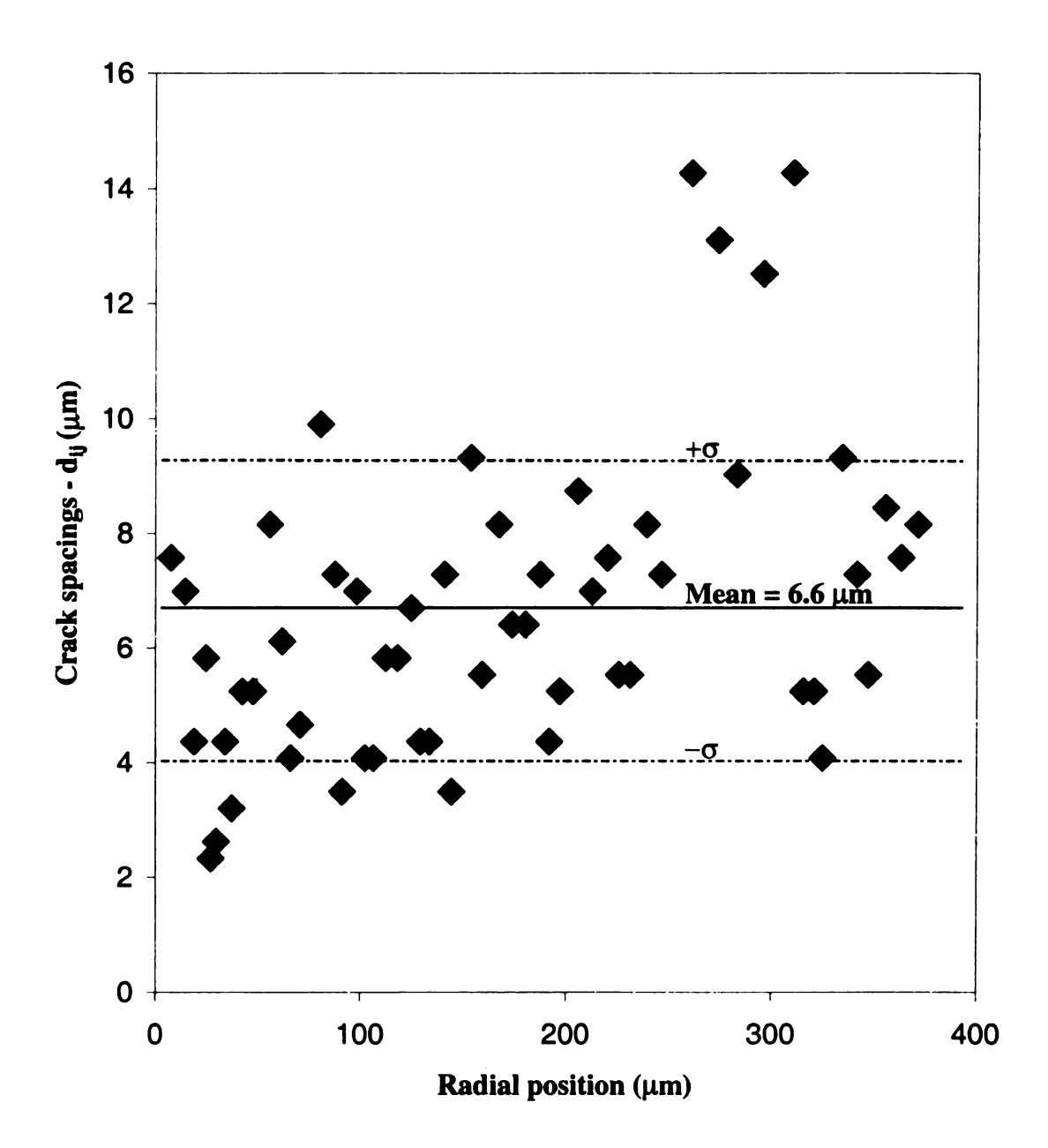


Figure 32. Crack spacing data d_{ij} , for a Vickers indent made at a load of 98 N, on an silica coated BMI specimen cured at 175° C for one hour (CR3, Appendix C), plotted against the radial position from the center of the indent.

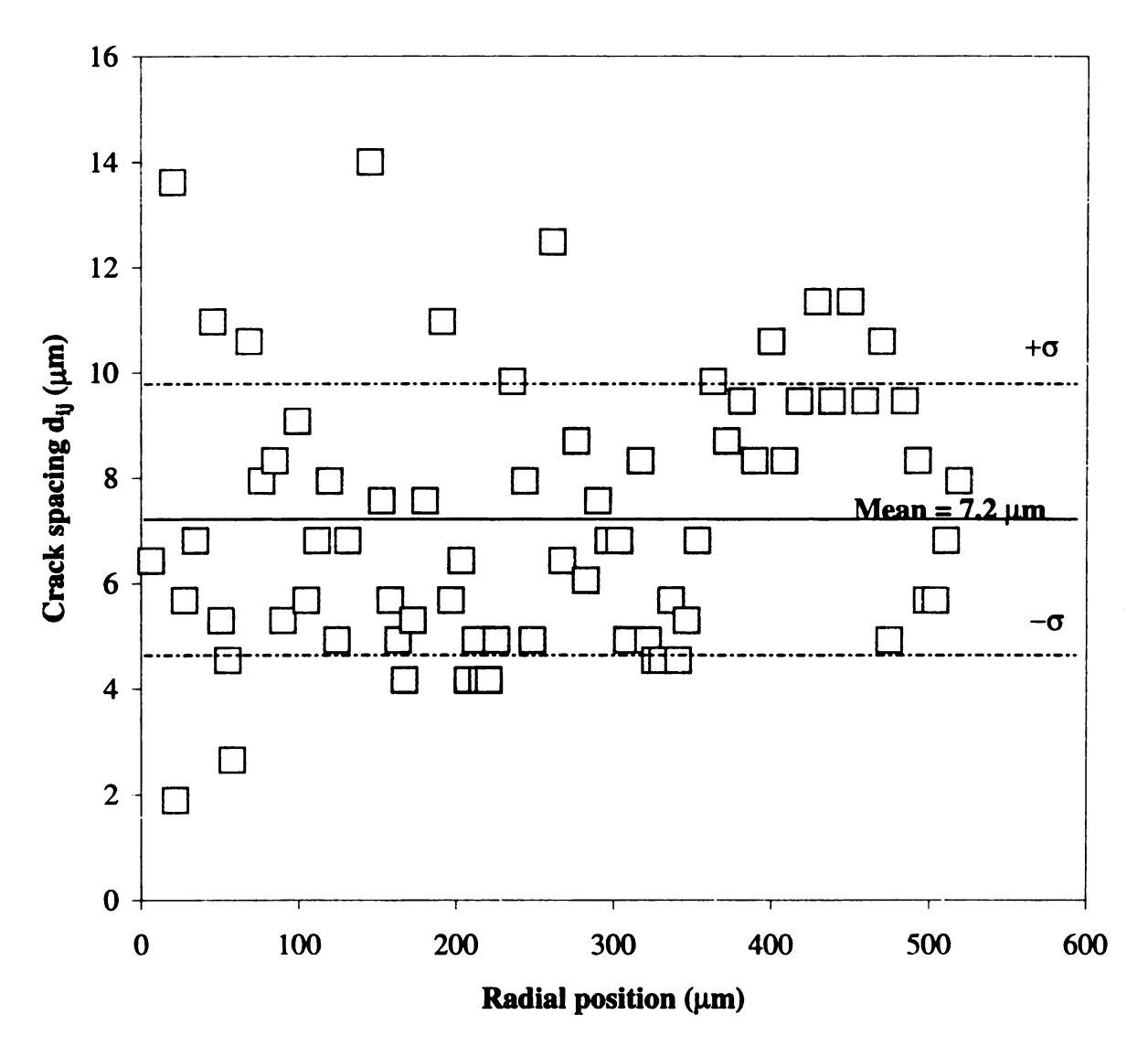


Fig 33. Crack spacing data d_{ij}, for a Vickers indent made at a load of 196 N, on an silica coated BMI specimen cured at 175°C for one hour (CR3, Appendix C), plotted against the radial position from the center of the indent.

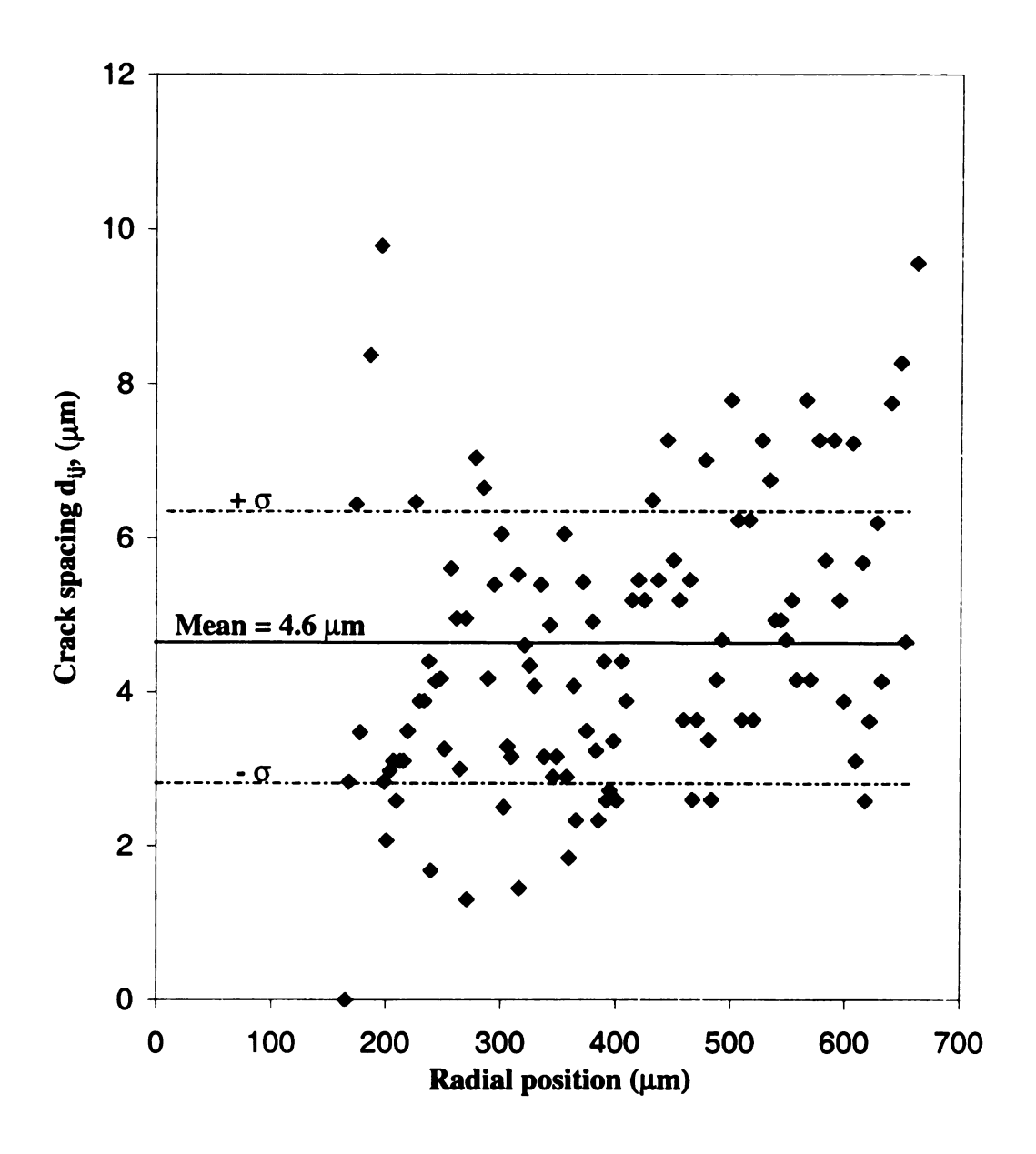


Figure 34. Crack spacing data d_{ij} , for a Hertzian indent made on the HRF scale, on specimen SUA3 (Appendix C), plotted against the radial position from the center of the indent impression.

3.5.2 Comparison of scatter in spacing of abraded coatings versus unabraded coatings at constant loads.

The standard deviation, σ , from the mean crack spacing values for Vickers indentations at 2.94 N, 4.9 N, 9.8 N, 49 N, 98 N and 196 N for BMI specimens with unabraded coatings cured at 150° C for twenty minutes (Figures 20, 21, 22, 23, 24 and 25) were $\sigma_{2.94} = 2.1 \,\mu\text{m}$, $\sigma_{4.9} = 2.1 \,\mu\text{m}$, $\sigma_{9.8} = 1.9 \,\mu\text{m}$, $\sigma_{4.9} = 1.9 \,\mu\text{m}$, $\sigma_{98} = 2.1 \,\mu\text{m}$ and $\sigma_{1.96} = 1.6 \,\mu\text{m}$ (Table 9) respectively. For the BMI specimens with unabraded coatings cured at 175° C for one hour the σ values varied from 1.6 μ m to 3.0 μ m (Table 9, Figures 28, 29, 30, 31, 32 and 33), for indentation loads of 2.94 N to 196 N.

For indentation loads of 9.8 N and 49 N the specimen with the coating abraded abraded (on 0.03 μ m alumina polishing wheel, Section 2.7) prior to indentation showed standard deviations in mean spacing values of $\sigma_{9.8} = 1.2 \,\mu$ m (Figure 26, Table 9) and $\sigma_{49} = 1.0 \,\mu$ m (Figure 27, Table 9) respectively.

The statistical differences between the standard deviations of the crack spacing data for the unabraded specimen versus the abraded specimen were explored using the F-test [33]. The statistical analysis was performed using MS Excel software. The F-test returns a P value for two sets of data. The two data sets are not required to have the same number of items. In our case the two data sets were the crack spacings for the unabraded coated BMI (SUA1) and the abraded coated BMI (SA1). The spacing data was compared between SUA1 and SA1 for both the 9.8N as well as the 49N indent. As the P value increases, the statistical significance of the difference in standard deviations of the two data sets decreases. The maximum P value is 1 and the minimum P value is zero. The cutoff P value used generally is 0.05, below which values the statistical significance of

the difference in standard deviation values are considered to be significant [33]. Thus if the two data sets returned P values less than 0.05 then the difference in standard deviations of the two data sets can be considered significant.

The P value for the corresponding spacing data of the 9.8 N indents on abraded (SA1 – data set from figure 16) and unabraded silica coated BMI (SUA1 – data set from Figure 14) specimens worked was P = 0.046. Similarly the P value for the corresponding spacing data of the 49 N indents on abraded (SA1 – data set from Figure 17) and unabraded silica coated BMI (SUA1 – data set from Figure 15) specimens worked out to be $P = 9.97 \times 10^{-6}$.

From the low P values (P = 4.6 X 10^{-2} and 9.97 X 10^{-6} < 0.05), for both the 9.8 N and 49 N sets of crack spacing data, and the fact that the σ values for crack spacing data on the silica coated BMI specimen with unabraded coating { $\sigma_{49.8} = 1.9 \mu m$, $\sigma_{49} = 1.9 \mu m$ } are greater than the standard deviations for the BMI specimen with an abraded coating { $\sigma_{9.8} = 1.2 \mu m$, $\sigma_{49} = 1.0 \mu m$ }, we can conclude that abrading the coating prior to indentation considerably reduces the scatter.

The dimensions of the indentation-damaged zone was larger for the abraded coatings (SA1 and SA2, Appendix C) at the same load than for the unabraded coatings (SUA1, SUA2 and SUA3, Appendix C). The half-diagonal length of the diamond shaped region "a" for the unabraded coatings at 9.8 N was approximately 116 microns, where as for abraded coatings it is approximately 135 microns. Similarly the radius of the overall crack dimension D in the specimens with unabraded coatings at 49N was approximately 260 microns, where as for the specimen with abraded coatings it is approximately 295

microns. That is, BMI with abraded coatings have crack dimensions around 1.15 times greater than that of BMI specimens with unabraded coatings.

Table 9. The standard deviations from mean crack spacings for BMI specimens with unabraded and abraded coatings cured at 150°C for twenty minutesand BMI specimens with unabraded coatings cured at 175°C for one hour.

| Indentation load | σ (SUA)* | σ (SA)** | σ (CR)∀ |
|------------------|---------------|---------------|----------------|
| (Newtons) | (μ m) | (μ m) | (μ m) |
| 2.94 | 2.1 | | 1.6 |
| 4.9 | 2.1 | | 2.2 |
| 9.8 | 1.9 | 1.2 | 1.8 |
| 49 | 1.9 | 1.0 | 3.0 |
| 98 | 2.1 | | 2.7 |
| 196 | 1.6 | | 2.5 |

3.5.3 Scatter increase with distance from the center of indent.

The scatter in the crack spacing measurements increased with increasing radial distance from the indent center (Figures 20, 21, 22, 23, 24 and 25) for the BMI specimens with unabraded coatings cured at 150° C for twenty minutes. For an interval from the indent center to a point ϕ , the scatter in crack spacing was markedly less compared to the scatter from ϕ to the edge of the cracked region. The point ϕ depends on the indentation load. When normalized by the radial crack field dimension "a", ϕ corresponds to approximately 0.4 irrespective of the indentation load (Figure 35).

Point ϕ , was determined by using MS Excel software. For each indentation load the crack spacing data was subdivided into two sets. If there were "n" items in a set of crack spacing data "z", the F-test was performed for two data sets "Z1" and "Z2". Minimum number of items in either set "Z1" or "Z2" was fixed to be = n/3, as a criterion, to get good results from the F-test, where,

Set
$$Z1 = d_{1,2}$$
 to $d_{M-1,M}$, and Set $Z2 = d_{M,M+1}$ to $d_{N-1,N}$ (6)

$$2n/3 > M > n/3 \tag{7}$$

and "d" represents measured crack spacing values.

The F-test was performed for the range of, M, specified by equation (7). The M that corresponded to the minimum P value (i.e. if P < 0.05), M^* , was calculated and used to calculate ϕ in the following manner.

$$\phi = \sum_{1,2}^{m-1,m} d_{i,j} \tag{8}$$

The minimum P value was determined using a Visual basic macro program (Appendix H) which was run using MS Excel software.

Thus the F-test was also performed on individual sets of crack spacing data comparing data for two different regions on the same crack region. One data set represented the crack spacings for cracks positioned between the indent center and point ϕ , and the other data set represented crack spacings for cracks located between point ϕ and the outer edge of the indentation crack field.

Point ϕ was determined (Figure 35, Table 10) using the method explained above for the six different loads (2.94 N, 4.9, 9.8 N, 49 N, 98 N and 196 N) for unabraded coated specimens (SUA1, SUA4, Appendix C). For the 2.94 N indentation load the point ϕ was determined to be 36.1 microns from the center of the indent (Table, Figures 20 and 35). The P value for the F-test carried out on the two sets of data for the 2.94 N indent was PR = 0.03 (i.e. PR < 0.05).

Similarly for the 4.9 N, 9.8 N, 49 N, 98 N and 196 N indentation loads ϕ was calculated to be 39.8 μ m, 46.6 μ m, 94.3 μ m, 162.1 μ m, 214.6 μ m respectively. The P values for the 4.9 N, 9.8 N, 49 N, 98 N and 196 N were 0.01, 0.0004, 0.00003, 0.007, 0.0001 (i.e. P < 0.05) respectively.

The standard deviations from mean crack spacing, for crack spacing data from the center of the 2.94 N indent to point $\phi = 36.05$ microns, and from point ϕ to the end of the indent were 1.30 microns and 3.49 microns respectively. Now let the ratio of the distances from point ϕ to the edge of the indent and center of the indent to point ϕ be

$$\frac{\sigma_{\phi-end}}{\sigma_{C-\phi}} = \eta \tag{9}$$

where

 $\sigma_{\phi \text{-end}}$ = Standard deviation of the crack spacing data from the mean for the data ranging from point ϕ , to the end of the indent.

 $\sigma_{C-\phi}$ = Standard deviation of the crack spacing data from the mean for the data ranging from center of the indent to point ϕ .

The η values for the 2.94 N, 4.9 N, 9.8 N, 49 N, 98 N and 196 N indentation loads were calculated using equation 9. Table 10 lists the ϕ , $\sigma_{O\text{-end}}$, $\sigma_{C\text{-}O}$ and η values for the 2.94 N, 9.8 N, 49 N and 196 N indentation loads. From the greater than one, η values (ranged from 1.8 to 2.7, Table 10), we can conclude that the standard deviations from mean crack spacing for the crack spacings in the region in between point ϕ , to the end of the indent is greater compared to the standard deviations from mean crack spacings for the crack spacings in between the region from the center of the indent to point ϕ .

Table 10. The distance of point ϕ from the center of the indent, along with the η values (equation 9), for various loads.

| Specimen | Load | C- # | σ _{C-φ} | σ _{φ-end} | η |
|----------|-----------|-----------|------------------|--------------------|----------|
| | (Newtons) | (microns) | (microns) | (microns) | unitless |
| SUA4 | 2.94 | 36.5 | 1.3 | 3.5 | 2.68 |
| SUA1 | 4.9 | 39.8 | 1.2 | 2.8 | 2.31 |
| SUA1 | 9.8 | 46.6 | 1.2 | 2.5 | 2.09 |
| SUA1 | 49 | 94.3 | 1.0 | 2.1 | 2.01 |
| SUA1 | 98 | 162.1 | 1.1 | 2.0 | 1.80 |
| SUA4 | 196 | 214.6 | 1.0 | 1.8 | 1.77 |

^{*} $C-\phi$ represents the distance from the center of the indent to the point ϕ .

Thus from the low P values (i.e. < 0.05) and the η values, that are greater than one (1.8 to 2.7) we conclude that the scatter is considerably greater in the region from the center of the indent to point ϕ than for the region between point ϕ and end of the cracked region.

A similar test was performed on the abraded specimen to determine if scatter is high towards the end of the crack region as in the abraded specimen (SA1, Appendix C). For the abraded coatigns P values for loads of 9.8 N and 49 N were 0.86 and 0.54 respectively (i.e. P > 0.05).

The P values for the abraded BMI are greater than 0.05 (0.54 to 0.86). Thus the difference in, σ values from mean crack spacings for a region in-between the center of the indent and point ϕ compared to the σ values from mean crack spacing for a region in-between point ϕ and end of the indent is not statistically significant. Thus we can conclude that the scatter in crack spacings from the mean does not increase with radial position from the center of the indent for the BMI with abraded coatings as compared to the BMI with unabraded coatings were scatter increased with radial position from center of the indent.

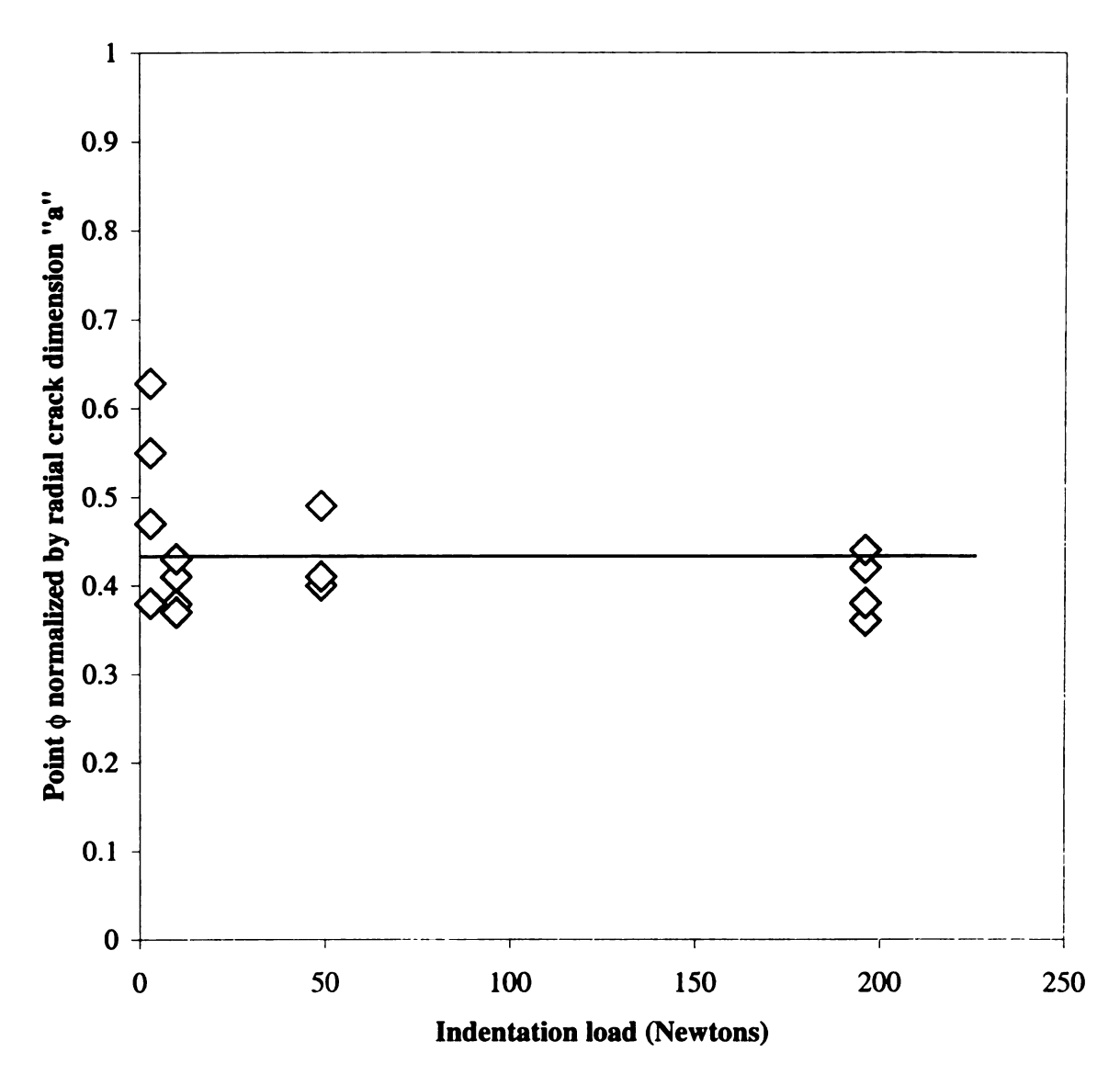


Figure 35. Point " ϕ ", normalized by radial crack field dimension "a" for coated BMI specimens (SUA1, SUA4, Appendix C), plotted as a function of indentation load.

3.5.4 Order statistics study to determine distribution of crack spacings

If we assume an uniform crack spacing, then the residuals (difference between the observed value and expected value) and are normally distributed [34]. This is consistent with a random variation with respect to the mean crack spacing. The assumption that the residuals are distributed in a manner similar to the crack spacings itself is true for any distribution [34].

An order statistics study [34] compared the distribution of the crack spacings with the uniform distribution. For the crack spacing data for a single indentation, mean crack spacings, μ , was subtracted from each individual crack spacing d_{ij} , for one particular indent, to obtain the residual crack spacings. The residual crack spacings were arranged in ascending order and numbered 1 through N, where N was the total number of crack spacings for that particular data set. We label the order set of crack spacings is an ordered statistic of the experimental data R.

The set S is defined by

$$S_1 = (I-3/8)/(N+1/4)$$
 (10)

where

 S_1 = The Ith item in the new data set S_1

I = 1 through N,

N = defined earlier as total number of items.

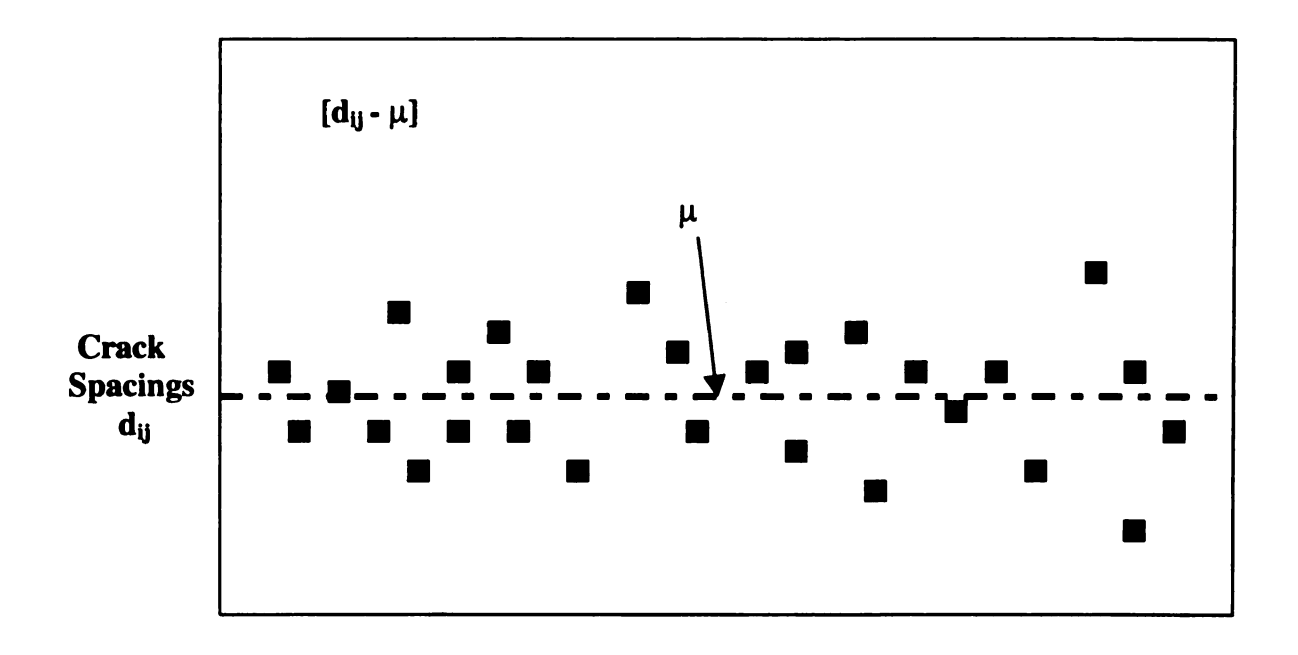
Equation 10, removes a bias that is based on a detailed explanation in [34].

From set S, a new set E was created using the NORMSINV function in MS Excel software. NORMSINV returns the inverse of the standard normal cumulative distribution

(standard normal deviate) [34] with a mean of zero and standard deviation of one. Set E is the expected value of order statistic.

The ordered residual spacings (set R) from measured values was plotted against the expected order statistic values using MS Excel software (Figures 37, 38, 39, 40, 41, 42, 43, 44, 45, 46, 47, 48, 49, 50 and 51). The least squares fit for the figures, gave very good R-square values ranging from 0.904 to 0.986. Thus we can say the distribution of our residual spacings is a Gaussian [34]. Since the distribution of residuals is a gaussian, we can conclude that the assumption we had made of the crack spacings being uniformly distributed is true.

Similar plots of ordered residual crack spacings were plotted against expected order statistic values for the crack spacings data for an indentation load in the region inbetween the center of the indent to point ϕ , and for regions in-between point ϕ and the end of the indent dimension (Figures 52, 53, 54 and 55). The least-squares fit for the figures 37 though 55, gave R^2 values ranging from 0.971 to 0.986. Thus we can say that the crack spacings are also uniformly distributed in regions between center of indent and point ϕ , and in regions in-between point ϕ , and end of the indent.



Radial position

Figure 36. Schematic, describing uniform distribution of crack spacings.

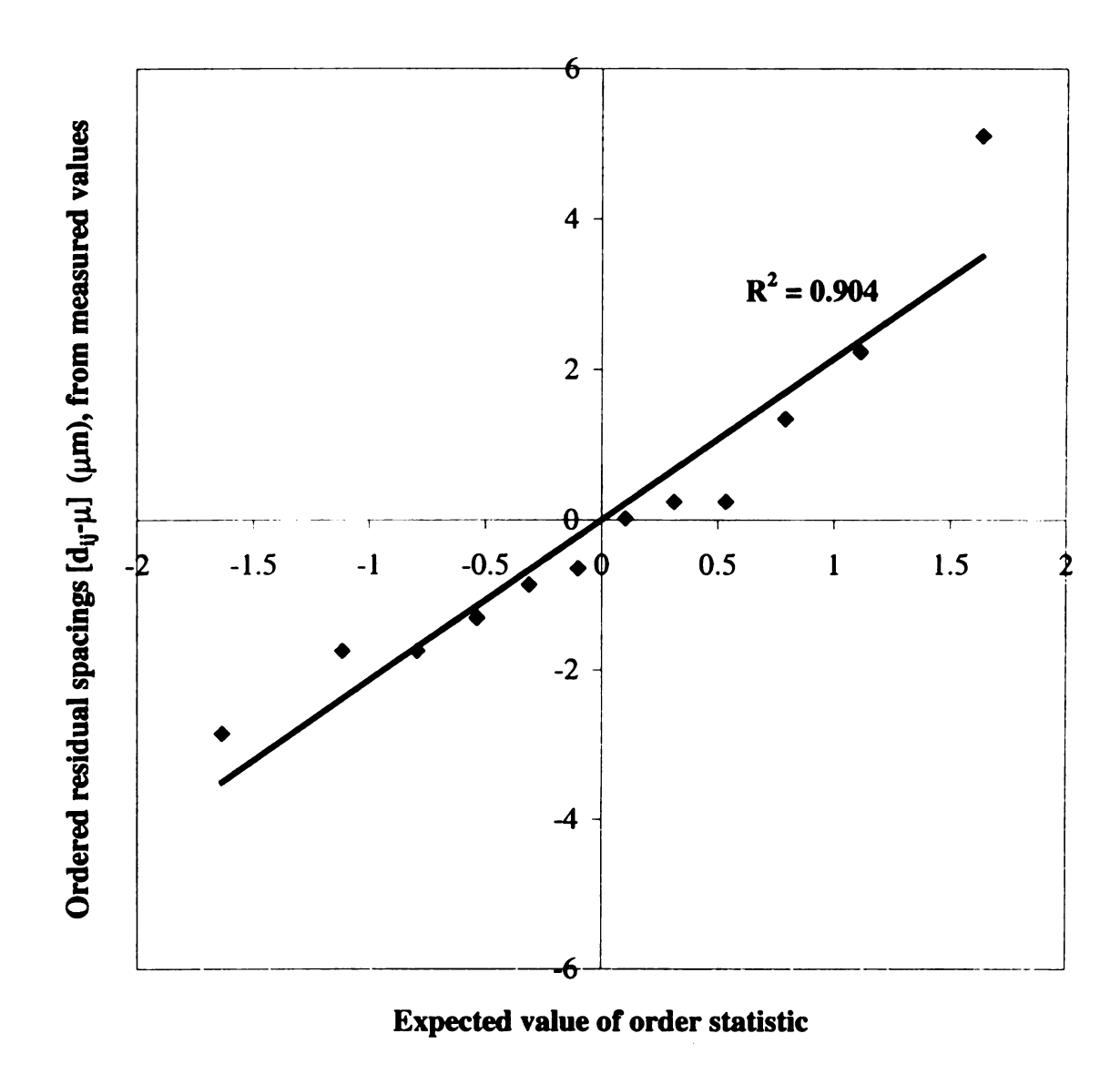


Figure 37. For the distance between the ith and jth crack, d_{ij}, ordered residual spacings versus expected value of order statistics for a 2.94 N indent on an silica coated BMI specimen (SUA4, Appendix C) with an unabraded coating.

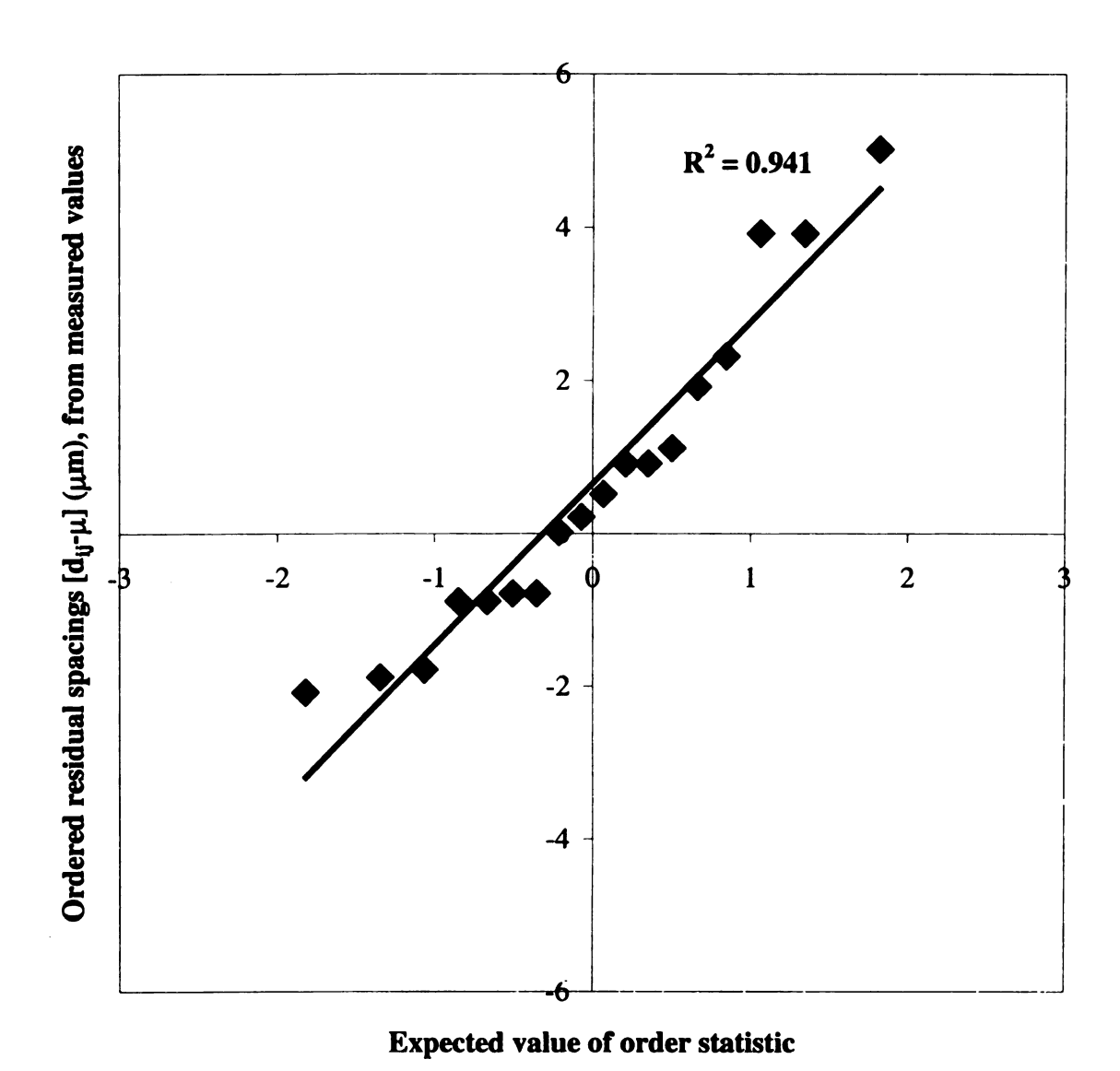


Figure 38. For the distance between the i^{th} and j^{th} crack, d_{ij} , ordered residual spacings versus expected value of order statistics for a 4.9 N indent on an silica coated BMI specimen (SUA4, Appendix C) with an unabraded coating.

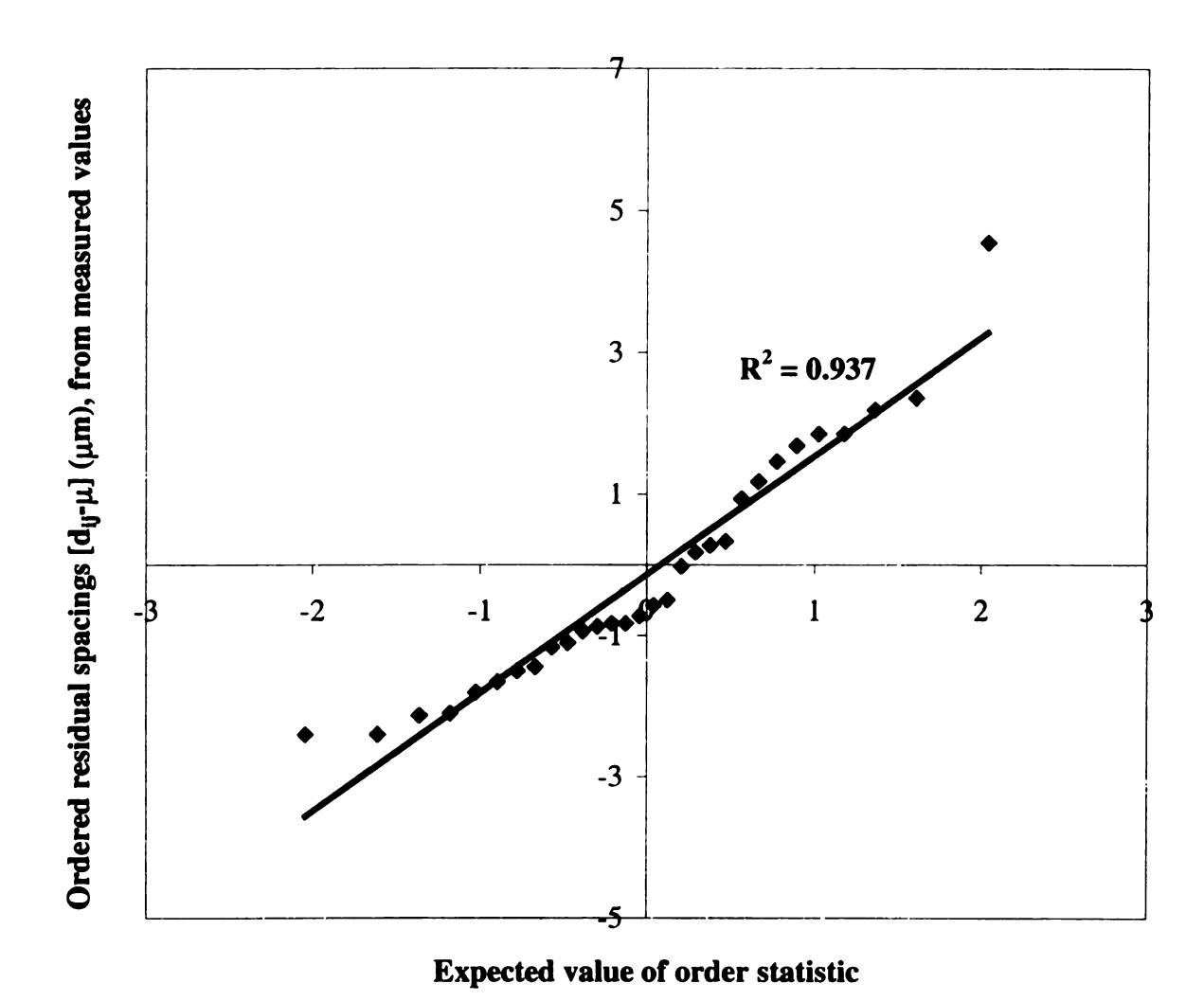


Figure 39. For the distance between the ith and jth crack, d_{ij}, ordered residual crack spacings versus expected value of order statistics for a 9.8 N indent on an silica coated BMI specimen (SUA1, Appendix C) with an unabraded coating.

| | | | , |
|--|--|--|---|
| | | | |
| | | | |
| | | | |
| | | | |
| | | | |
| | | | |
| | | | |
| | | | |
| | | | |
| | | | |
| | | | |
| | | | |
| | | | |
| | | | |
| | | | |
| | | | |
| | | | |
| | | | |
| | | | |
| | | | |
| | | | |
| | | | |
| | | | |

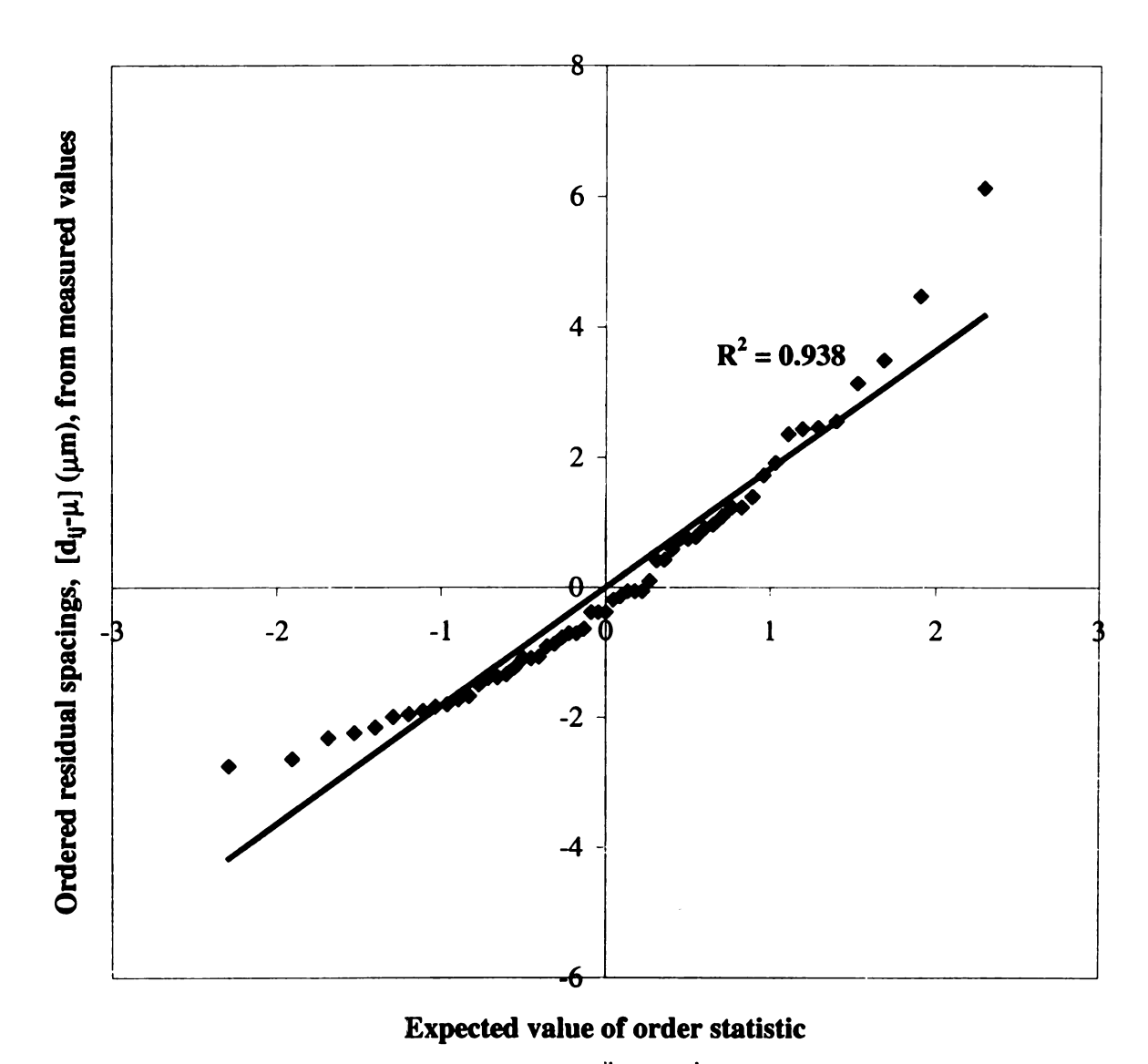


Figure 40. For the distance between the i^{ih} and j^{th} crack, d_{ij} , ordered residual spacings versus expected value of order statistics for a 49 N indent on an silica coated BMI specimen (SUA1, Appendix C), with an unabraded coating.

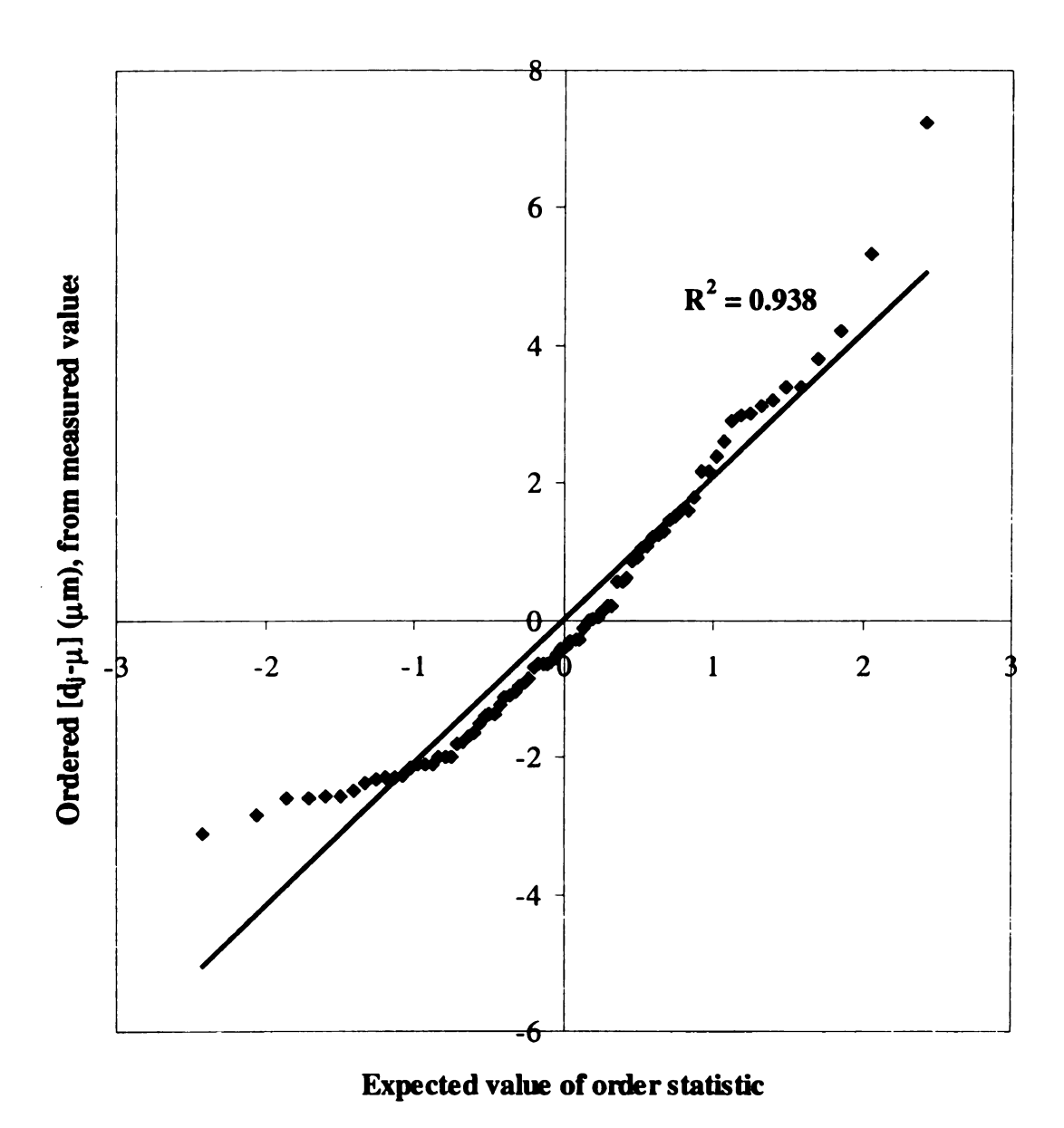


Figure 41. For the distance between the i^{th} and j^{th} crack, d_{ij} , ordered residual crack spacings versus expected value of order statistics for a 98 N indent on an silica coated BMI specimen (SUA4, Appendix C), with an unabraded coating.

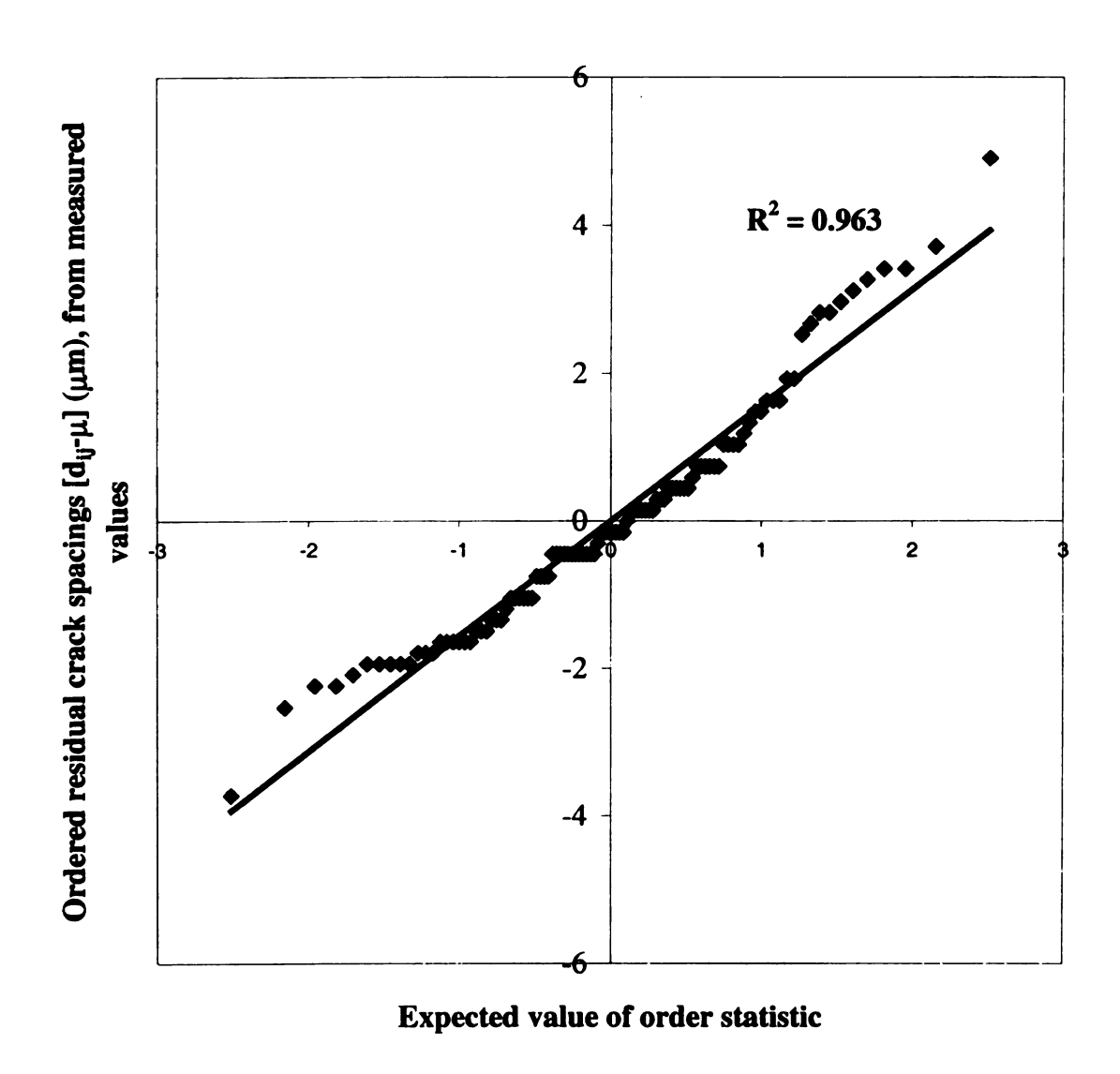


Figure 42. For the distance between the ith and jth crack, d_{ij}, ordered residual crack spacings versus expected value of order statistics for a 196 N indent on an silica coated BMI specimen (SUA4, Appendix C), with an unabraded coating.

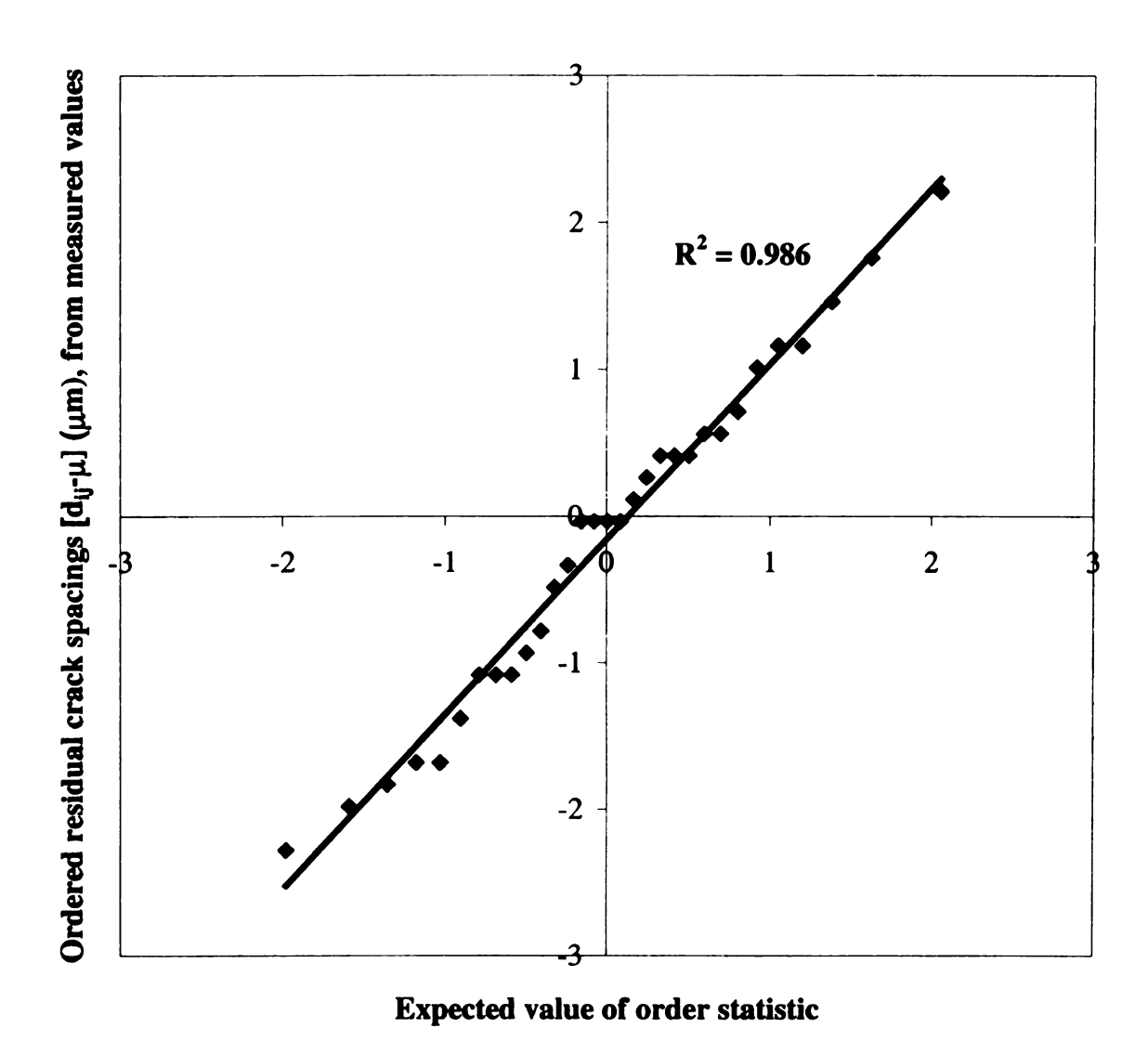


Figure 43. For the distance between the ith and jth crack, d_{ij}, ordered residual spacings versus expected value of order statistics for a 9.8 N indent on a coated BMI specimen (SA1, Appendix C) with an abraded silica film.

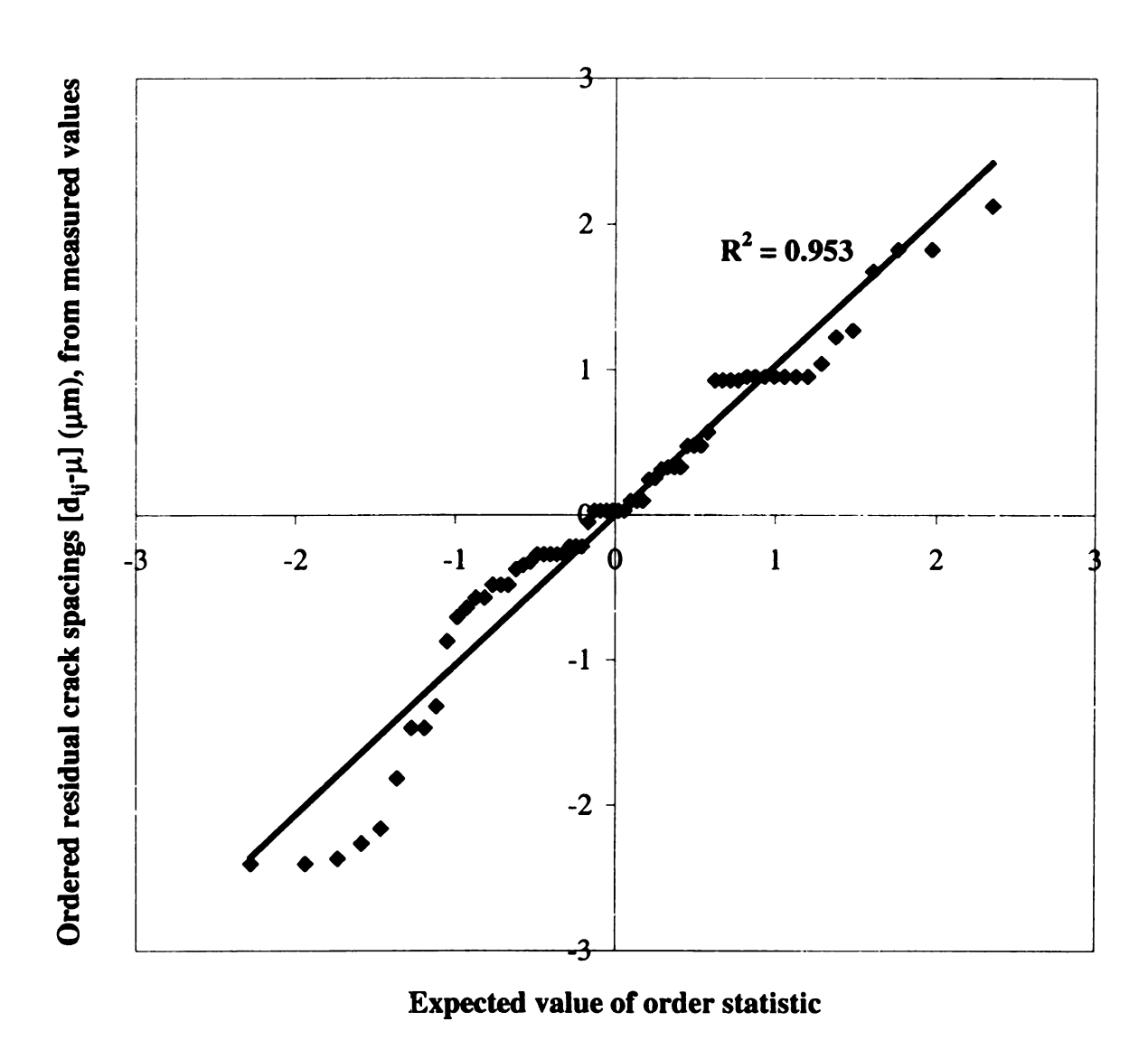


Figure 44. For the distance between the i^{ih} and j^{th} crack, d_{ij} , ordered residual spacings versus expected value of ordered statistics for a 49 N indent on a coated BMI specimen (SA1, Appendix C) with an abraded silica film.

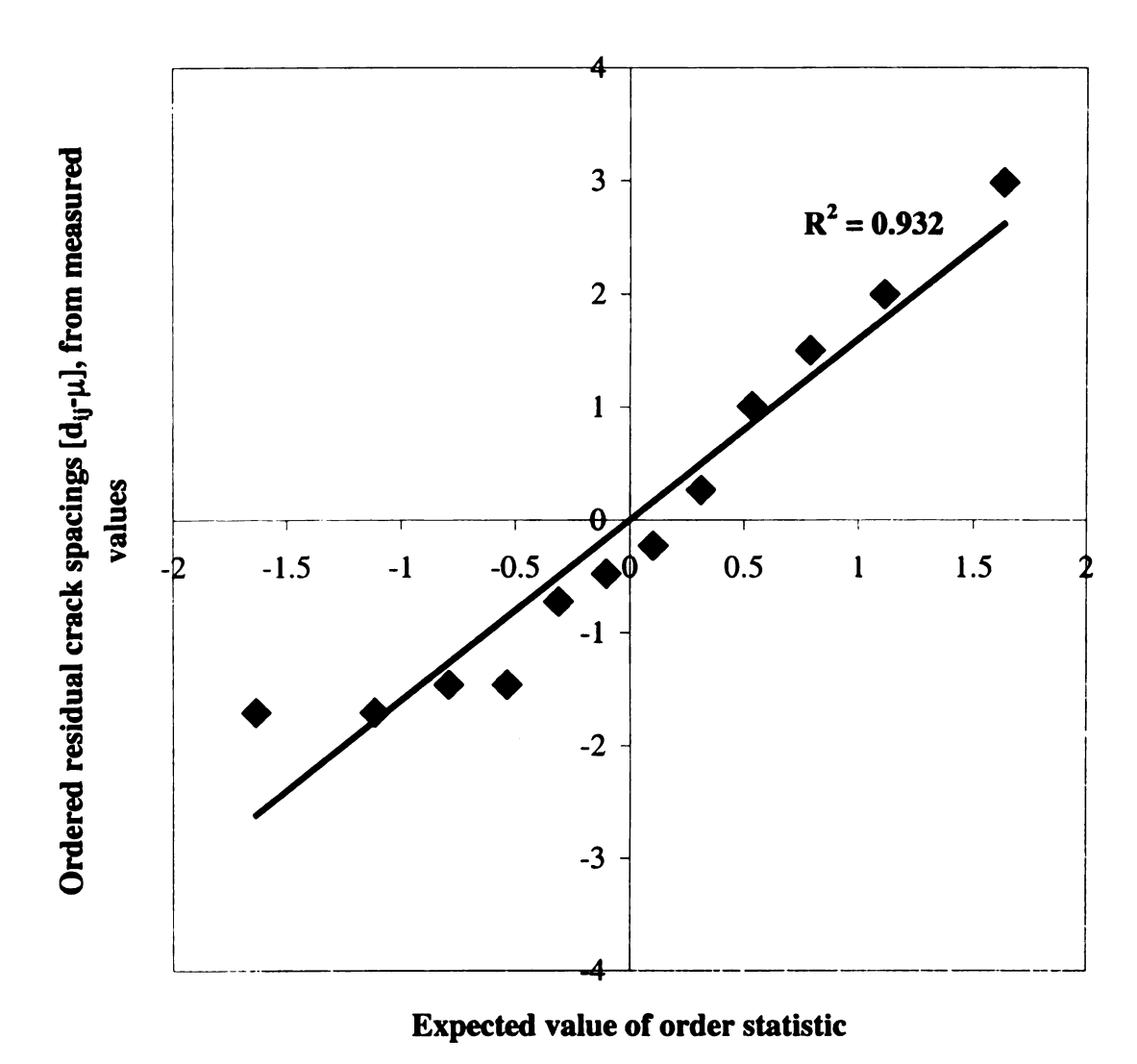


Figure 45. For the distance between the ith and jth crack, d_{ij}, ordered residual spacings versus expected value of ordered statistics for a 2.94 N indent on a coated BMI specimen cured at 175°C for one hour (CR3, Appendix C) with an abraded silica film.

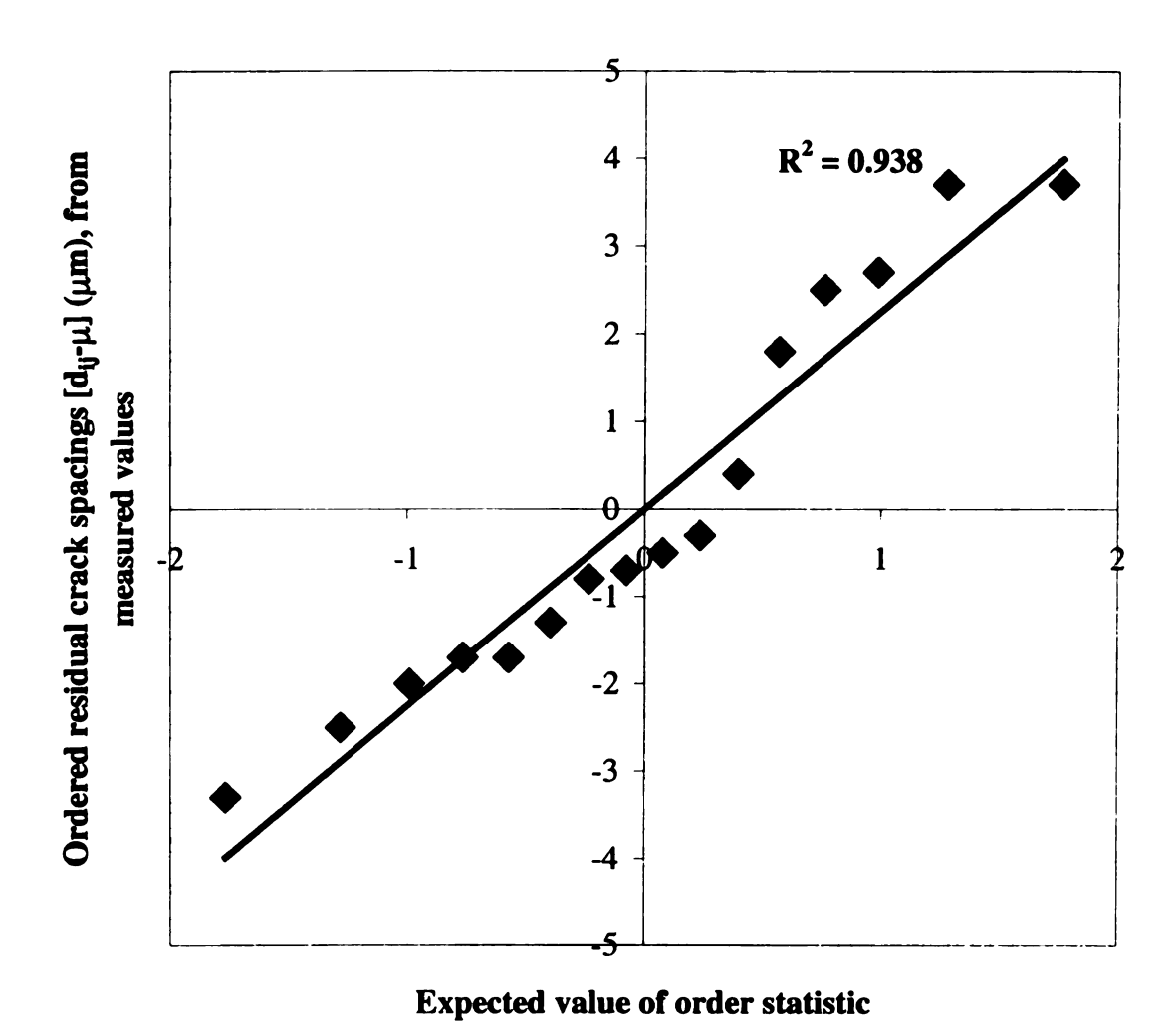


Figure 46. For the distance between the ith and jth crack, d_{ij}, ordered residual spacings versus expected value of ordered statistics for a 9.8 N indent on a coated BMI specimen cured at 175°C for one hour (CR3, Appendix C) with an abraded silica film.

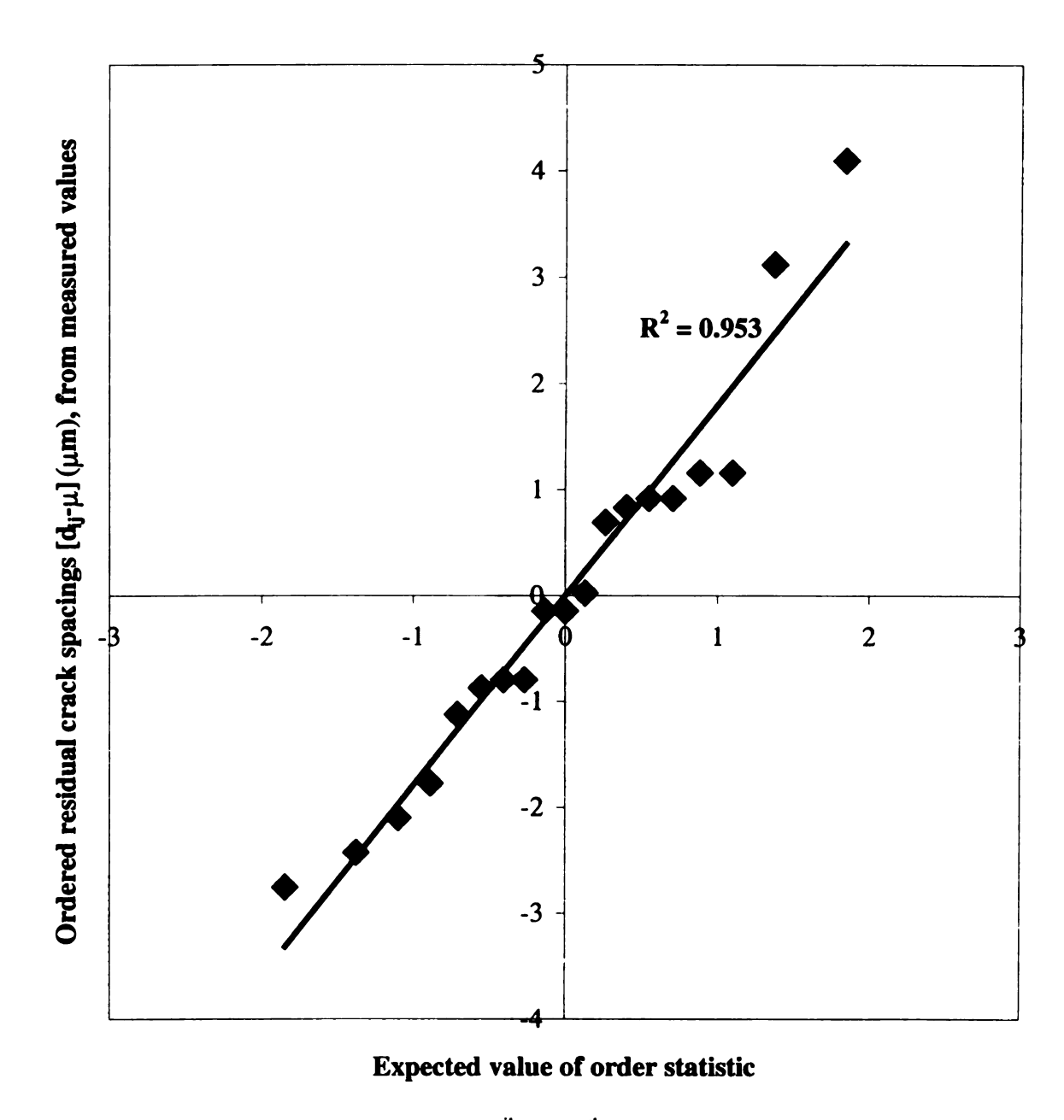


Figure 47. For the distance between the ith and jth crack, d_{ij}, ordered residual spacings versus expected value of ordered statistics for a 9.8 N indent on a coated BMI specimen cured at 175°C for one hour (CR3, Appendix C) with an abraded silica film.

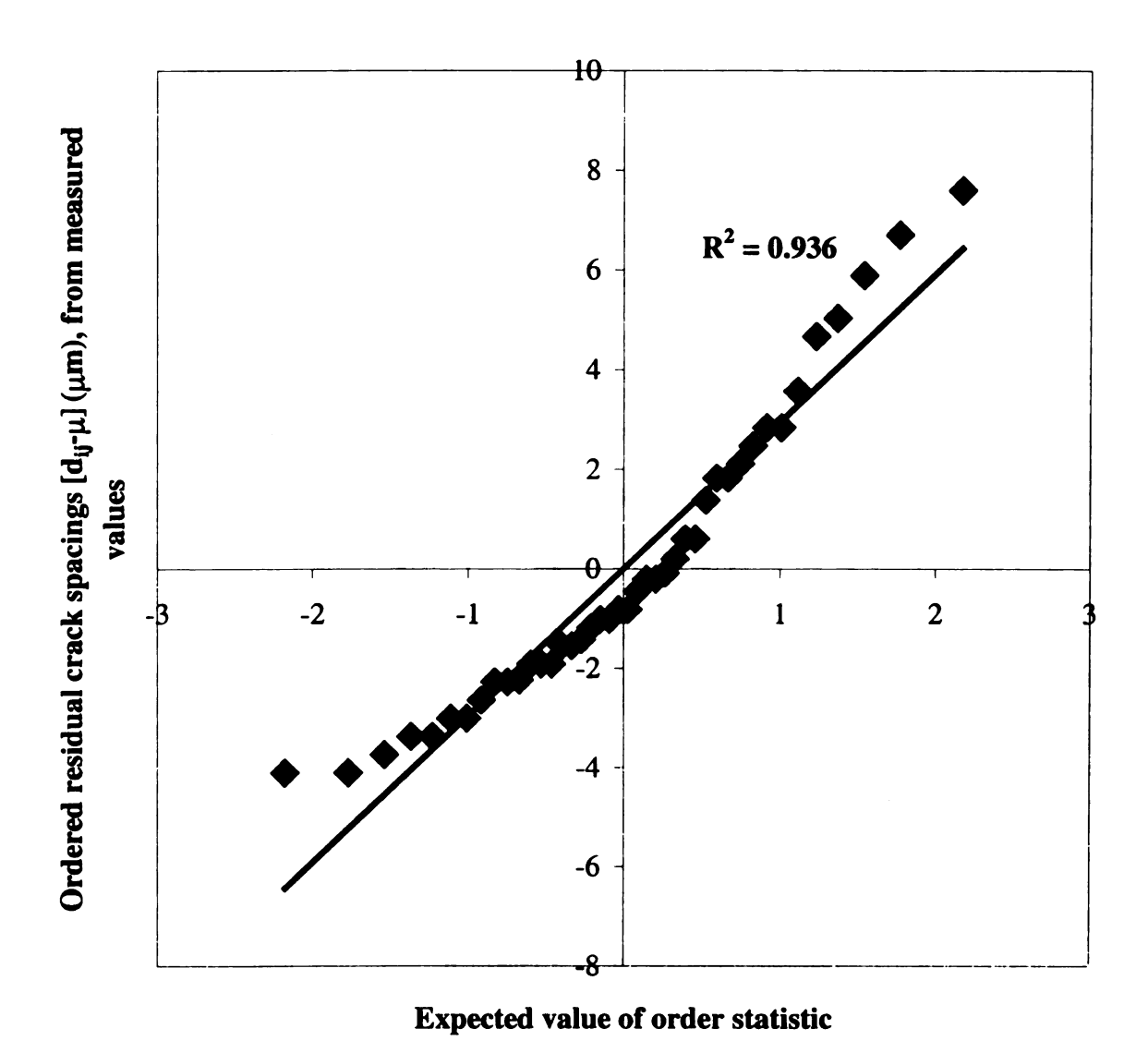


Figure 48. For the distance between the ith and jth crack, d_{ij}, ordered residual spacings versus expected value of ordered statistics for a 49 N indent on a coated BMI specimen cured at 175^oC for one hour (CR3, Appendix C) with an abraded silica film.

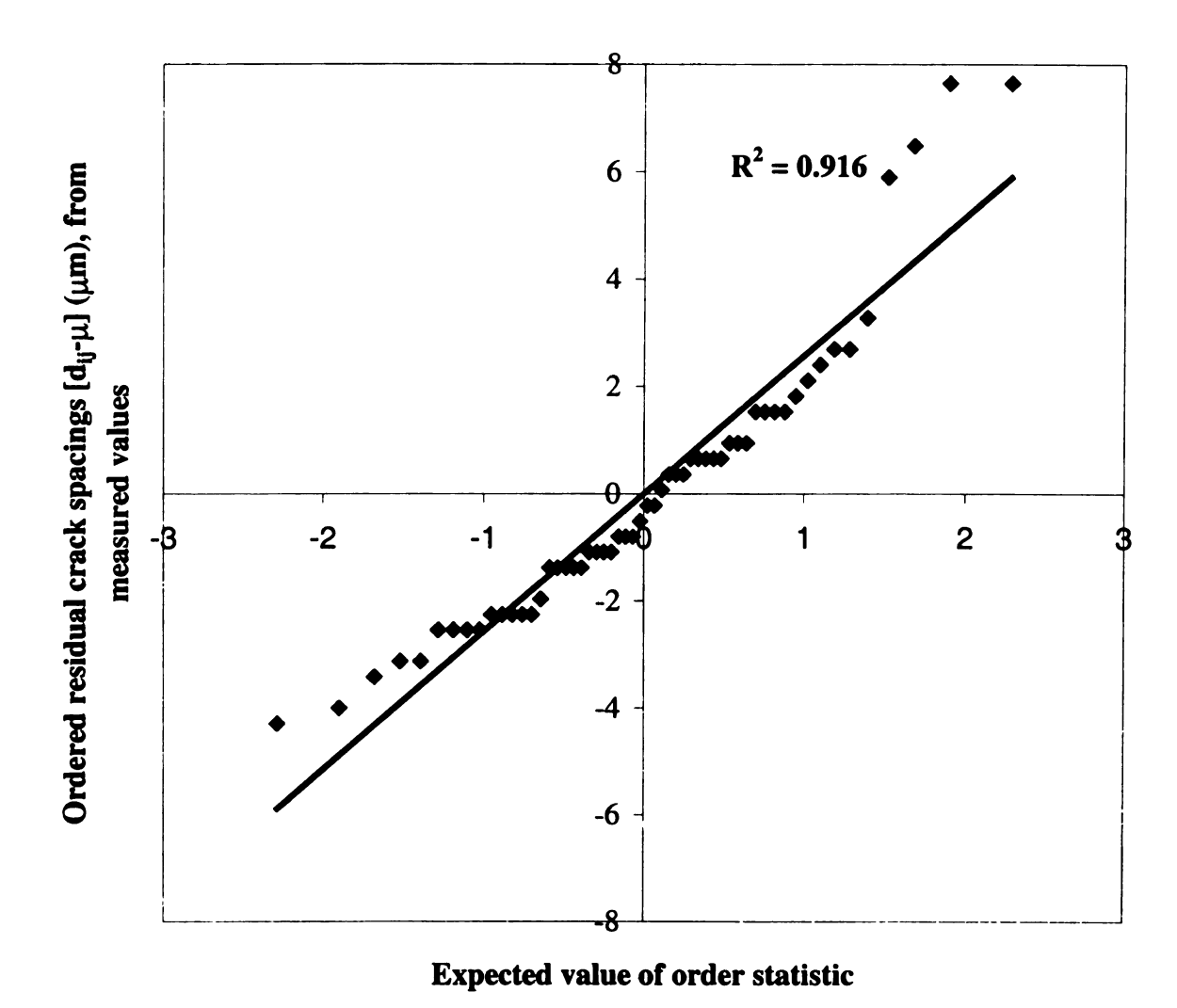


Figure 49. For the distance between the i^{ih} and jth crack, d_{ij}, ordered residual spacings versus expected value of ordered statistics for a 98 N indent on a coated BMI specimen cured at 175°C for one hour (CR3, Appendix C) with an abraded silica film.

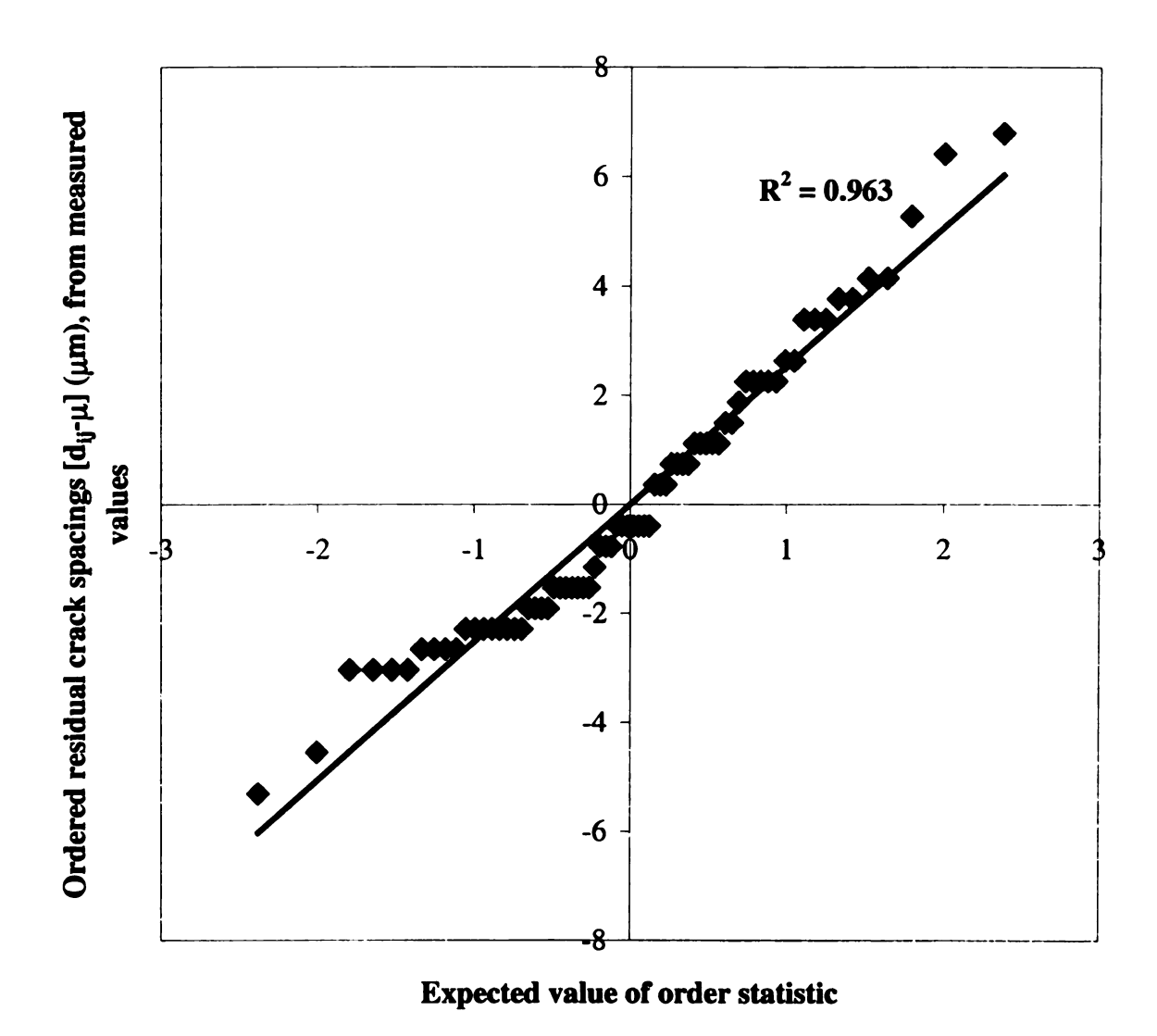


Figure 50. For the distance between the ith and jth crack, d_{ij}, ordered residual spacings versus expected value of ordered statistics for a 196 N indent on a coated BMI specimen cured at 175°C for one hour (CR3, Appendix C) with an abraded silica film.

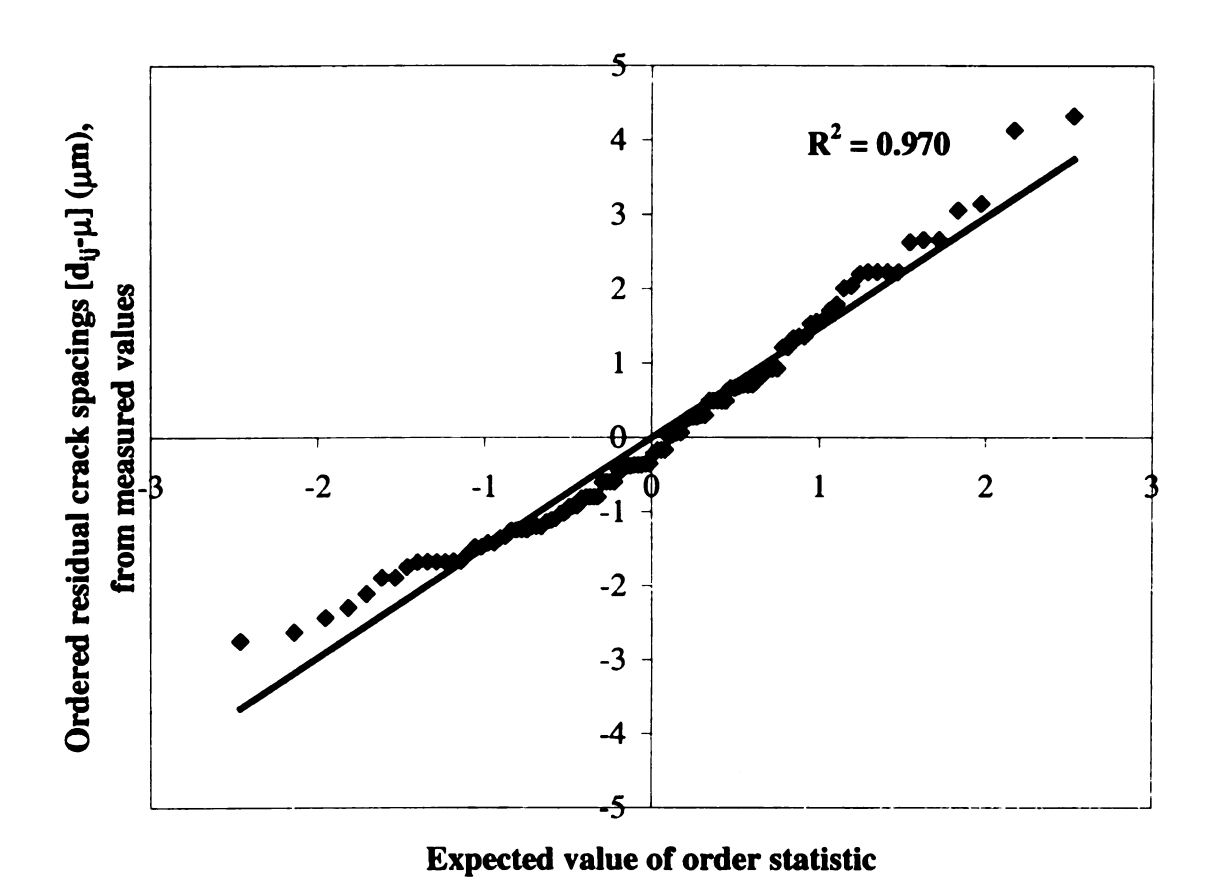


Figure 51. For the distance between the ith and jth crack, d_{ij}, ordered residual spacings versus expected value of order statistics for a Rockwell indent on a coated BMI specimen (SUA3, Appendix C), with an unabraded silica film.

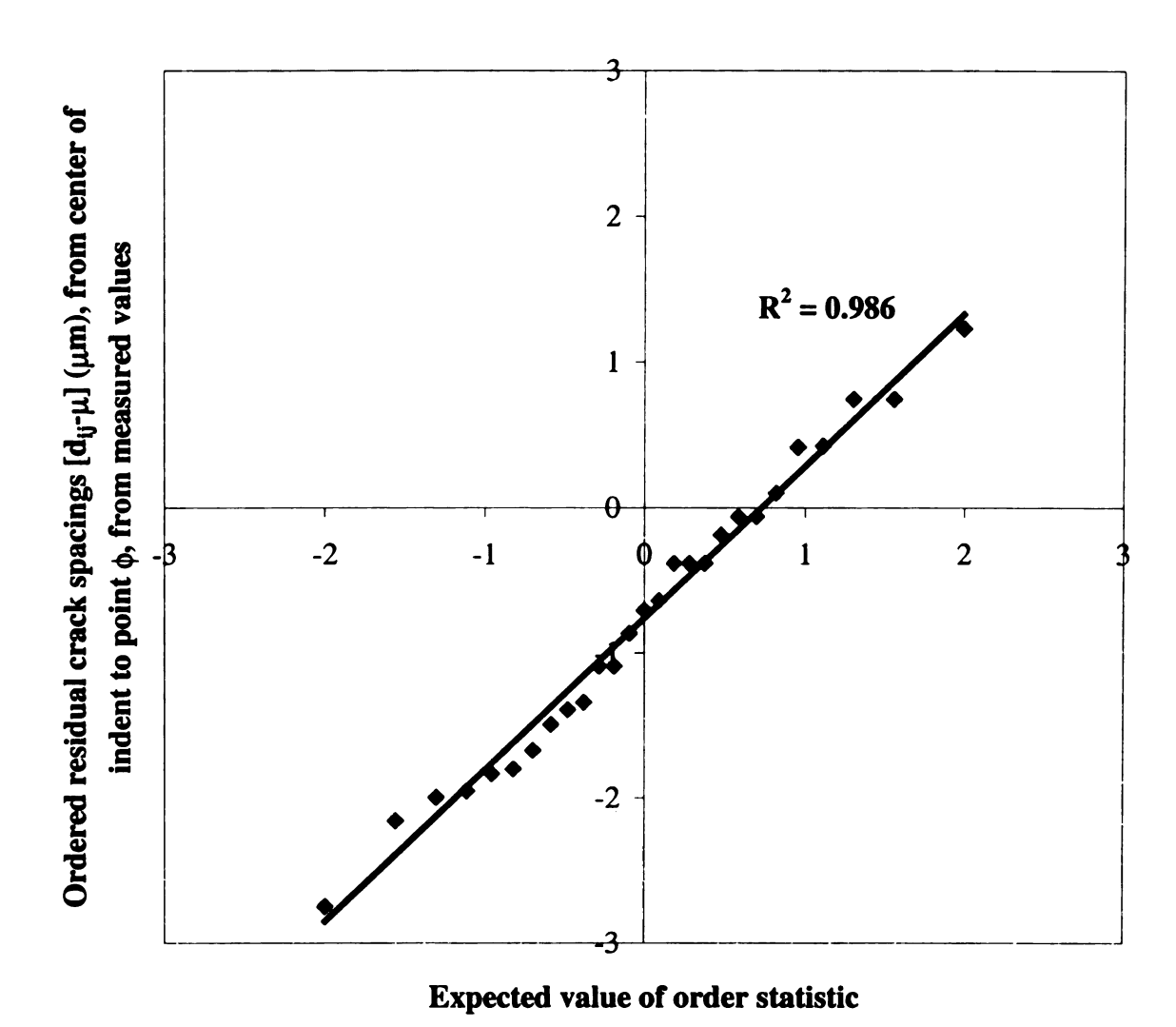


Figure 52. For the distance between the i^{th} and j^{th} crack, d_{ij} , from the center of the indent until the point ϕ , ordered residual spacings versus expected value of order statistics for a 49 N Vickers indent on a coated BMI specimen (SUA1, Appendix C), with an unabraded silica film.

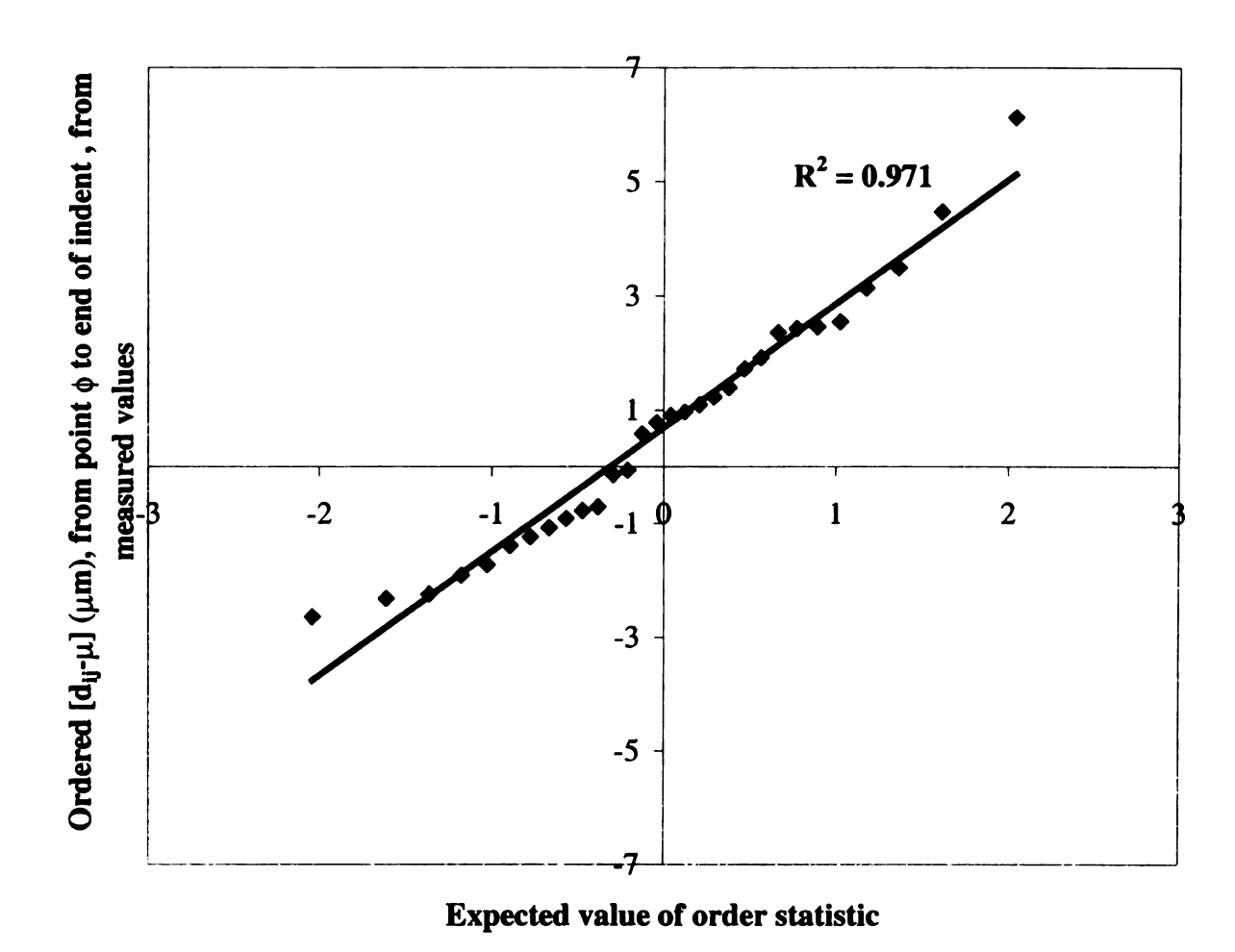


Figure 53. For the distance between the i^{th} and j^{th} crack, d_{ij} , from the point ϕ to the end of the indent, ordered residual spacings versus expected value of order statistics for a 49 N Vickers indent on a coated BMI specimen (SUA1, Appendix C), with an unabraded silica film.

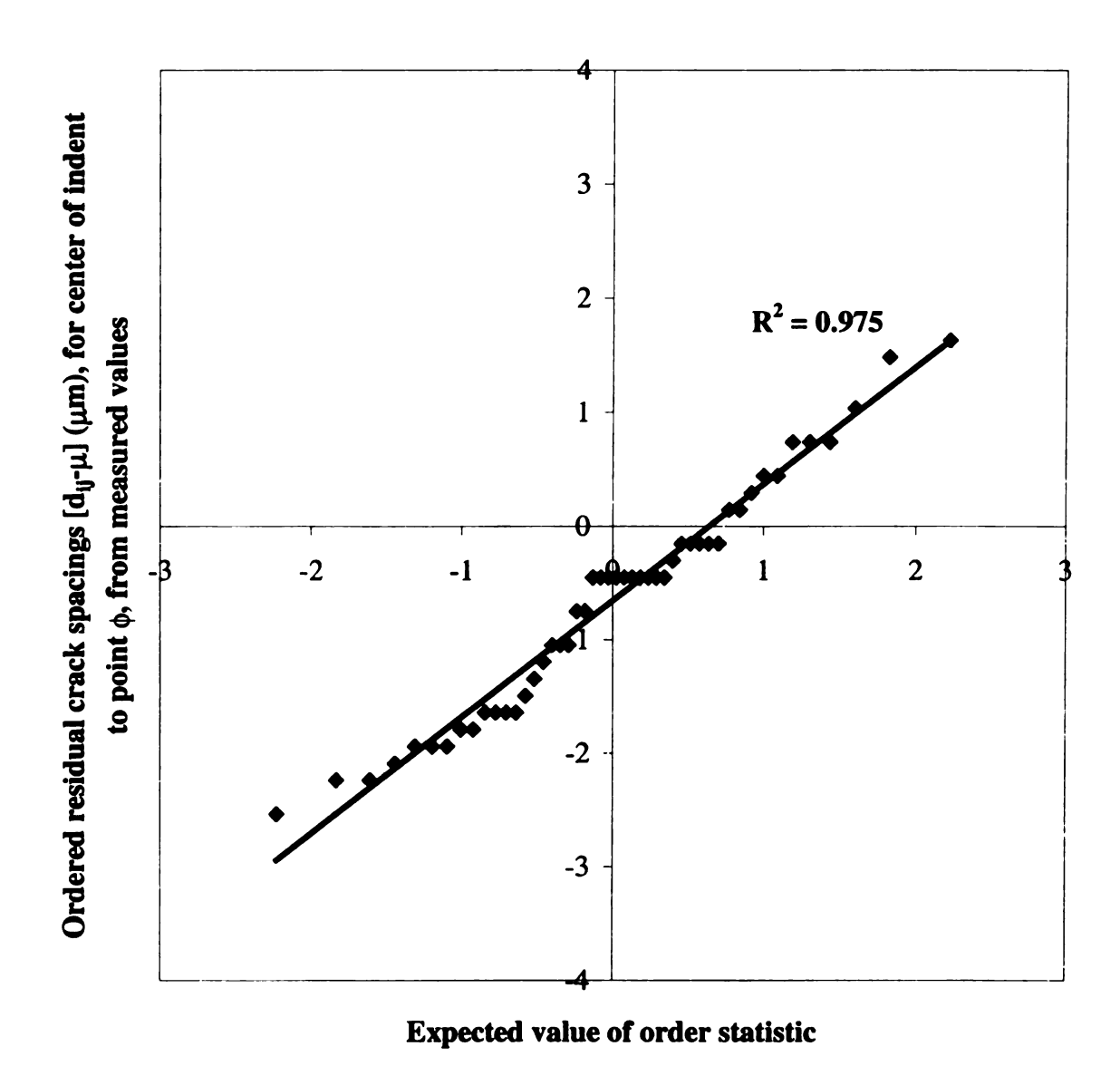
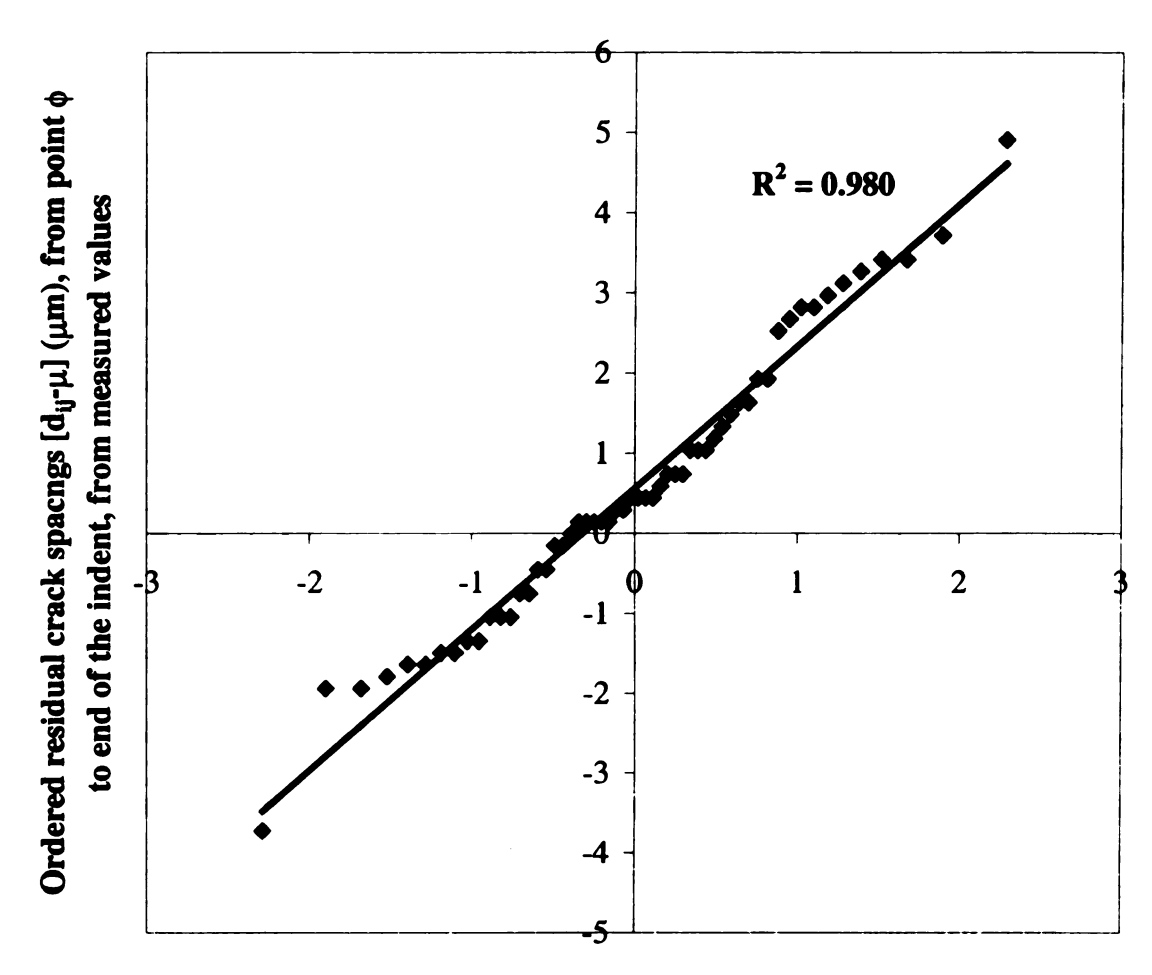


Figure 54. For the distance between the i^{th} and j^{th} crack, d_{ij} , from the center of the indent until the point ϕ , ordered residual spacings versus expected value of order statistics for a 196 N Vickers indent on a coated BMI specimen (SUA4, Appendix C), with an unabraded silica film.



Expected value of order statistic: Standard normal distribution

Figure 55. For the distance between the i^{th} and j^{th} crack, d_{ij} , from the point ϕ to the end of the indent, ordered residual spacings versus expected value of order statistics for a 196 N Vickers indent on a coated BMI specimen (SUA4, Appendix C), with an unabraded silica film.

3.6 Mass change measurements

An expression for the mass change as a function of time due to the diffusion of water into the BMI specimens can be developed by first considering the concentration C(x,t) for a semi-infinite medium with a planar interface [35] with the time independent concentration C_I defined as $C(0,t) = C_I$ and the initial concentration $C(x,0) = C_0$, then C(x,t) can be written as [35]

$$\frac{C(x,t) - C_1}{C_0 - C_1} = erf \frac{x}{2\sqrt{Dt}} \tag{11}$$

where $C_1 = C(0,t) = \text{time-independent}$ concentration at the planar interface and $C_0 = C(x,0) = \text{initial}$ concentration of diffusant in the host. From Fick's first law, the flux, J, of water diffusing into the BMI specimen (Figure 56) is related to the concentration gradient by [35]

$$J = -\left(D\frac{\partial C}{\partial x}\right)_{x=0} = \frac{D(C_0 - C_1)}{\sqrt{\pi Dt}}$$
 (12)

where D is the diffusivity of water in the BMI. The total mass of water, M_{τ} , which has diffused into BMI in time τ , is given by

$$M_{\tau} = \int_0^{\tau} J dt. \tag{13}$$

Upon integration M_{τ} can be written as

$$M_{\tau} = 2(C_0 - C_1)(\frac{Dt}{\pi})^{\frac{1}{2}} + k \tag{14}$$

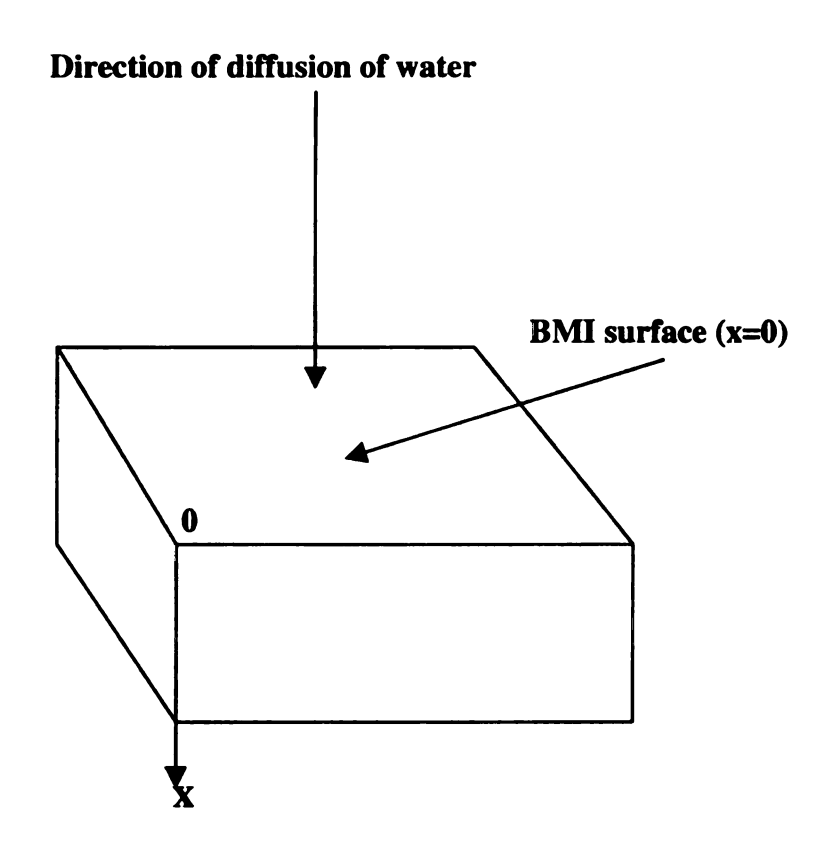


Figure 56. Schematic of the diffusion of water into the BMI during water immersion testing.

which displays parabolic kinetics (that is, the mass change is a function of the square root of time). Physically, the constant k corresponds to M_0 . In terms of the M_7 , we can rewrite equation (14) as

$$M_{\tau} - M_0 = 2(C_0 - C_1)(\frac{D}{\pi})^{\frac{1}{2}} \tau^{\frac{1}{2}}$$
 (15)

We define the normalized mass change M_N per unit surface area as

$$M_{N} = \frac{(M_{r} - M_{0})}{M_{0}A} \tag{16}$$

where M_{τ} is the instantaneous mass at time $t = \tau$, M_0 is the initial mass at time t = 0 hours, and A is the total specimen surface area. Thus the time dependence of M_{τ} can be written as in terms of M_N

$$M_{N} = \frac{(M_{\tau} - M_{0})}{M_{0}A} = \alpha t^{\frac{1}{2}}$$
 (17a)

In equation 17a, for t = 0, $M_N = 0$ since $M_{\tau} = M_0$ at time t = 0. However, we fit the M_N versus $t^{1/2}$ data to equation 17b

$$M_{N} = \alpha t^{\frac{1}{2}} + \beta \tag{17b}$$

where the coefficients α and β are determined from the least-squares fit, and β allows for a non-zero intercept of the regression line. The α values for coated and uncoated BMI (Table 11) show that at any time, t, the mass change of coated BMI will be less than the

uncoated BMI. Comparing with equation (15), we can see that physically the coefficient α corresponds to

$$\alpha = 2 \frac{(C_0 - C_1)}{M_0 A} (\frac{D}{\pi})^{\frac{1}{2}}$$
 (18)

Thus, α is the slope of the M_N versus $t^{1/2}$ curve (Figure 57), where α is a function of the concentration difference (C_0-C_I) as well as the diffusivity D, specimen surface area A, and initial specimen mass M_0 . A least-squares fit of the M_N versus $t^{1/2}$ data (Figure 57) shows a linear trend for both the coated and uncoated BMI, where coefficient of determination, R^2 , is 0.992 and 0.946 for the uncoated and coated specimens respectively.

If τ_{SAT} is the time required for the BMI to become saturated with water then for time $\tau << \tau_{SAT}$ we expect parabolic kinetics, as predicted by equation 14. In this study, after ten hours of immersion in water at 21°C the values of the relative mass change $\Delta M/M_0 = (M_\tau - M_0)/M_0$ were 0.0032 and 0.0048, for the uncoated and the coated specimens, respectively. However, for BMI at water saturation, $\Delta M_{SAT}/M_0 = (M_{SAT} - M_0)/M_0$ = about 0.04 to 0.05 [17], where M_{SAT} denotes the specimen mass in the water-saturated condition. Thus the relative mass change, $\Delta M/M_0$, observed in this experiment is about an order of magnitude less than $\Delta M_{SAT}/M_0$, which is again consistent with the parabolic kinetics, observed in this study [35].

As described in Section 3.2, "islands" of the silicate coating were observed by optical microscopy for the four specimen "edges" of the specimen, although the larger specimen surfaces were coated continuously and uniformly. The discontinuous silica coating on the four edges of the specimen was likely the reason that the moisture uptake

by the coated BMI specimens was higher than would be expected for a perfectly continuous coating. Methods for producing a more uniform silicate coating on all specimen surfaces, including the edges, will be explored in future work, including methods in which the coating is brushed or sprayed on the edges.

Table 11. Coefficients α and β obtained from the least-squares fit of equation (17b) to the M_N versus $t^{1/2}$ data.

| Uncoated | Coated | |
|----------|---|--|
| 4.2266 | 2.4172 | |
| 0.179 | 0.391 | |
| 4.24% | 16.16% | |
| 0.3652 | 0.6508 | |
| 0.318 | 0.401 | |
| 87% | 61.7% | |
| | 4.2266 0.179 4.24% 0.3652 0.318 | |

s.e.e = standard error estimate, determined by Sigmaplot^R software

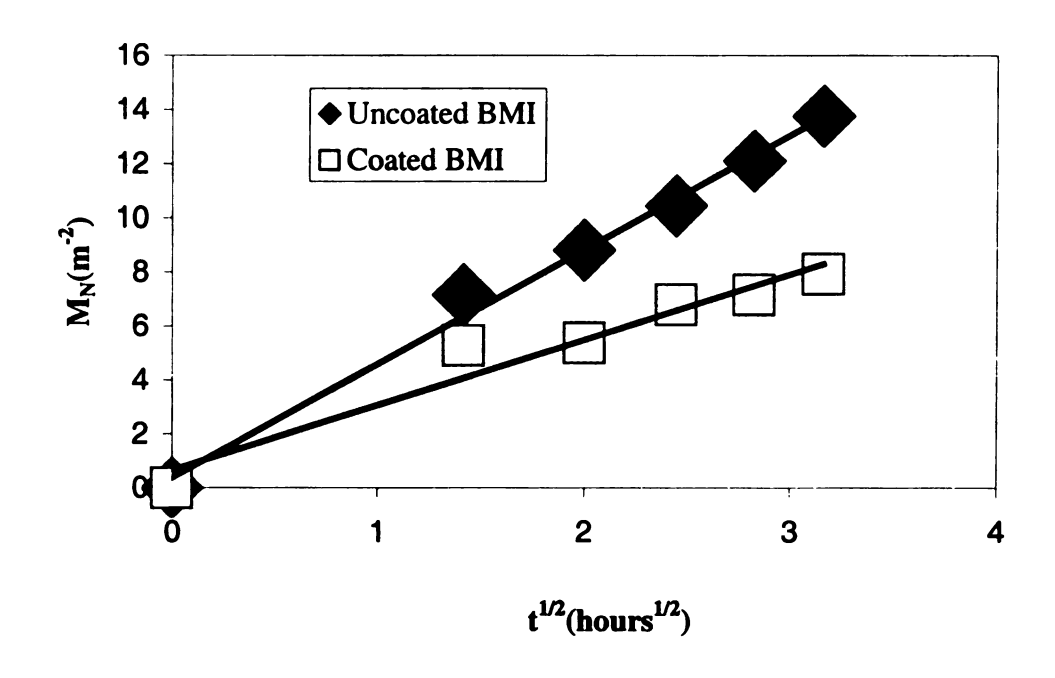


Figure 57. Normalized mass change, M_N , versus $t^{1/2}$ for BMI specimens with (a) all 6 sides coated and (b) uncoated BMI specimens (BMPM:DABPA = 1:0.82). The solid curves represent a least -squares fit of the data to equation (17b).

4. **CONCLUSIONS**

This study employed a total of 72 specimens in all. Using a spin-on process, neat (unreinforced) precured BMI polymeric substrates were coated with a silicate coating. Six specimens each of T1, T2, T3, T4 and three specimens of T7 (Appendix A) were used to determine coating thicknesses as a function of the spin-rate. Curing the coated specimen at 150°C for 20 minutes produced silicate coatings roughly 0.15 to 2.5 microns thick. The silica coating thickness decreases as the speed increases, however the coating thickness becomes relatively constant at 0.15 microns for spin rates greater than 3000 rpm.

The surfaces of six specimens each of T5, T6, T7 types (Appendix A) were observed using optical microscopy and scanning electron microscopy. For coating thickness in the thickness range between 1.66 (1000 rpm) to 2.5 microns (500 rpm), the coating was discontinuous. For coatings spun at 500 rpm and 1000 rpm, islands of silica coating (Figure 2) were observed. For the 500 rpm specimens the distance between the silica islands was on average about 12 microns, and for 1000 rpm specimen the distance between the islands was about 6.3 microns. Coatings spun at 1500 rpm (coating thickness ≈ 0.6 microns) had parallel cracks with spacings of about 100 to 150 microns with lengths ranging from 3 to 4 mm, with occasional side branching cracks that ranged in length from about 1mm to 2.5mm. Coating spun at 2000 rpm and greater speeds were uniform and continuous, and showed no cracking or gaps when observed using optical microscopy and scanning electron microscopy. For the BMI specimens included in this

study the minimum spinning speed required to obtain a uniform and continuous coating is approximately 2000 rpm.

For Vickers indentation experiments 12 specimens (Appendix D) were used, of which 4 were uncoated. A concentric, diamond shaped array of cracks were induced in the silica coatings upon loading with a Vickers indentor (Figures 4b, 7a, 7band 8). Over a load range from 0.098 N to 196 N the diagonal length of the crack array 2a (Figures 4b, 5a, and 5b) for the coated specimens were essentially identical to the radial crack length for the uncoated specimens (Figures 4a, 5a and 5b). Within the crack array there was only very minor spalling of the coating from the BMI substrate (roughly 22 percent) and coating delaminations were not observed in any of the indents (Figure 10), but one indentation (Figure 11).

Vickers indentation dimension was found to be independent of indentation load times in the range of 5 seconds to 35 seconds (Figure 12). These dimensions were measured right after making the indents and also 72 hours later. The recovery after 72 hours was minimal (Figure 12). Thus the BMI is not viscoelastic enough to affect the indentation dimension readings with loading time, which is used to determine hardness values using equation (2). Also varying loading rate experiments were carried out, and the indentation dimension did not change much with loading rate (13).

Two coated BMI specimens (Appendix E) were indented using a Rockwell-F scale, which uses a steel ball indentor with a diameter of 1.5875*10⁻³ and a load of 588N.

A concentric, circular shaped array of cracks was produced, and no delamination was

observed. Fraction of the region spalled of was 0.08. Thus, it appears that the silica coatings adhered exceptionally well to the polymeric substrates.

Seven specimens (Appendix C) in all were studied for observing the crack spacings. Since the MSF values for the silica coated BMI specimens cured at 150^{0} C for twenty minutes ranged between 0.97 to 1.02 (Table 7, Section 3.5.1) we can say that the mean spacing is a very weak function of the indentation load if at all. Also the mean crack spacing for the rockwell indent was within \pm 2% of the various vickers indents (Table 7, Section 3.5.1). Thus on changing the indentor material and shape the mean crack spacing did not change much. Thus mean crack spacings was independent of the indentation load and material for BMI specimens with unabraded and abraded coatings cured at 150^{0} C for twenty minutes.

However for BMI specimens with unabraded coatings cured at 175° C for one hour (Appendix C, CR3), the mean crack spacing increased with indentation loads and was 47% greater than BMI with coatings cured at 150° C for twenty minutes at the highest load of 196 N. The mean crack spacing normalized with respect to half the total crack dimension when plotted against indentation load shows a power law relationship $u/a = \omega P^{\epsilon}$

for the two different curing temperatures, with similar pre-exponential factors of $\phi = 0.123 \pm 0.005$ and $\phi = 0.1224 \pm 0.006$ for curing conditions of 175^{0} C/1 hour and 150^{0} C/20 minutes respectively. However the exponent, ϵ , was significantly different for the two different curing conditions. For the 175^{0} C/1 hour and 150^{0} C/20 minute curing conditions the, ϵ , were $\epsilon = -0.4153 \pm 0.0230$ and -0.4153 ± 0.0253 respectively. Thus the exponent ϵ , may be varying with curing conditions.

The scatter in crack spacings is considerably reduced when the coating is abraded and the crack region seems to be bigger than that of the unabraded specimen (Section 3.5.2). The scatter in crack spacing is more towards the end of the crack region than near the indent (Section 3.5.3). The residual distribution is pretty much normal from the ordered statistics plot (Section 3.5.4).

For mass absorption experiments eight specimens (Appendix B) were studied, 4 of which were coated and 4 uncoated. The extent of water absorption was 1.7 times more for the coated BMI compared to the uncoated BMI (Figure 56). For immersion in deionized water at 21°C for 10 hours, M_N, the normalized mass change per unit surface area (equation 16) was 13.64 m⁻², for the uncoated BMI and 8.06 m⁻² for the coated BMI. The larger than expected mass change M_N for the coated BMI may be related to gaps in silica coating on the edges of the specimen.

5. FUTURE STUDIES

Future work should include coating BMI substrates with coatings having other chemistries (i.e. other than silicate coatings). Silica coating on substrates other than BMI should be investigated and a comparison made with the silica/BMI system, which would be of interest from an application and even, from a scientific point of view.

The silica coating should be subjected to more severe chemical and environmental attacks, than just absorption of DI water. A model connecting coating thickness, indentation load, crack spacings and surface strains should be developed. Reasons for why the silica coating adheres to the BMI substrate must be investigated thoroughly.

The effect of different curing temperatures on the exponent, ε , in equation 5 (Section 3.5.1), needs to be further investigated, to come up with an explanation for how the different curing conditions are related to the exponent ε .

The percentage of coating that spalls of on indentation for BMI with coatings cured at of 175°C ranges from 2% to 5%. An attempt to further reduce the percentage of coating that spalls off on indentation should be made, as that would show enhanced adhesion of silica coating to the BMI.

LIST OF REFERENCES

- 1. J. B. Park and R. S. Lake, pp. 154-155, 167 in <u>Biomaterials</u>, Second Edition, Plenum Press, New York (1992).
- 2. R. J. Crawford, Chapter One in <u>Plastics Engineering</u>, Second Edition, Pergamon Press, Oxford (1987).
- 3. M. Moskowitz, "Only the Strong Survive (fillers and reinforcements)", Plastics World, 51[3]: 47 50 (1993).
- 4. P. Duchatelard, G. Baud, J. P. Besse and M. Jacquet, "Alumina coatings on PMMA Optimization of adherence", Thin Solid Films, 250 [1-2]: 142-150 (1994).
- 5. P. Duchatelard, G. Baud, J. P. Besse, C. Caperaa and M. Jacquet, "Composition and adhesion strength of alumina coatings on PMMA", Vide-Science Technique Et Applications, 272, 614-617, Suppl. S (1994).
- 6. P. Duchatelard, G. Baud, J. P. Besse and M. Jacquet, "Plasma treatment and alumina coating for improved wettability of PMMA Journal of Dental Research, 74 [3]: 940 (1995).
- 7. R. J. Morgan, R.J. Jurek, A. Yen and T. Donnellan, Polymer, 34, 835 (1993).
- 8. M. A. Chaudhari, T. Galvin and J. King, SAMPE J., 21, 17 (1985).
- 9. B. J. Lee, M.A. Chaudhari and V. Blyakham, Polymer News, 13, 297 (1988).
- 10. Zahir, M.A. Chaudhari and J. King, Makromol. Chem., Macromol. Symp., 25, 141 (1989).
- 11. R. J. Morgan, "Thermal Characterization of Composites," in "Thermal Analyses of Polymers," Ed. E. Turi, Academic Press, New York, NY, Ch. 9 (1997).
- 12. R. J. Morgan, L.T. Drzal, A. Lee, and E.E. Shin, "Characterization of Critical Fundamental Aging Mechanisms of High Temperature Polymer Matrix Composites" AFOSR grant (1994-97).
- 13. R. J. Morgan, In "Advances in Polymer Science," Volume 12, "Epoxy Resins and Composites, I," K. Dusek, Ed., Springer-Verlag, Ch. 1., (1985).
- 14. Ciba-Geigy, Plastics Department, Product Data Sheet, Matrimid 5292 System, (1985).

- 15. E. E. Shin, R. J. Morgan, J. Zhou, J. E. Lincoln, R. J. Lurek and D. B. Curliss, "Hygrothermal durability and thermal aging behavior prediction of high temperature polymer matrix composites and their resins", Proceedings of the American Ceramic Society for composites, Twelfth Technical Conference, pp. 1113-1122 (1997).
- 16. J. E. Lincoln, A. Lee, R. J. Morgan and E. E. Shin, "Effects of cure and initial monomer stoichiometry on the moisture absorption behavior of Bismaleimide composite matrices", To be submitted to SAMPE Journal of Advanced Materials.
- 17. J. E. Lincoln, "Effects of cure and initial monomer stoichiometry on the physical, thermal and mechanical properties of Bismaleimide resins", B. S. Thesis, Michigan State University, pp. 103-106 (1998).
- 18. C. A. Gamlen, E. D. Case, D. K. Reinhard and B. Huang, "Adhesion of polycrystalline diamond thin-films on single-crystal silicon substrates", Applied Physics Letters, 59 [20]: 2529-2531 (1991).
- 19. D. G. Lee, J. M. Fitz-Gerald, and R. K. Singh, "Novel method for adherent diamond coatings on cemented carbide substrates", Surface and coatings technology, 101 [1-3]: 187-191 (1998).
- 20. D. F. Diao, K. Kato K and K. Hokkirigawa, "Fracture mechanisms of ceramic coatings in Indentation", Journal of Tribology-Transactions of the ASME, 116 [4]: 860-869 (1994).
- 21. B. R. Lawn, B. J. Hockey and H. Richter, "Indentation analysis application in the strength and wear of brittle materials", Journal of Microscopy Oxford, 130, 295-308 (1983).
- 22. G. E. Dieter, "Mechanical Metallurgy", McGraw Hill Book Company, New York, Second Edition, Page 509 (1976).
- 23. I. M. Low, G. Paglia and C. Shi, "Indentation responses of viscoelastic materials", Journal of applied polymer science, 70 [12]: 2349-2352 (1998).
- 24. B. R. Lawn, T. R. Jensen and A. Arora, "Brittleness as an indentation size effect", Journal of Materials Science, 11 [3]: 573-576 (1976).
- 25. B. R. Lawn and D. B. Marshall, "Hardness, toughness, and brittleness Indentation analysis", Journal of the American Ceramic Society, 62 [7-8]:347-350 (1979).
- 26. J. Li, E. T. Thostenson, T. W. Chou and L. Riester, "An investigation of thin-film coating/substrate systems by nanoindentation", Journal of Engineering Materials and Technology-Transactions of the ASME, 120 [2]: 154-162 (1998).

- 27. G. W. Mclellan and E. B. Shand, "Glass Engineering Handbook", McGraw Hill Book Company, New York, Third Edition, Chapter 2, Page 2-20, 1984.
- 29. A. Flores, F. J. B. Calleja and H. R. Kricheldorf, "Mechanical study of sintered aromatic polyesters as revealed by microindentation measurements, "Journal of Materials Science", 33 [14]: 3567-371 (1998).
- 30. G. H. Michler, M. Ensslen, F. J. Balta-Calleja, L. Konczol and W. Doll, "Mechanical properties of crazes investigated by ultramicrohardness", Philosophical magazine A Physics of condensed matter structure defects and mechanical properties, 79 [1]: 167-178 (1999).
- 31. B. J. Briscoe, L. Fiori and E. Pelillo, "Nano-indentation of polymeric surfaces", Journal of Physics D Applied Physics, 31 [19]: 2395-2405 (1998).
- 32. G. M. Pharr, "Measurement of mechanical properties by ultra-low load indentation", Materials Science and Engineering A Structural materials properties microstructure and processing, 253 [1-2]: 151-159 (1998).
- 33. J. Suwanprateeb, "A comparision of different methods in determining load and time dependence of Vickers hardness in polymers", Polymer Testing, 17 [7]: 495-506 (1998).
- 34. W. Volk, Statistics for engineers, McGraw Hill Book Company Inc., New York, 145-152 (1958).
- 35. J. Mandel, "Statistical analysis of experimental data", Interscience publishers, New York, 1964.
- 36. J. Crank, Mathematics of Diffusion, pp. 30-31, Clarendon Press, Oxford, pp 84-95 (1956).

Appendix A.

Table A. Curing and coating conditions for specimens used to measure coating thicknesses (Section 3.2).

| Specimen | Pre curing temp(°C) /time (hours) | Coati speed range (rpm) | : | Coating time (seconds) | Curing temp(°C) /time (mins) | No. of specimens | Dimensions l×b×h cm ³ |
|----------|---|----------------------------------|----|------------------------------|---------------------------------------|------------------|----------------------------------|
| *T1 | 200/1 | 500 4000 | to | 20 | 150/20 | 6 | 1×1×0.45 |
| *T2 | 200/1 | 500 4000 | to | 20 | 150/20 | 6 | 1×1×0.38 |
| *T3 | 200/1 | 500 4000 | to | 20 | 150/20 | 6 | 1×1×0.38 |
| **T4 | 200/1 | 500 4000 | to | 20 | 150/20 | 6 | 1×1×0.41 |
| *T5 | 200/2 | 500 4000 | to | 20 | 150/20 | 6 | 1×0.8×0.33 |
| **T6 | 200/1 | 500 4000 | to | 20 | 150/20 | 6 | 1×1×0.41 |
| ***T8 | 200/1 | 500 4000 | to | 201 | 150/20 | 6 | 1×1×0.36 |
| ***T8 | 200/1 | 500 4000 | to | 20 | 150/20 | 6 | 1×1×0.36 |

^{*} T1, T2, T3 and T5 specimens had a BMPM:DABPA = 1:1.13

^{* *} T4 and T6 specimens had a BMPM:DABPA = 1:1

^{****} T7 and T8 had a BMPM:DABPA = 1:0.82

Appendix B.

Table B. Curing and coating conditions for specimens used in mass absorption experiments, along with dimensions and time of water immersion (Section 3.6).

| Specimen* | Precuring temp(°C)/ time (hours) | Coating speed (rpm)/ Time (seconds) | Curing temp(°C)/ time (mins) | Time of immersion in water (hours) | Dimensions l×b×h cm ³ |
|-----------|---|-------------------------------------|---------------------------------------|------------------------------------|-------------------------------------|
| WC1 | 265/1 | 3000/20 | 150/20 | 10 | 1×1×0.42 |
| WUC1 | 265/1 | Uncoated | 150/20 | 10 | 1×1×0.42 |
| WC2 | 265/2 | 3000/20 | 150/20 | 10 | 1×1×0.42 |
| WUC2 | 265/2 | Uncoated | 150/20 | 10 | 1×1×0.42 |
| WC3 | 200/2 | 3000/20 | 150/20 | 10 | 1×1×0.42 |
| WUC3 | 200/2 | Uncoated | 150/20 | 10 | 1×1×0.42 |
| WC4 | 265/1 | 3000/20 | 150/20 | 500 | 1×1×0.42 |
| WUC4 | 265/1 | Uncoated | 150/20 | 500 | 1×1×0.42 |

^{*}All specimens had a BMPM:DABPA = 1:0.82

Appendix C.

Table C1. Curing and coating conditions for specimens used in scatter spacing measurements, along with mean spacing values at different loads (Section 3.5).

| Specimen* | Precuring temp(°C)/ time (mins) | Coating speed (rpm)/ time (seconds) | Curing temp(°C)/ time (mins) | Abraded (Yes/No) | Number of indents |
|-----------|--|-------------------------------------|---------------------------------------|---------------------|-------------------------|
| SUA1** | 200/60 | 4000/20 | 150/20 | NO | 8 |
| SUA2** | 200/60 | 4000/20 | 150/20 | NO | 8 |
| SUA3*** | 200/60 | 4000/20 | 150/20 | NO | 8 |
| SUA4** | 200/60 | 4000/20 | 150/20 | NO | 2 |
| SA1** | 200/60 | 4000/20 | 150/20 | YES | 8 |
| SA2** | 200/60 | 4000/20 | 150/60 | YES | 4 |
| CR3! | 200/60 | 4000/20 | 175/60 | NO | 6 |

^{*} All specimens had a BMPM:DABPA = 1:1

^{* *} SUA1, SUA2, SUA4, SA1, and SA2 were used to make Vickers indents only

^{***} SUA3 was used to make the Hertzian indent only

[!] CR3 specimen was also used in spalling area fraction calculations

Table C2. R-square values for order statistics plots for indentations made on specimens listed in table C1.

| Indentation | SUA1 | SUA4 | SUA3 | SA1 | CR3 |
|-------------------|----------------------|----------------------|----------------------|----------------------|----------------------|
| Load | (R ²) |
| (N) | | 0.904 | | | 0.932 |
| 2.94 | | (Figure 37) | | | (Figure 46) |
| 4.9 | | 0.941 (Figure 38) | | | 0.938 (Figure 47) |
| 9.8 | 0.937 (Figure 39) | | | 0.986 (Figure 43) | 0.953 (Figure 48) |
| 49 | 0.938 (Figure 40) | | | 0.953 (Figure 44) | 0.936 (Figure 49) |
| 98 | | 0.938 (Figure 41) | | | 0.916 (Figure 50) |
| 196 | | 0.963 (Figure 42) | | | 0.963 (Figure 51) |
| 588 (Rockwell) | | | 0.970 (Figure 45) | | |

Appendix D.

Table D. Curing and coating conditions for specimens used to make Vickers Indentations and study effect of not precuring specimens (Section 3.3.42 and Section 3.3.4).

| Specimen | Precuring temp(°C)/ time (hours) | Coating speed (rpm)/ Time(s) | BMPM: DABPA | Curing temp(°C) /time (mins) | Load range (N) | Dimensions l×b×h cm ³ |
|---------------|---|------------------------------|----------------|---------------------------------------|-------------------|-------------------------------------|
| A | 200/1 | Uncoated | 1:1 | 150/20 | 2.94-196 | 1×1×0.45 |
| В | 200/1 | 3000/20 | 1:1 | 150/20 | 2.94-196 | 1×1×0.38 |
| С | 200/1 | 4000/20 | 1:1 | 150/20 | 2.94-196 | 1×1×0.45 |
| D | 200/1 | Uncoated | 1:0.82 | 150/20 | 2.94-196 | 1×1×0.38 |
| E | 200/1 | 3000/20 | 1:0.82 | 150/20 | 2.94-196 | 1×1×0.38 |
| A1 | 200/1 | Uncoated | 1:1 | 150/20 | 0.245-9.8 | 1×1×0.38 |
| B1 | 200/1 | 3000/20 | 1:1 | 150/20 | 0.245-9.8 | 1×1×0.38 |
| C1 | 200/1 | 4000/20 | 1:1 | 150/20 | 0.245-9.8 | 1×1×0.38 |
| F3 | 200/1 | Uncoated | 1:1.13 | 150/20 | 2.94-196 | 1×1×0.45 |
| F4 | 200/1 | 3000/20 | 1:1.13 | 150/20 | 2.94-196 | 1×1×0.45 |
| G1 | 200/1 | 3500/20 | 1:1 | 150/20 | 588 | 1×1×0.36 |
| G2 | 200/1 | 3500/20 | 1:1 | 150/20 | 588 | 1×1×0.36 |
| K1 Ki-yong | Not pre | 3000/20 | 1:1 | 150/20 | 9.8-98 | 1×1×0.36 |
| K2 | 200/1 | 3000/20 | 1:1 | 150/20 | 9.8-98 | 1×1×0.45 |

Ar Ta (S

1

Appendix E.

Table E. Curing and coating conditions for specimens used to study Hertzian indents (Section 3.4).

| *Specimen | Pre curing temp(°C) /time (hours) | Coating speed (rpm) | Coating time (seconds) | Curing temp(°C)/ time (mins) | No. of indents | Dimensions l×b×h cm ³ |
|-----------|---|---------------------|------------------------------|---------------------------------------|----------------|-------------------------------------|
| R1 | 200/1 | 3500 | 20 | 150/20 | 3 | 1×1×0.45 |
| R2 | 200/1 | 3500 | 20 | 150/20 | 3 | 1×1×0.45 |

^{*}All specimens had a BMPM:DABPA = 1:1.13

Appendix F.

Table F. Curing conditions and dimensions for uncoated specimens used in varying load time and loading rate Vickers indentations (Section 3.3.5).

| Specimen | BMPM:DABPA | Precuring temp(°C)/time (hours) | Dimensions l×b×h cm ³ |
|----------|------------|---------------------------------|-------------------------------------|
| L1 | 1:1 | 200/1 | 1×1×0.45 |
| L2 | 1:0.82 | 200/1 | 1×1×0.45 |
| L3 | 1:1.13 | 200/1 | 1×1×0.45 |

Appendix G.

Table G. Curing and coating conditions for specimens used to calculate fractional spalled of area from indentations (Section 3.3.3).

| *Specimen | Pre curing temp(°C) /time (hours) | Coating speed (rpm)/ Time (s) | Curing temp(°C)/ Time (mins) | No. of indents | Dimensions l×b×h cm ³ |
|-----------|---|-------------------------------|---------------------------------------|----------------|-------------------------------------|
| CR1 | 200/1 | 3500/20 | 150/20 | 24 | 1×1×0.45 |
| CR2 | 200/1 | 3500/20 | 150/20 | 30 | 1×1×0.45 |
| CR3! | 200/1 | 3500/20 | 175/60 | 24 | 1×1×0.45 |
| CR4 | 200/1 | 3500/20 | 175/60 | 30 | 1×1×0.45 |

^{*} All specimens had a BMPM:DABPA = 1:1

[!] CR3 specimen also used in crack spacing measurements

Appendix H. Visual basic macro program to determine point ϕ , corresponding to the lowest P value in a set of crack spacings for any given indentation load (Section 3.5.3). The program compares a series of P values comparing two sets for the same indent and returns the minimum P value obtained. Section 3.5.3 describes the procedure in detail.

Private Sub CommandCancel_Click()

FormTestSeries.Hide

End Sub

Private Sub CommandOkay_Click()

Dim ThisSheet As Worksheet

D im FTestResults As Range

Dim RangeNum As Integer

Dim RangeS, RangeE As Integer

Dim NOver3 As Integer

Dim FTestR As Double

Dim TopEnd, BottomStart As Integer

RangeS = Val(Right(RangeStart.Text, Len(RangeStart.Text) - 1))

RangeE = Val(Right(RangeEnd.Text, Len(RangeEnd.Text) - 1))

Col = Left(RangeStart.Text, 1)

RangeNum = RangeE - RangeS + 1

NOver3 = Int(RangeNum / 3)

TopEnd = RangeS + NOver3

BottomStart = RangeE - NOver3

Worksheets(TextSheetName.Text).Activate

Set ThisSheet = Worksheets(TextSheetName.Text)

Set Results = Worksheets.Add

Set FTestResults = Results.Range("A1:A" & NOver3)

Do While BottomStart > NOver3

FTestR = Application.WorksheetFunction.FTest(ThisSheet.Range(RangeStart.Text & ":"

& Col & Format(TopEnd)), ThisSheet.Range(Col & Format(BottomStart) & ":" &

RangeEnd.Text))

FTestResults(TopEnd - RangeS - NOver3 + 1, "A") = FTestR

BottomStart = BottomStart - 1

TopEnd = TopEnd + 1

Loop

MinFTest = Application.WorksheetFunction.Min(FTestResults)

FTestResults(1, "B") = MinFTest

MsgBox (MinFTest)

FormTestSeries.Hide

End Sub

Appendix I.

Table I. Raw crack spacings data for 2.94 N and 4.9 N indentation loads for BMI specimen with unabraded silica coating cured at 150°C for 20 minutes (Figures 20 and 21) and 175°C for one hour (Figures 28 and 29).

| SUA1 (2.94 N) | CR1 (2.94 N) | SUA1 (4.9 N) | CR1 (4.9 N) |
|---------------|--------------|--------------|-------------|
| 7.1 | 6.4 | 4.2 | 9.1 |
| 3.1 | 3.2 | 5.3 | 4.7 |
| 3.1 | 3.2 | 4.7 | 5.8 |
| 5.1 | 3.5 | 6.5 | 4.1 |
| 5.1 | 3.5 | 2.4 | 3.7 |
| 4.0 | 4.7 | 8.1 | 5.1 |
| 4.9 | 6.9 | 3.3 | 7.9 |
| 4.2 | 7.9 | 9.2 | 2.9 |
| 6.2 | 5.9 | 3.4 | 3.7 |
| 10.0 | 5.2 | 3.4 | 4.9 |
| 2.0 | 4.4 | 2.1 | 8.1 |
| 3.5 | 4.2 | 5.1 | 9.1 |
| | | 8.1 | 7.2 |
| | | 4.4 | 4.6 |
| | | 5.1 | 2.1 |
| | | 2.3 | 3.4 |
| | | 6.1 | |
| | | 3.3 | |

Appendix J.

Table J. Raw crack spacings data for 9.8 N and 49 N indentation loads for BMI specimen with unabraded silica coating cured at 150°C for 20 minutes (SUA1, Figures 22 and 23) and 175°C for one hour (CR1, Figures 30 and 31) and, BMI with abraded coating cured at 150°C for 20 minutes.

| SUA1 (9.8 N) | CR1 (9.8 N) | | SUA1 (49 N) | CR1 (49 N) | SA1 (49 N) |
|--------------|-------------|-----|-------------|------------|------------|
| 2.5 | 10.1 | 2.2 | 2.8 | 9.1 | 3.8 |
| 2.4 | 9.1 | 2.8 | 2.3 | 4.8 | 2.3 |
| 4.2 | 5.2 | 3.7 | 2.9 | 3.3 | 2.0 |
| 2.1 | 4.9 | 4.9 | 2.5 | 2.2 | 2.1 |
| 1.8 | 5.9 | 5.2 | 2.4 | 4.0 | 2.6 |
| 1.8 | 3.6 | 5.1 | 4.4 | 3.7 | 4.4 |
| 4.5 | 7.2 | 5.1 | 5.5 | 2.6 | 4.7 |
| 6.5 | 7.2 | 6.3 | 3.4 | 5.5 | 4.6 |
| 6.4 | 6.8 | 4.5 | 5.0 | 5.9 | 4.1 |
| 2.7 | 5.9 | 4.5 | 4.7 | 4.4 | 4.6 |
| 3.0 | 3.3 | 5.7 | 4.2 | 4.0 | 3.8 |
| 5.4 | 4.2 | 6.0 | 2.1 | 2.9 | 4.1 |
| 4.4 | 5.2 | 5.7 | 2.6 | 4.4 | 5.7 |
| 3.4 | 3.9 | 3.4 | 4.2 | 5.1 | 4.9 |
| 3.4 | 6.9 | 3.6 | 5.0 | 4.4 | 4.8 |
| 6.0 | 6.7 | 4.9 | 3.2 | 9.1 | 5.4 |
| 6.0 | 5.1 | 2.7 | 2.9 | 3.3 | 5.4 |
| 3.7 | 7.0 | 4.0 | 4.1 | 5.5 | 5.4 |
| 4.5 | 6.0 | 3.4 | 2.3 | 11.3 | 4.0 |
| 3.3 | | 4.5 | 3.2 | 6.2 | 4.0 |
| 3.5 | | 4.6 | 1.5 | 7.7 | 4.0 |
| 3.6 | | 4.8 | 4.7 | 4.8 | 5.4 |
| 8.7 | | 6.7 | 3.6 | 2.2 | 5.4 |
| 5.1 | | 4.9 | 3.9 | 2.9 | 5.4 |
| 5.9 | | 4.5 | 3.9 | 8.4 | 5.4 |
| 5.7 | | 5.5 | 3.9 | 13.9 | 4.9 |
| 3.1 | | 2.8 | 3.5 | 9.9 | 4.9 |
| 2.1 | | 3.1 | 5.5 | 8.8 | 4.5 |
| 3.3 | | 4.2 | 1.6 | 5.3 | 4.8 |
| 2.7 | | 3.4 | 5.2 | 8.1 | 5.4 |
| | | 2.5 | 4.8 | 4.1 | 2.1 |
| | | | 3.5 | 6.1 | 4.5 |
| | | | 7.7 | 6.5 | 4.2 |
| | | | 6.6 | 11.0 | 4.2 |

| | | 1.9 | 13.0 | 3.6 |
|----------|---|------|------|-----|
| | | 5.6 | 4.9 | 3.9 |
| | | 2.3 | 6.9 | 4.5 |
| | | 2.0 | 5.3 | 4.5 |
| | | 3.0 | 6.1 | 4.2 |
| | | 5.0 | 12.2 | 6.1 |
| | | 8.7 | 6.9 | 4.2 |
| | | 6.7 | 8.1 | 4.5 |
| | | 4.2 | | 5.7 |
| | | 5.2 | | 6.3 |
| | | 2.5 | | 4.8 |
| | | 6.2 | | 4.5 |
| <u> </u> | | 6.8 | | 4.8 |
| | | 3.5 | | 5.4 |
| | | 4.1 | | 3.0 |
| | | 10.3 | | 3.1 |
| | | 5.3 | | 3.0 |
| | | 6.0 | | 4.2 |
| | | 7.4 | | 3.9 |
| | | 2.9 | | 6.3 |
| | | 6.7 | | 5.4 |
| | | 3.3 | | 6.6 |
| | | 3.2 | | 5.4 |
| | | | | 5.5 |
| | | | | 4.2 |
| | | | | 2.2 |
| | | | | 5.0 |
| | | | | 4.2 |
| | | | | 4.2 |
| | | | | 4.6 |
| | | | | 4.7 |
| | | | | 4.1 |
| 1 | l | Li | | |

Appendix K.

Table K. Raw crack spacings data for 98 N and 196N indentation loads for BMI specimen with unabraded silica coating cured at 150°C for 20 minutes (SUA1, Figures 24 and 25) and 175°C for one hour (CR1, Figures 32 and 33).

| SUA1 (98 N) | C for one hour (CR1, F CR1 (98 N) | SUA1 (196 N) | CR1 (196 N) |
|-------------|--------------------------------------|--------------|-------------|
| 2.9 | 7.6 | 4.5 | 6.4 |
| 2.4 | 7.0 | 4.8 | 13.6 |
| 3.1 | 4.4 | 4.5 | 1.9 |
| 2.6 | 5.8 | 4.5 | 5.7 |
| 2.5 | 2.3 | 3.3 | 6.8 |
| 4.6 | 2.6 | 3.6 | 11.0 |
| 5.8 | 4.4 | 5.1 | 5.3 |
| 3.6 | 3.2 | 5.7 | 4.5 |
| 5.3 | 5.2 | 4.5 | 2.6 |
| 4.9 | 5.2 | 4.5 | 10.6 |
| 4.4 | 8.2 | 3.0 | 7.9 |
| 2.2 | 6.1 | 3.3 | 8.3 |
| 2.7 | 4.1 | 4.2 | 5.3 |
| 4.4 | 4.7 | 3.1 | 9.1 |
| 5.3 | 9.9 | 3.3 | 5.7 |
| 3.3 | 7.3 | 3.4 | 6.8 |
| 3.0 | 3.5 | 2.8 | 7.9 |
| 4.3 | 7.0 | 2.7 | 4.9 |
| 2.4 | 4.1 | 2.4 | 6.8 |
| 3.3 | 4.1 | 3.9 | 14.0 |
| 1.6 | 5.8 | 4.2 | 7.6 |
| 4.9 | 5.8 | 3.0 | 5.7 |
| 3.8 | 6.7 | 3.1 | 4.9 |
| 4.1 | 4.4 | 5.2 | 4.2 |
| 4.1 | 4.4 | 3.3 | 5.3 |
| 4.1 | 7.3 | 4.5 | 7.6 |
| 3.7 | 3.5 | 4.5 | 11.0 |
| 6.3 | 9.3 | 4.5 | 5.7 |
| 1.9 | 5.5 | 5.1 | 6.4 |
| 5.9 | 8.2 | 4.5 | 4.2 |
| 5.6 | 6.4 | 4.5 | 4.9 |
| 4.1 | 6.4 | 4.8 | 4.2 |
| 8.9 | 7.3 | 4.8 | 4.2 |
| 7.6 | 4.4 | 4.6 | 4.9 |
| 2.1 | 5.2 | 5.4 | 9.8 |

| 6.5 | 8.7 | 4.8 | 7.9 |
|------|------|-----|------|
| 2.7 | 7.0 | 5.4 | 4.9 |
| 2.3 | 7.6 | 5.7 | 12.5 |
| 3.5 | 5.5 | 6.5 | 6.4 |
| 5.8 | 5.5 | 6.4 | 8.7 |
| 10.0 | 8.2 | 4.8 | 6.1 |
| 7.7 | 7.3 | 3.9 | 7.6 |
| 4.8 | 14.3 | 3.0 | 6.8 |
| 6.0 | 13.1 | 3.7 | 6.8 |
| 2.9 | 9.0 | 5.7 | 4.9 |
| 7.1 | 12.5 | 6.0 | 8.3 |
| 7.8 | 14.3 | 3.9 | 4.9 |
| 4.0 | 5.2 | 2.7 | 4.5 |
| 4.7 | 5.2 | 5.1 | 4.5 |
| 11.9 | 4.1 | 5.1 | 5.7 |
| 6.1 | 9.3 | 3.1 | 4.5 |
| 6.9 | 7.3 | 7.7 | 5.3 |
| 8.5 | 5.5 | 6.8 | 6.8 |
| 3.3 | 8.4 | 4.2 | 9.8 |
| 7.7 | 7.6 | 3.4 | 8.7 |
| 3.8 | | 8.3 | 9.5 |
| 3.7 | | 5.4 | 8.3 |
| 7.9 | | 3.9 | 10.6 |
| 4.7 | | 6.5 | 8.3 |
| 3.2 | | 6.0 | 9.5 |
| 2.6 | | 6.4 | 11.3 |
| 5.9 | | 6.5 | 9.5 |
| 8.1 | | 5.7 | 11.3 |
| 2.4 | | 5.2 | 9.5 |
| 3.6 | | 6.8 | 10.6 |
| 6.2 | | 8.0 | 4.9 |
| 5.6 | | 5.1 | 9.5 |
| 4.3 | | 5.4 | 8.3 |
| 2.4 | | 5.1 | 5.7 |
| 2.1 | | 8.6 | 5.7 |
| 4.4 | | 6.1 | 6.8 |
| 6.3 | | 7.6 | 7.9 |
| 2.7 | | 3.3 | |
| 7.3 | | 3.6 | |
| 2.1 | | 5.4 | |

| 4.2 | 4.8 | |
|-----|------------|--|
| 8.1 | 6.0 | |
| 5.3 | 4.5 | |
| 4.7 | 9.8 | |
| 2.1 | 6.0 | |
| 6.9 | 7.9 | |
| 2.6 | 6.3 | |
| | 4.2 | |
| | 7.7 | |
| | 3.4 | |
| | 3.9 | |
| | 8.2 | |
| | 7.4 | |
| | 8.3 | |
| | | |
| | 5.2 4.9 | |
| | | |
| | 5.5 | |
| | 3.0 | |
| | 5.7 | |
| | 4.8 | |
| | 3.0 | |
| | 3.9 | |
| | 5.4 | |
| | 3.6 | |
| | 3.3 | |
| | 5.1 | |
| | 4.5 | |
| | 1.2 | |
| | 5.7 | |
| | | |

Appendix L.

Table L. Indent dimension raw data, which was included in Figures 5a and 5b. Averages of indent dimensions (6 to 10 indents) were taken, when plotting indentation dimension versus indentation load.

| Specimen | Indentation Load | Indent dimension – 2a | Average |
|----------|------------------|--|------------------------------------|
| | (A) | (μ m) | Indent |
| | (N) | | dimension |
| A | 2.94 | 132.2, 133.5, 135.8, 133.3, 135.4, | – 2a (μ m) 134.5 |
| A | 2.54 | 136.8, 132.8, 136.1 | 134.3 |
| A | 4.9 | 172.3, 176.1, 178.0, 177.6, 175.3, | 176.0 |
| A | 1.7 | 176.2, 175.8, 176.7 | 170.0 |
| A | 9.8 | 237.1, 235.8, 238.5, 238.9, 237.9, | 237.6 |
| | | 236.0, 238.8, 237.8 | |
| A | 49 | 521.1, 523.4, 527.4, 524.7, 525.2, | 524.4 |
| | | 523.6 | |
| A | 98 | 746.2, 741.1, 745.6, 748.3, 742.9, | 745.3 |
| | | 747.7 | |
| A | 196 | 1036.3, 1027.9, 1031.5, 1033.1, | 1031.9 |
| | | 1035.9, 1028.1 | |
| В | 2.94 | 120.2, 126.4, 121.1, 124.3, 120.4, | 122.3 |
| | ļ | 121.4, 123.1, 121.5 | |
| В | 4.9 | 170.1, 168.8, 167.2, 166.3, 166.1, | 167.7 |
| D | 0.0 | 170.4, 165.7, 166.9 | 220.5 |
| В | 9.8 | 238.1, 239.7, 241.6, 238.4, 242.3, 237.6, 238.0, 240.1 | 239.5 |
| В | 49 | 523.4, 526.1, 529.0, 527.9, 525.1, | 526.9 |
| D | 49 | 529.9 | 320.9 |
| В | 98 | 746.8, 751.1, 751.7, 749.2, 748.8, | 749.7 |
| D | | 750.6 | , , , , , |
| В | 196 | 1044.5, 1041.9, 1045.8, 1042.1, | 1043.4 |
| _ | | 1046.0, 1040.1 | |
| С | 2.94 | 134.9, 133.6, 132.0, 129.5, 129.8, | 132.5 |
| | | 133.2, 134.9, 132.1 | |
| C | 4.9 | 169.4, 167.2, 166.1, 168.9, 170.3, | 167.9 |
| | | 166.6, 169.4, 167.7 | |
| C | 9.8 | 226.7, 229.2, 234.1, 234.4, 232.4, | 231.1 |
| | | 228.7, 230.1, 233.3 | |
| C | 49 | 519.2, 516.5, 516.7, 521.3, 517.0, | 517.8 |
| | | 516.1 | |
| C | 98 | 740.7, 743.9, 747.6, 748.1, 740.2, | 744.3 |
| | | 746.2, 745.6 | 1015 |
| <u>C</u> | 196 | 1035.6, 1039.3, 1047.4, 1049.2, | 1042.3 |

| [| | 1044.5, 1038.8 | |
|----------|--------|---|----------------|
| D | 2.94 | | 122.0 |
| שו | 2.94 | 121.5, 125.2, 122.9, 126.8, 121.4, | 123.9 |
| D | 4.0 | 124.4, 1245.1, 122.8 | 165.5 |
| D | 4.9 | 166.2, 162.7, 173.3, 164.3, 163.8, | 165.5 |
| | + | 164.3, 166.2, 163.2 | |
| D | 9.8 | 235.6, 229.1, 233.2, 232.6, 235.2, | 232.2 |
| | | 231.0, 230.8, 232.9 | |
| D | 49 | 514.7, 509.7, 510.5, 514.5, 509.3, | 511.6 |
| | | 510.9 | |
| D | 98 | 722.9, 717.6, 719.3, 725.1, 719.8, | 721.1 |
| | | 721.9 | |
| D | 196 | 1040.5, 1037.2, 1033.8, 1032.3, | 1036.8 |
| | | 1038.8, 1038.3 | |
| E | 2.94 | 128.1, 130.3, 133.9, 132.3, 135.6, | 132 |
| 1 | | 129.4, 131.8, 134.6 | |
| E | 4.9 | 164.9, 166.8, 170.1, 168.5, 167.4, | 167.2 |
| ~ | | 166.1, 169.3, 164.5 | 107.2 |
| E | 9.8 | 236.4, 235.3, 230.9, 237.7, 233.6, | 234.1 |
| | 7.0 | 233.2, 235.9, 229.8 | 254.1 |
| E | 49 | 517.9, 511.5, 520.4, 513.9, 516.8, | 516.3 |
| | 1 | 517.3 | 310.5 |
| E | 98 | 724.3, 729.9, 725.6, 725.4, 733.8, | 728.6 |
| E | 96 | | 728.0 |
| E | 106 | 732.6 | 1042.1 |
| E | 196 | 1034.9, 1042.4, 1045.6, 1044.1, | 1042.1 |
| <u> </u> | 0.000 | 1047.8, 1037.8 | 20.1 |
| A1 | 0.098 | 20.5, 19.8, 20.6, 19.1, 18.7, 20.5, 22.3, | 20.1 |
| A 4 | 0.045 | 18.9, 20.2, 20.4 | 20.1 |
| A1 | 0.245 | 32.1, 28.9, 28.4, 29.3, 33.5, 29.6, 30.5, | 30.1 |
| | | 28.3, 30.0, 30.4 | |
| A1 | 0.49 | 45.4, 46.9, 49.1, 48.2, 44.6, 48.1, 49.7, | 47.7 |
| | | 43.5, 47.9, 53.6 | |
| A1 | 0.98 | 68.9, 73.2, 71.7, 69.3, 70.5, 74.2, 68.4, | 71.2 |
| | | 70.3, 75.1, 70.4 | |
| A1 | 1.96 | 106.8, 104.5, 103.3, 101.6, 105.6, | 102.9 |
| | | 102.8, 99.0, 100.6, 99.2, 105.6 | |
| A1 | 2.94 | 126.8, 129.3, 128.1, 135.7, 127.6, | 129.1 |
| | | 133.4, 128.7, 123.2 | |
| A1 | 4.9 | 170.4, 178.6, 173.9, 176.7, 179.1, | 175.1 |
| | | 175.6, 177.2, 169.3 | |
| A1 | 9.8 | 236.9, 234.2, 231.4, 237.8, 240.1, | 236.4 |
| | | 235.3, 238.5, 237.0 | |
| B1 | 0.098 | 19.3, 22.9, 20.6, 18.1, 20.2, 20.9, 22.1, | 20.3 |
| | | 18.8, 19.9, 20.2 | |
| B1 | 0.245 | 33.5, 29.6, 31.8, 34.1, 28.5, 34.6, 32.5, | 32.9 |
| | 0.2.15 | 33.2, 32.7, 38.5 | - - |
| B1 | 0.49 | 50.4, 46.9, 48.1, 48.4, 50.3, 47.2, 49.5, | 48.8 |
| 44 | 1 0.77 | [JUIT, TUIZ, TUIT, JUIJ, TILE, TIJ,] | 70.0 |

| | | 50.2, 47.1, 49.9 | |
|------|-------|---|----------------|
| B1 | 0.98 | 70.1, 73.2, 68.6, 70.7, 69.4, 67.9, 72.7, 73.6, 69.0, 69.8 | 70.5 |
| B1 | 1.96 | 96.3, 100.5, 104.9, 97.2, 95.6, 100.3, 95.2, 101.9, 96.7, 102.4 | 99.1 |
| B1 | 2.94 | 123.7, 120.9, 126.3, 125.4, 124.8, 128.3, 121.1, 123.9 | 124.3 |
| B1 | 4.9 | 167.2, 163.8, 164.5, 166.3, 162.9, 168.4, 162.6, 165.9 | 165.2 |
| B1 | 9.8 | 234.1, 239.3, 235.5, 233.8, 234.7, 236.9, 237.3, 242.0 | 236.7 |
| C1 | 0.098 | 21.9, 18.9, 20.2, 18.1, 19.3, 22.5, 18.4, 19.3, 20.7, 17.7 | 19.7 |
| C1 | 0.245 | 30.6, 27.2, 29.3, 26.8, 27.5, 28.1, 26.9, 27.9, 30.5, 32.2 | 28.7 |
| C1 | 0.49 | 48.3, 49.9, 45.4, 46.7, 46.1, 44.8, 50.2, 47.6, 45.1, 47.9 | 47.2 |
| C1 | 0.98 | 72.3, 69.4, 67.3, 71.8, 69.7, 68.1, 65.3, 75.8, 70.2, 68.1 | 69.8 |
| C1 | 1.96 | 104.6, 100.3, 102.7, 105.1, 104.8, 108.3, 99.3, 103.5, 104.1, 107.3 | 104 |
| C1 | 2.94 | 122.1, 123.9, 127.2, 126.8, 130.3, 120.4, 123.7, 129.6 | 125.5 |
| C1 | 4.9 | 163.1, 160.2, 161.7, 162.4, 161.6, 160.9, 161.3, 167.2 | 162.3 228.5 |
| C1 | 9.8 | 233.8, 227.1, 229.5, 226.3, 228.2, 224.9, 230.8, 227.4 132.4, 127.9, 128.7, 133.6, 135.4, | 130.8 |
| F1 | 2.94 | 126.1, 127.2, 135.1 | 171.6 |
| F1 | 9.8 | 172.2, 175.9, 168.9, 170.4, 174.3, 171.9, 169.7, 169.5 235.7, 236.3, 232.2, 238.1, 234.1, | 234.9 |
| F1 | 49 | 230.5, 233.6, 238.7 516.9, 522.4, 523.7, 518.6, 519.2, | 521.2 |
| F1 | 98 | 526.4 728.1, 724.3, 722.8, 730.1, 726.3, | 725.2 |
| F2 | 2.94 | 719.6 125.9, 118.7, 120.1, 119.3, 117.7, | 120.4 |
| F2 | 4.9 | 118.5, 116.4, 126.6 163.9, 164.8, 168.6, 162.5, 163.6, | 164.6 |
| F2 | 9.8 | 161.9, 169.4, 162.1 224.6, 223.2, 227.9, 220.1, 228.8, | 224.8 |
| F2 | 49 | 224.2 510.9, 513.8, 519.4, 516.1, 514.7, | 514.3 |
| F2 | 98 | 510.7 510.7 728.1, 725.3, 724.4, 722.6, 729.3, | 725.8 |
| 1' 4 | 1 70 | 120.1, 123.3, 127.7, 122.0, 127.3, | , 45.0 |

| | | 725.1 | |
|-----|-----|-------|--------|
| G1* | 588 | | 1339.1 |
| G2* | 588 | | 1312.8 |

A total of 514 Vickers indents made in this study.

